THE THERMODYNAMICS OF THE ^{4}HE SUBMONOLAYER FILM ADSORBED ON GRAFOIL

Thesis by

Robert Lawrence Elgin

In partial Fulfillment of the Requirements

for the Degree of

Doctor of Philosophy

California Institute of Technology

Pasadena, California

1973

(Submitted May 23, 1973)

ACKNOWLEDGMENTS

I would like to express my appreciation to Dr. David L. Goodstein for his guidance, advice, and tolerance during this long project. Thanks also to Alex Stewart, Jeff Greif, and Harris Notarys for many helpful discussions. I would also like to thank Dr. J. G. Dash and the low temperature physics group at the University of Washington for their generous sharing of ideas and prepublication results.

The financial support of the National Science Foundation, both through a graduate fellowship and a research grant is gratefully acknowledged.

ABSTRACT

The heat capacity and vapor pressure of thin films of helium adsorbed on graphite have been measured simultaneously. Sufficient data were taken for a complete model-independent thermodynamic analysis from 4.5 K to 15 K and from 0.01 to 1.2 monolayer. Heat capacity down to 1.4 K showed reproducibility with other laboratories.

The data allow definitive tests of many models suggested for these films. Large heat capacity peaks at the melting transition are shown to be the result of interactions with the second layer and the bulk gas phase. Large deviations from ideal gas behavior at low densities are explained quantitatively by interactions with inhomogeneities in the substrate. The data may therefore be corrected to determine experimentally the behavior of strictly two-dimensional helium on a completely homogeneous surface.

TABLE OF CONTENTS

Introduction		1
Chapter 1		
	The adsorption system	3
	The helium-Grafoil system	7
Chapter 2		
	Experimental apparatus	25
	Methods of data reduction	31
Chapter 3		
	Two-dimensional thermodynamics	42
	Tabulation of results	52
Chapter 4		
	Subsystem identification	60
	Model generation	70
	Model analysis	84
Chapter 5		
	Conclusions	103
Appendix I		
	Table I Main results	107
	Table II Lattice gas	122
	Table III Survey data	123
	Table IV Low temperature results	125
Appendix II		
	Thermal transpiration	126
Bibliography		131

LIST OF FIGURES

Figure		Page
1	Experimental Accessibility	8
2	Bulk Phase Diagram	10
3	2-D Phase Diagram	13
4	2-D Solid and Melting	15
5	2-D and 3-D Melting Line	16
6	2-D and 3-D Debye θ	17
7	Ordered Lattice Gas	19
8	Intermediate Region	20
9	Inhomogeneity Compressed Region	22
10	Calorimeter	26
11	Argon Isotherm at 63.5 K	57
12	Direct and Indirect Pressures	58
13	Excited State Energy	63
14	Binding Energy Estimates	64
15	Binding Energy Distribution	67
16	Fit to Virial Gas + Inhomogeneity	76
17	Pressure Isotherms	78
18	Isosteric Heat	80
19	Bulk P-V-T Diagram	81
20	Film ϕ-A-T Diagram	82

21	Lattice Gas Phases	90
22	Spreading Pressure	92
23	Constant Pressure Heat Capacity	96
24	Chemical Potential Plot	100

To my spouse, Dr. Sarah Carlisle Roberts Elgin, the most liberating person I know.

INTRODUCTION

The forces responsible for physical adsorption are nearly as ubiquitous as gravity. All atoms have instantaneous dipole moments which induce dipoles in nearby atoms causing an attractive interaction. Near a material surface, this gives a force varying approximately as the inverse fourth power of the distance. In rough analogy to planetary atmospheres held by gravity, this causes solids to be completely covered with a film of foreign material at normal temperatures and pressures. This invisible layer keeps "touching" metal surfaces from fusing and greatly accelerates many industrial reactions (catalysts) and biological processes (enzymes).

In spite of the simple force law and numerous practical uses, the nature of the film is poorly understood. In part this is caused by the wide range of systems available. Earliest experiments used practical catalysts with strongly convoluted surfaces and dense films of reactive molecules to maximize interactions, whereas the earliest theories analyzed inert films in the limit of infinite dilution on ideally smooth planes. Great strides have been made

in recent years to narrow this gap. Calculations are now available on effects of the crystalline structure of the substrate and of many body interactions in dense films. Experimentalists have worked toward smooth, reproducible, well-characterized substrates covered with pure inert gases.

Chapter 1 gives a general description of the adsorption system and a comparison with earlier systems. Chapter 2 describes the experimental apparatus and the techniques used for measuring the chemical potential and the heat capacity. Chapter 3 develops the thermodynamic identities relevant to two dimensions and uses them to transform the data into a complete thermodynamic description of the system. Chapter 4 separates the contributions due to substrate inhomogeneities and multilayer formation from those intrinsic to the two-dimensional film and compares the results with theoretical models. Chapter 5 summarizes the current understanding of the system and suggests interesting remaining problems.

CHAPTER 1

The adsorption system

Although physical adsorption will occur in almost any system consisting of a solid and a gas that are not chemically reactive, most such systems are not suitable for study by thermodynamic methods. The general problem is the ratio of surface signal to bulk background. For example, 1 mg of N_2 gas occupies only 0.8 STP cm^3 but, when adsorbed, it covers 3.5 m^2 of surface with a monolayer. The obvious solution is to use a substrate with a large surface to mass ratio.

Early experiments on adsorbed helium used such substrates as porous glass and powders of "amorphous" carbon, ferric oxide (jeweler's rouge) and titanium dioxide (anatase) (Long & Meyer 1953) (1). Such materials often had more than 100 m^2 of surface per gram. A large number of adsorption (pressure) isotherms were reported as well as a careful measurement of the heat capacity near the superfluid transition

---

1. Author references are listed alphabetically in the bibliography.

(Frederikse 1949). However, the reproducibility was poor and almost no data were published on films of less than a monolayer. All the above substrates are poor heat conductors at low temperatures, especially as loose powders. For thick films, the bulk gas provides rapid thermal equilibrium, but the pressure becomes unmeasurably small slightly below a monolayer. So just where pressure measurements become impossible the heat capacity measurements become inaccurate.

A systematic solution to these problems was provided by argon-precoated sintered-copper sponges (Goodstein, McCormick, & Dash 1966). Copper is among the best thermal conductors and argon is among the weakest adsorbing substrates. So the combination allowed the pressure to be measured to less than half a layer (Wallace & Goodstein 1970) and the heat capacity to only a tenth of a layer (Stewart & Dash 1970). The immediate discovery of heat capacities consistent with a two-dimensional Debye solid suggested that the system was now simple enough to understand (McCormick, Goodstein, & Dash 1968). However, the pressure varied too much and the heat capacity too little: The pressure varied by up to two orders of magnitude at the same temperature and coverage (two-dimensional density) on what were supposed to be very similar substrates

(Dash, Peierls, & Stewart 1970). Debye-solid-like heat capacities persisted to low densities and high temperatures, a very unlikely region for a solid (Princehouse 1972).

The above results indicate that the binding energy varies considerably over the surface as well as between samples. It may be that metal powders cannot be smoothed to the scale needed by sintering. During sintering, surface tension rounds all the sharp edges. This exposes a large variety of crystal planes, each with a slightly different binding energy. Even if perfect surfaces could be prepared, copper is very susceptible to oxidation. Even at 77 K, a full monolayer of Cu_2O will form within seconds of exposure to even traces of oxygen (Rhodin 1950). The area to volume ratio of common sintered sponges is such that one leak from vacuum up to atmospheric air will oxidize about 10% of the surface.

Volatile oxides and a single type of crystalline face may be combined with a large surface area by using graphitized carbon (Dacey 1967). It was discovered 20 years ago that heat-treated carbon black develops sharp steps in adsorption isotherms indicative of high homogeneity (Polley, Schaeffer, & Smith 1953; Singleton & Halsey 1954). The powdered carbon P-33(2700°) is now the

most thoroughly investigated substrate in the world (Halsey 1967). The main drawback has been that, although the thermal conductivity of graphite along its basal plane is tolerable, the conductivity of the randomly oriented powders is abysmal.

Fortunately, a high-surface-area graphitized carbon with aligned planes may be made by exfoliation. Metal vapors exposed to graphite will often intercalate in widely spaced layers. Rapid heating will cause the metal to boil and the graphite to flake off (exfoliate) (Bretz, Dash, Hickernell, McLean, & Vilches 1973). Substrates made in this manner give even steeper steps than graphitized carbon black (Duval & Thomy 1964; Thomy & Duval 1969, 1970). Reproducibility is improved at the cost of some uncertainty in the method of preparation by the use of Grafoil (2). With careful attention to providing good thermal contact between the Grafoil sheets and the calorimeter walls, the thermal conductivity is completely adequate (Bretz & Dash 1971a).

---

2. GTA grade Grafoil^{R} is produced commercially by Union Carbide.

The helium-Grafoil system

The binding energy is fixed at about 140 K (3), the substrate thickness at 40 nm, and the separation at 60 nm (4) by the choice of Grafoil as the substrate and helium as the adsorbate. These parameters closely circumscribe the region over which two-dimensional behavior may be studied. The temperature and density must be sufficiently low so that most of the helium is in the surface layer. However, if the density is too low the heat capacity of the carbon will swamp the signal from the helium and if the temperature is too low the pressure will be unmeasurably small.

These limitations are evaluated in Fig. 1 using the data of this paper. The coverage, $1/\alpha$, in atoms per nm^2 is plotted against the temperature, T, in kelvins. The region over which both heat capacity and pressure are accurately measurable is bounded as follows: On the right, desorption corrections to the heat capacity exceed the film heat capacity

---

3. Energies will be expressed in kelvins throughout by suppressing the gas constant, R. 1 kelvin = 8.3143 J/mol = 1.9872 calories/mol = 1.3806×10^{-16} ergs/atom.

4. 1 nm = 10 Å. This implies 60 layers of carbon, and free space equivalent to 80 layers of liquid helium at 4.2 K for each exposed surface.

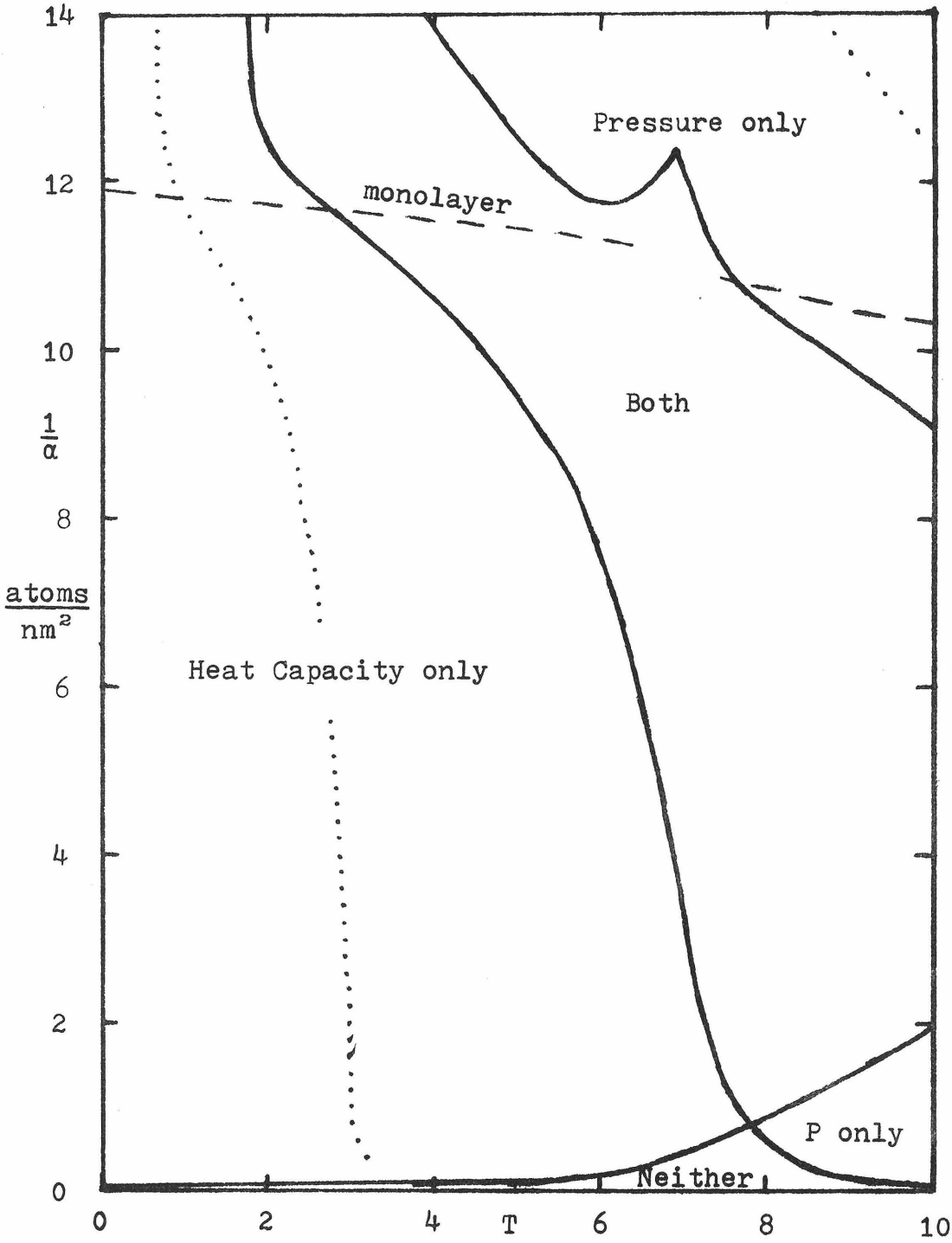

Figure 1 Experimental Accessibility

($P \approx 2$ torr) (5). At the bottom, the carbon heat capacity exceeds three times the film heat capacity. On the left, the pressure falls below the 10^{-5} torr limit of capacitive manometry. In the upward direction, the data are measurable up to 80 layers, but strictly two-dimensional behavior stops at the beginning of the second layer, defined in the figure by a minimum in the film entropy. Changes in instrumentation will move these boundary curves only moderately. The dotted line on the left locates the unmeasurably small bulk gas density of 1 atom/cm^3 ($P \approx 10^{-19}$ torr). The coverage itself becomes inaccurate beyond the dotted line in the upper right where most of the helium is not adsorbed ($P \approx 300$ torr).

Now that we know what is accessible, it remains to determine what is interesting. As a first approximation, we may examine the bulk phases in the same coordinates (6). These are shown in Fig. 2 (Ahlers 1970; Glassford & Smith 1966; McCarty 1972). There is one gas

---

5. 1 torr = 1/760 atmosphere = 101325/760 N/m^2.

6. In scaling between dimensions, it would seem reasonable to compare systems with the same intermolecular spacing, ℓ. For close packed spheres such as solid helium, the n-dimensional volume per "sphere" is $\sqrt{n+1}(\ell/\sqrt{2})^n$. Specializing to 2 and 3 dimensions gives $\alpha = \sqrt{3}(v/2)^{2/3} = 1.091\, v^{2/3}$. The same scaling was used at nonsolid densities.

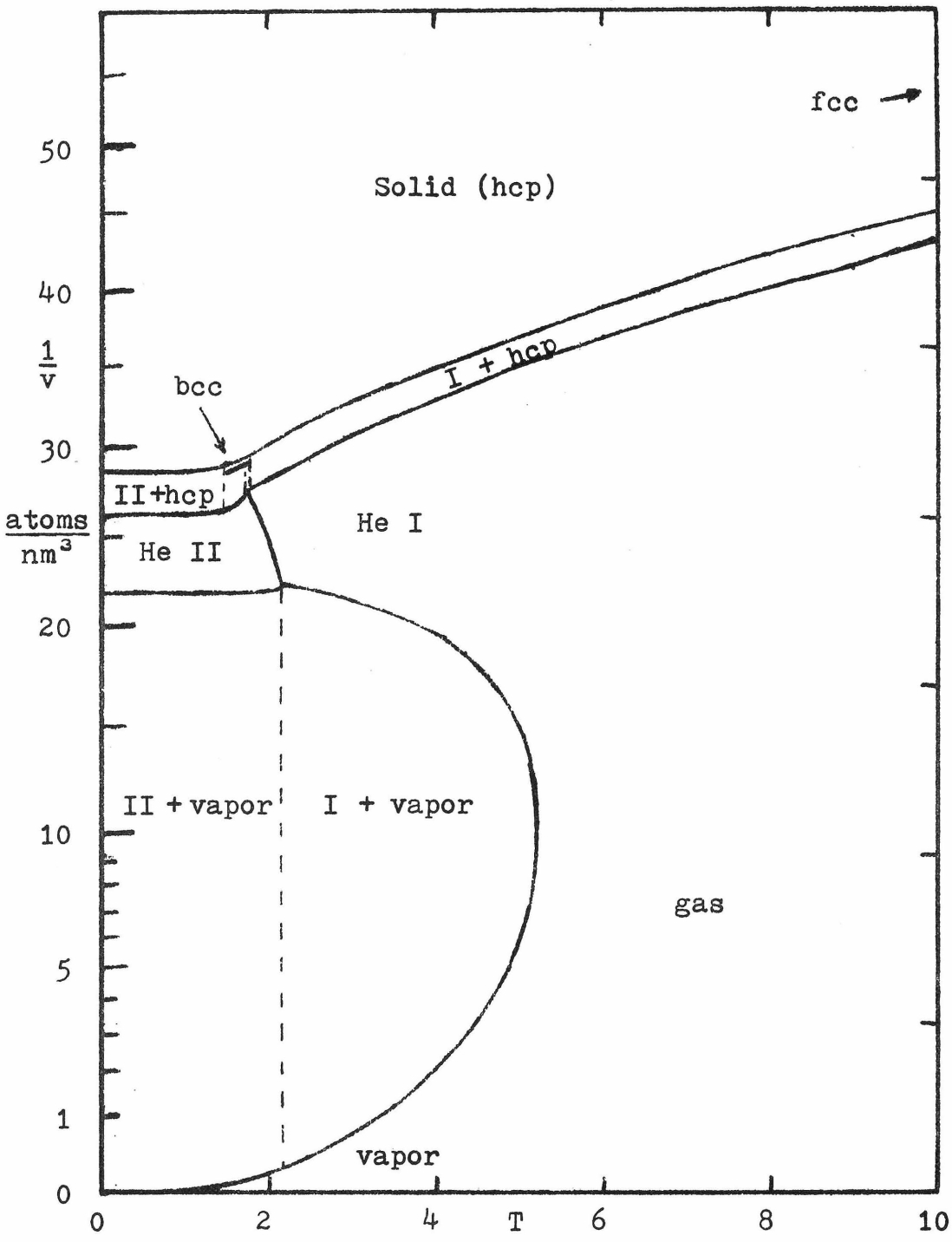

Figure 2 Bulk Phase Diagram

or vapor, two fluids - normal (He I) and superfluid (He II), and three solids - hexagonal close packed (hcp), body-centered cubic (bcc), and face-centered cubic (fcc). The actual density is shown on the nonlinear scale on the left. Comparing figures 1 and 2 we see that, except for solids above the critical temperature, all coverages corresponding to bulk phase transitions are easily accessible to heat capacity measurement but inaccessible to pressure measurement. This explains why all the early work with helium on Grafoil reported heat capacity results almost exclusively (Bretz & Dash 1971a, 1971b; Bretz, Huff, & Dash 1972; Hickernell, McLean, & Vilches 1972).

While heat capacity results alone can be very interesting and locate phase boundaries, they are seriously deficient. A detailed understanding of phase equilibria is impossible without knowledge of the chemical potential. This includes equilibrium with the bulk gas, the second layer, and substrate inhomogeneities as well as with other two-dimensional phases. The chemical potential cannot be found from heat capacity data alone, but can be found trivially from the pressure and temperature of a practically ideal gas. This project has concentrated on the region from 4.5 K to 15 K in order to have combined

knowledge of the pressure and the heat capacity. It will be shown in chapter 3 that one can use the heat capacity data to extend measurements of the pressure to lower temperatures with the same rigor with which one can extend the entropy to higher temperatures by integrating the heat capacity.

The actual phase diagram for ^{4}He adsorbed on Grafoil is shown in Fig. 3. Each dot or horizontal line represents an observed peak in the heat capacity; the heat capacity remains within 10% of its maximum value over the temperature interval given by the length of the line. All data summarized in Bretz et al (1973) and in this paper are shown. The major regions summarized below will be analyzed in detail in chapter 4.

The multilayer region may be identified in many ways. The energy gained by binding to the graphite will be counterbalanced by the energy required to compress the film at a bulk density of 0.31 g/cm^3 under a pressure of 760 atmospheres. This equals 47 atoms/nm^3 or 12 atoms/nm^2. The minimum in the entropy used for Fig. 1 is expected to indicate multilayer formation because adding atoms at constant volume lowers the entropy of a solid but raises the entropy of a gas. At low temperatures a gas-like constant heat capacity from the second layer can be seen in addition to

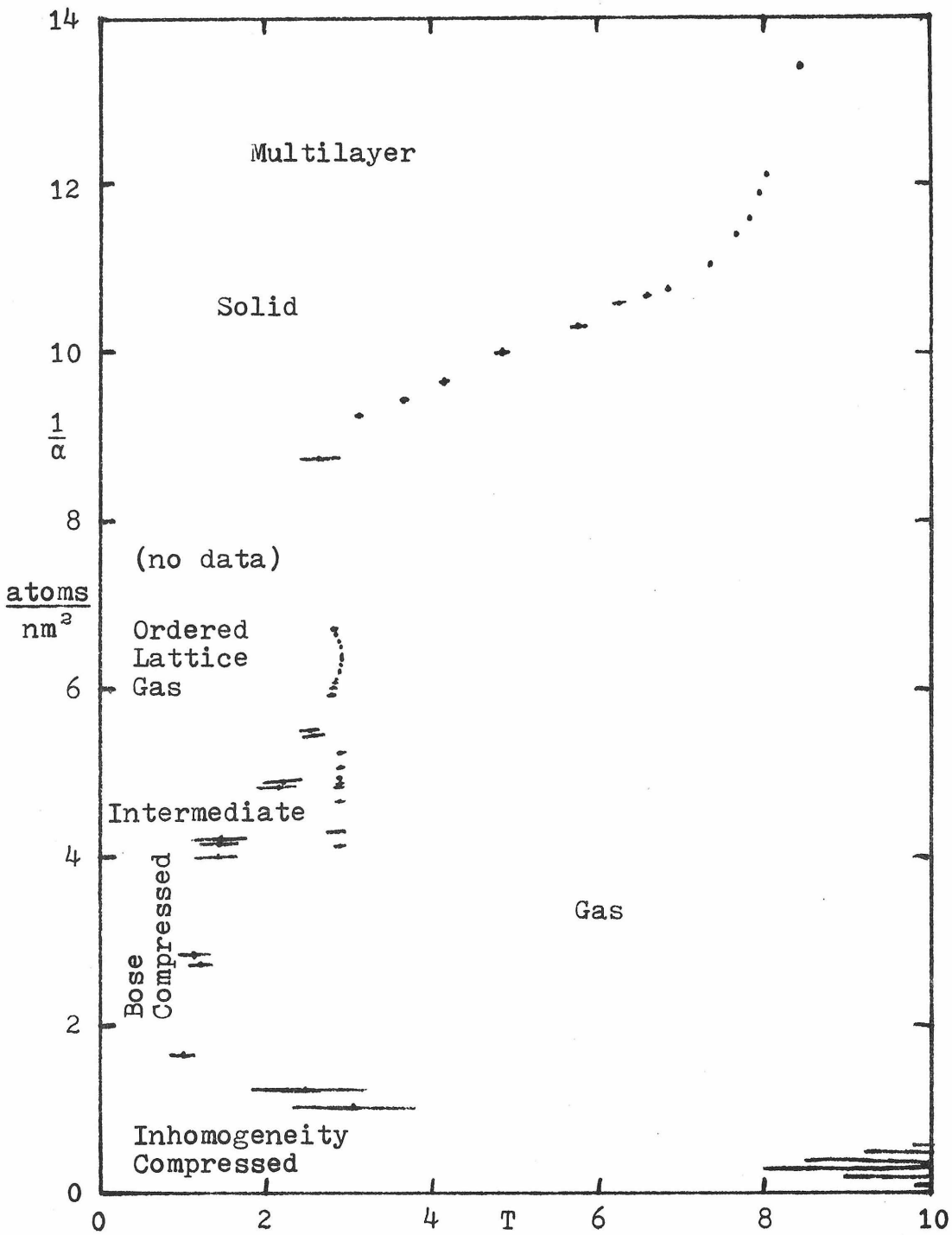

Figure 3 2-D Phase Diagram

that proportional to T^2 from the first layer. Most dramatically, the heat capacity peaks due to melting sharpen rapidly where the second layer forms. This effect is explained in chapter 4 where the curves shown in Fig. 4 are calculated.

The solid region is in remarkable coincidence with the bulk solid. A series of heat capacity peaks observed in the film (Bretz, Huff, & Dash 1972, data shown on Fig. 4) fall right in the liquid-solid two-phase region of bulk helium as shown enlarged in Fig. 5 (7). The split symbols show corrections for the second layer as explained in chapter 4. The heat capacity well below the peaks fits well to a two-dimensional Debye solid. The Debye temperatures in the bulk (+) (Ahlers 1970) are compared with those in the film (o) (Bretz, Huff, & Dash 1972) in Fig. 6. It is even possible to interrelate the data with elastic solid theory with consistent results (Stewart, Siegel, and Goodstein 1973).

The ordered lattice gas is centered at 6.366 ± .002 atoms/nm^2. Its density is well known because the lattice is provided by the graphite. The ordered gas occupies every third hexagonal site, forming a triangular array. The heat capacity peak occurs when the gas disorders

---

7. Note that $\alpha = 10$ $\mathring{A}^2$/atom is the same coverage as $1/\alpha = 10$ atoms/nm^2.

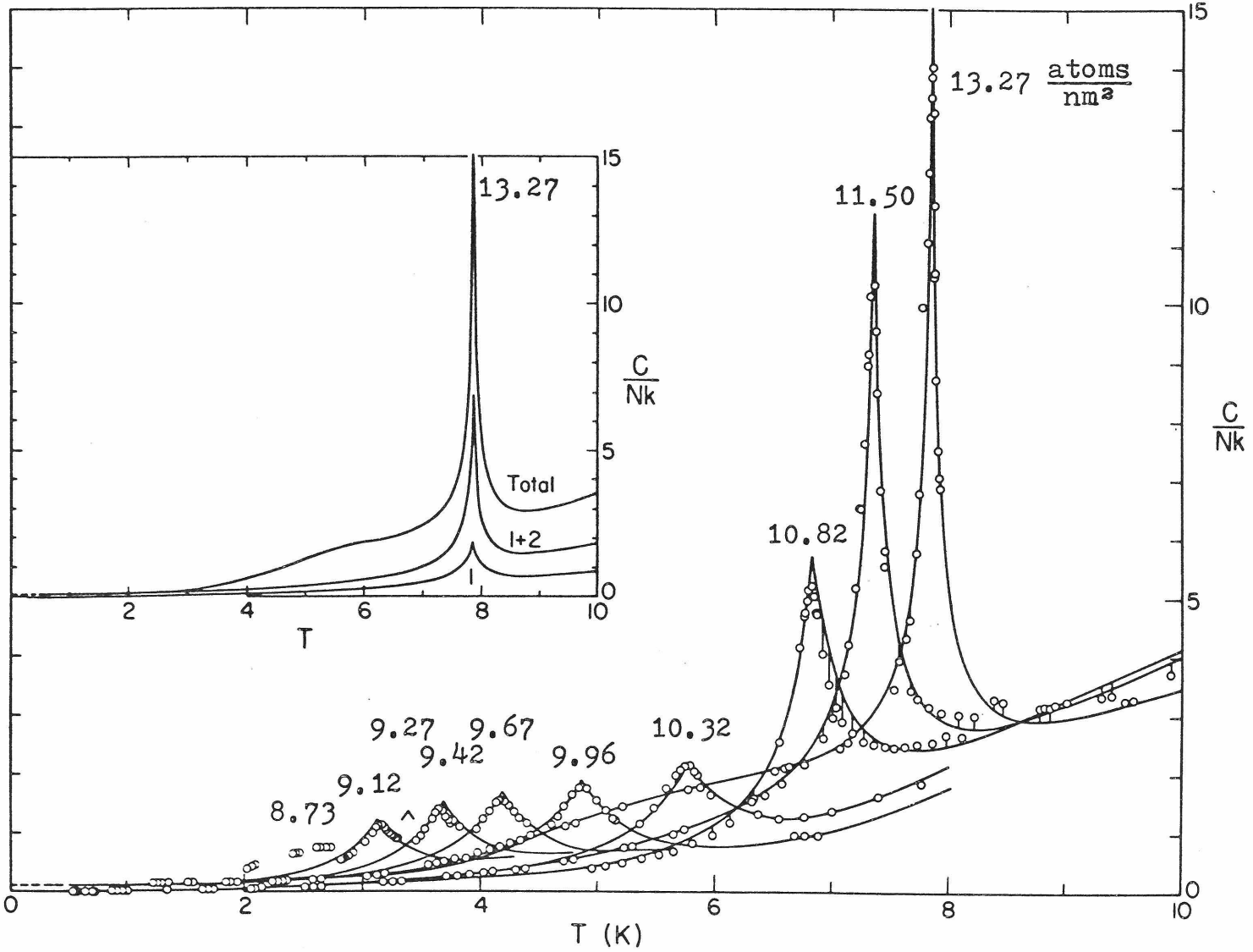

Figure 4 2-D Solid & Melting

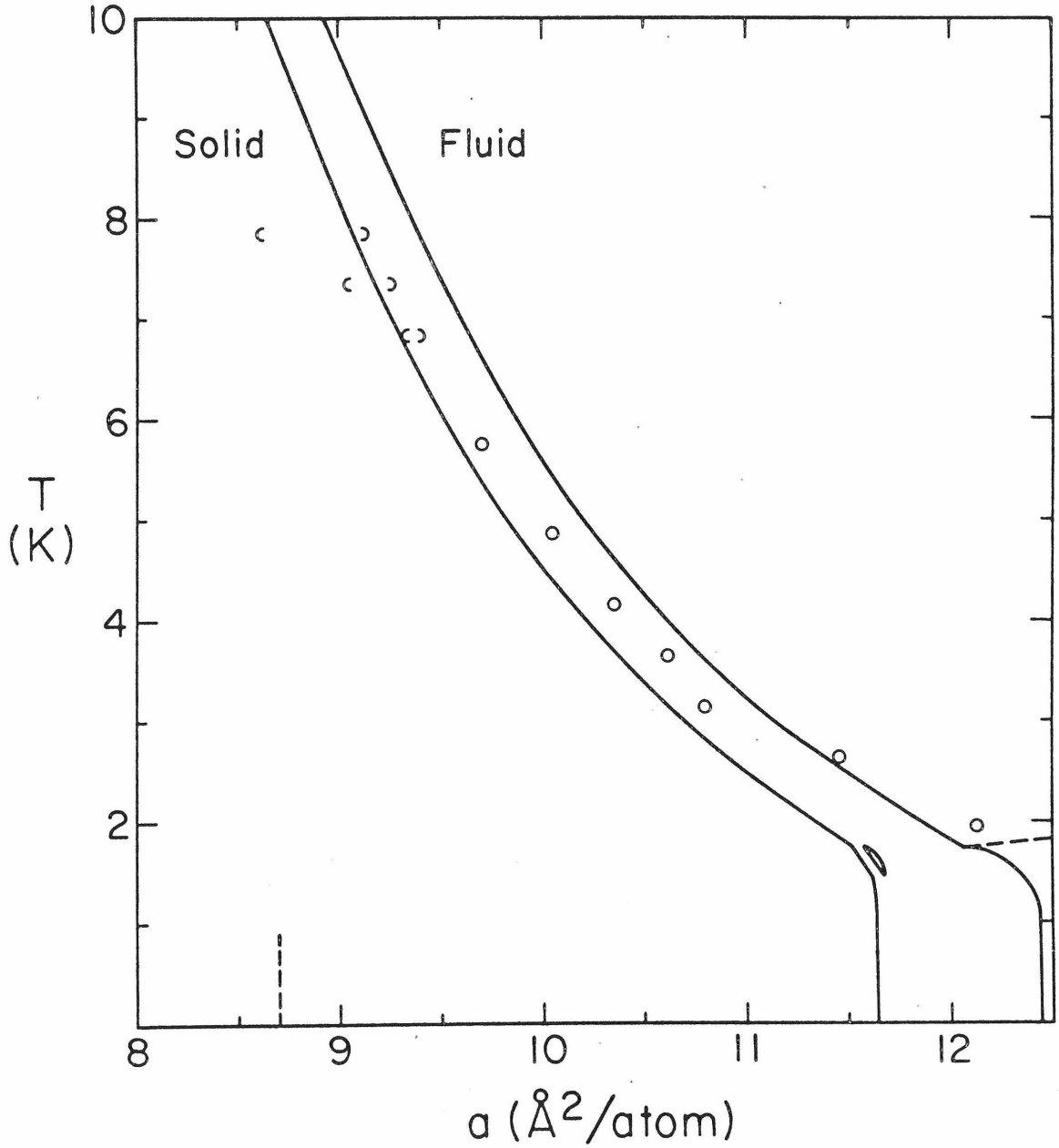

Figure 5 2-D & 3-D Melting Line

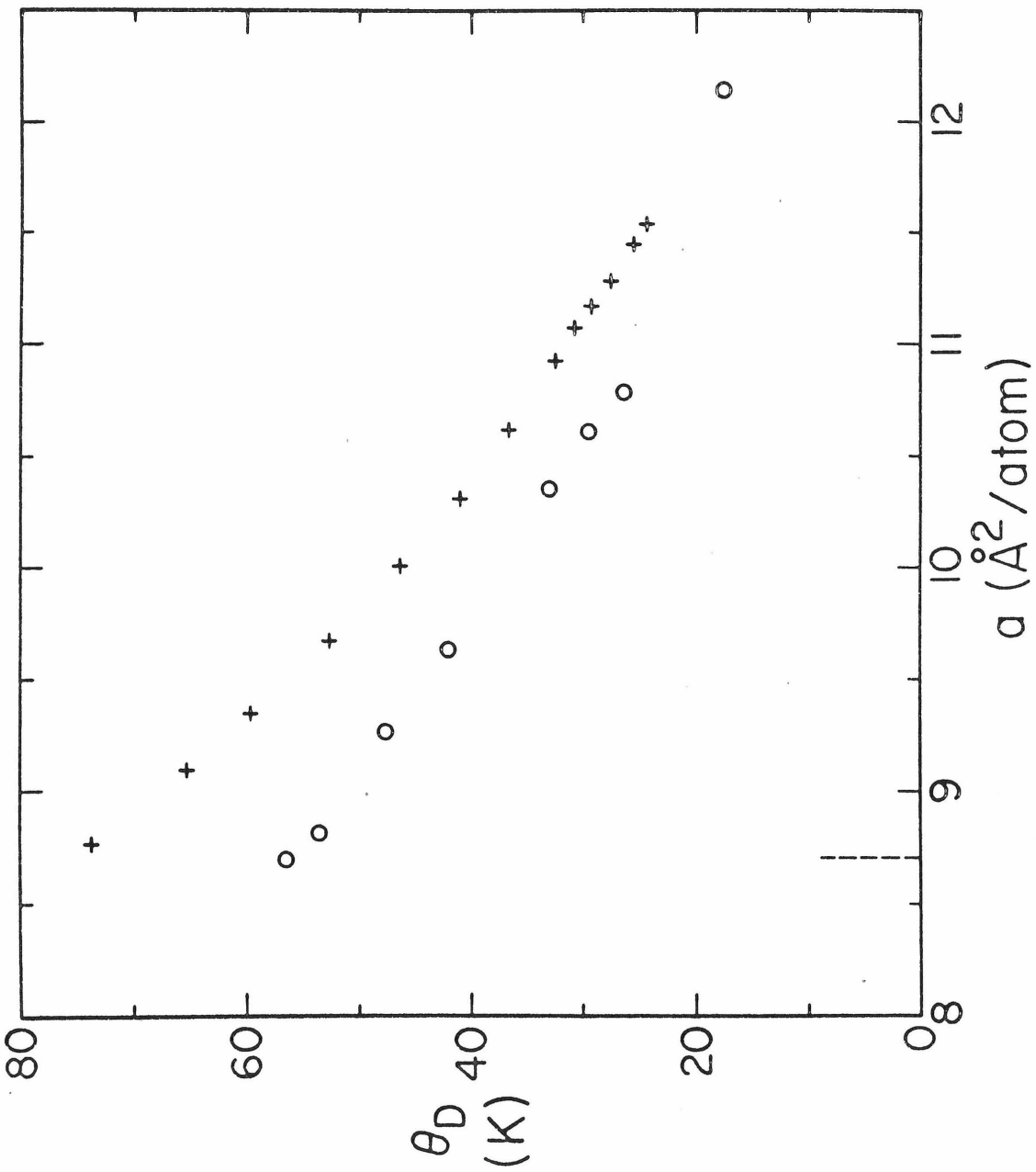

Figure 6 2-D & 3-D Debye θ

on heating. The peak is strongly coverage dependent as shown in Fig. 7. The coverage is shown on the right and the heat capacity zero has been shifted for each coverage. Measurements are shown for 4 cells. Cells A (circles) and B (diamonds) were used by Bretz et al (1973). Some early work of the author used cell C (open rectangles), but the main results reported here used cell D (solid rectangles). The coverage dependence and reproducibility of this peak has made it ideal as a fiducial mark for intercalibrating separate cells. The observed variation of temperature with coverage at the heat capacity peak has been shown to be consistent with a lattice gas order-disorder transition (Campbell & Schick 1972). The ordered lattice gas has also been shown to be the most stable arrangement at this coverage (Novaco 1973).

In the bulk, equilibrium is very slow near the critical density (10.5 atoms/nm^3 = 4.4 atoms/nm^2). The same appears to hold in the film at this intermediate density, for the data vary erratically as shown by Fig. 8. The solid symbols represent the most recent data for the systems defined in the preceding figure. All data available over an extended temperature range are shown. Only the true equilibrium state should have zero entropy at 0 K, so it should have the greatest

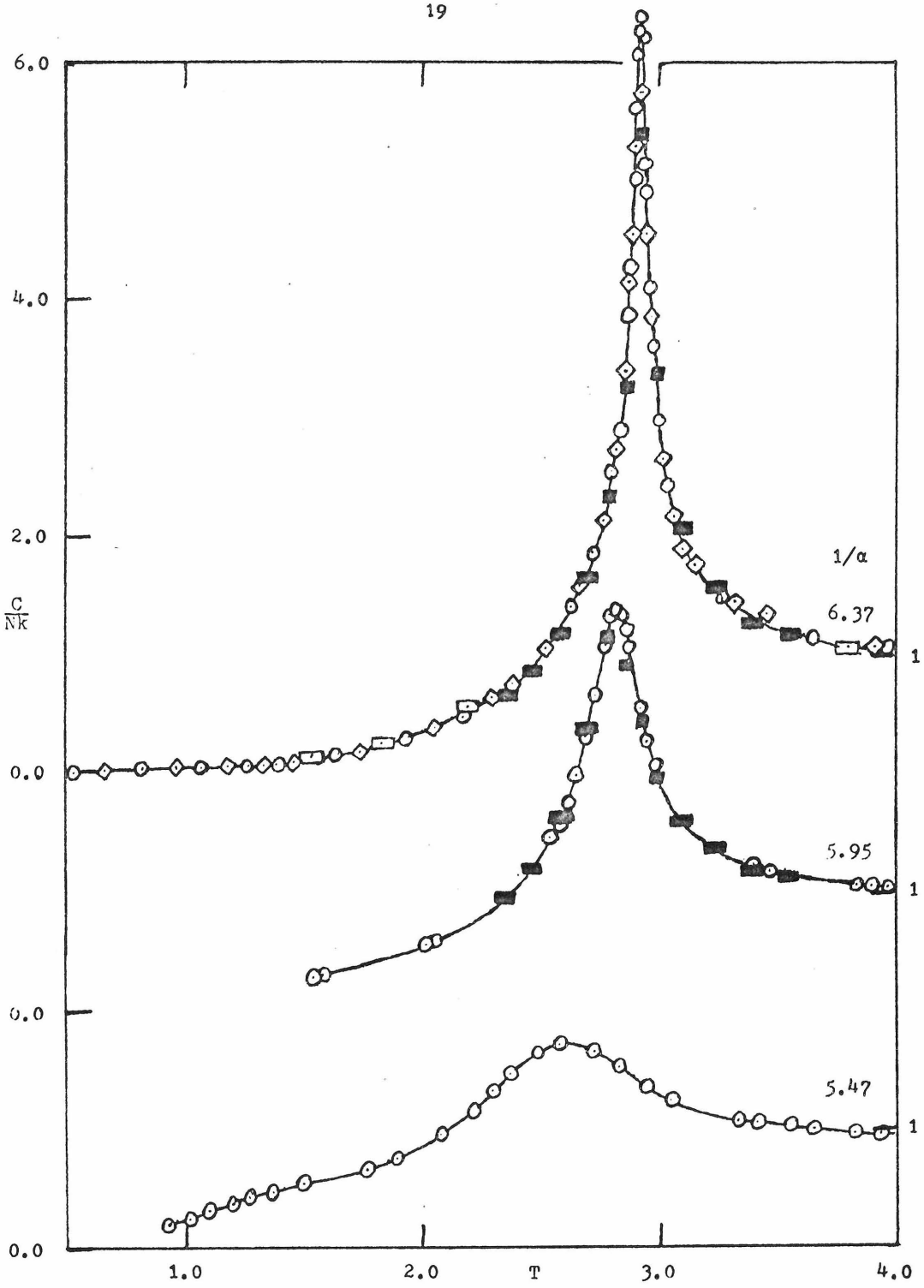

Figure 7 Ordered Lattice Gas

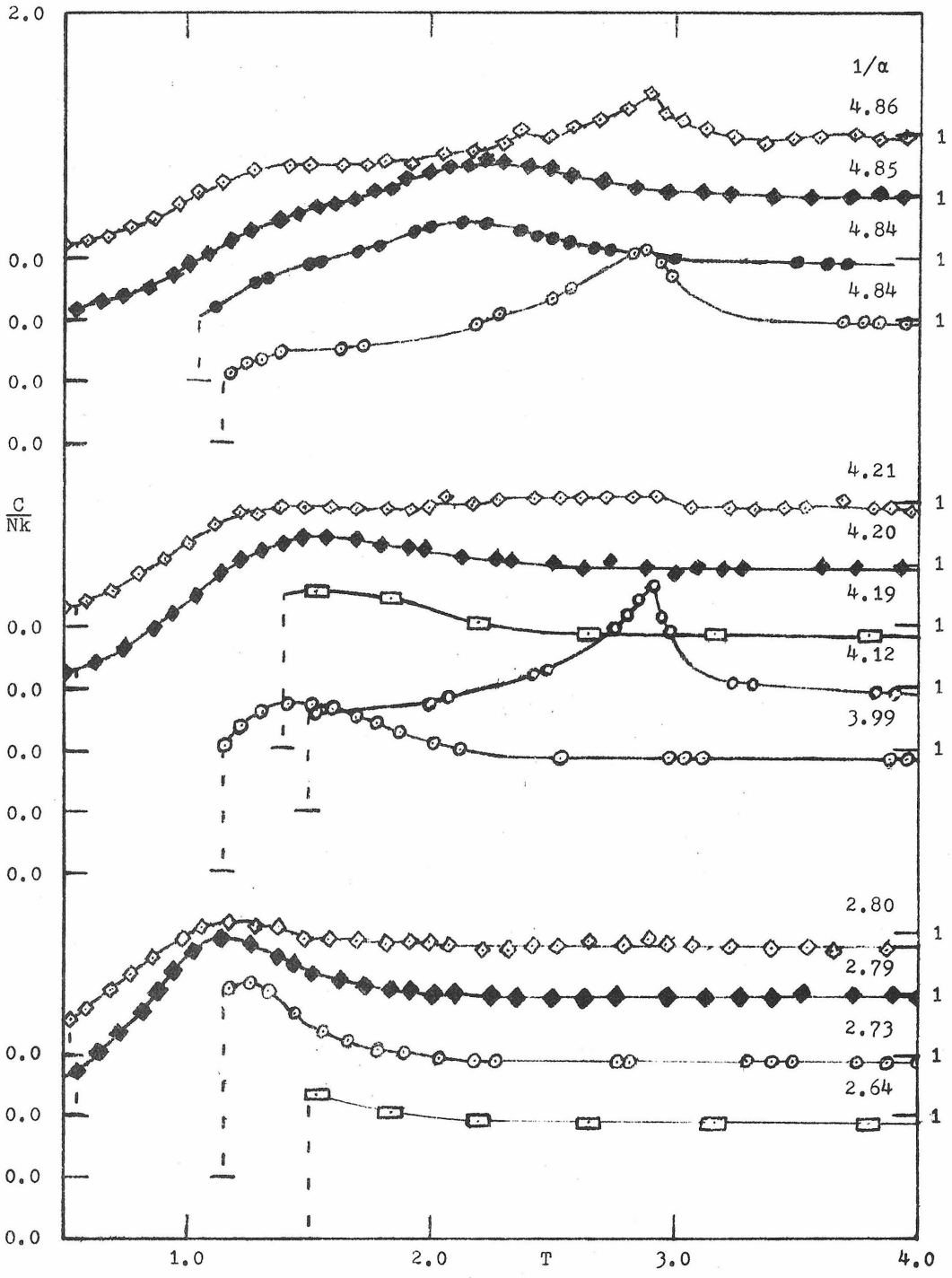

Figure 8 Intermediate Region

entropy increase on heating. By this criterion, the high temperature peaks are anomalous and the true phase boundary interpolates smoothly between the lattice gas and bose regions.

The label bose compressed was chosen mainly for its ambiguity. It has been shown that bosons with hard cores will give a heat capacity peak in two dimensions in this region (Siddon & Schick 1973). This says only that the Bose-Einstein statistics are equivalent to an attractive interaction. There is no hard evidence for the macroscopic occupation of the zero momentum state that is normally implied by the term bose condensation. The condensation here is in real space and may even be to a liquid state. Whatever the details, a single phenomenon occurs over the range $1.5 < 1/\alpha < 4.2$ atoms/nm^2, as shown at the bottom of Fig. 8 and the top of Fig. 9.

The inhomogeneity compressed region does not really belong on a two-dimensional phase diagram. Where two surfaces make contact the total binding energy is increased. At low coverages, this small substrate inhomogeneity leads to a very inhomogeneous film because the atoms are preferentially adsorbed in these high energy crevices. A large energy is required to promote these atoms to normal sites on heating.

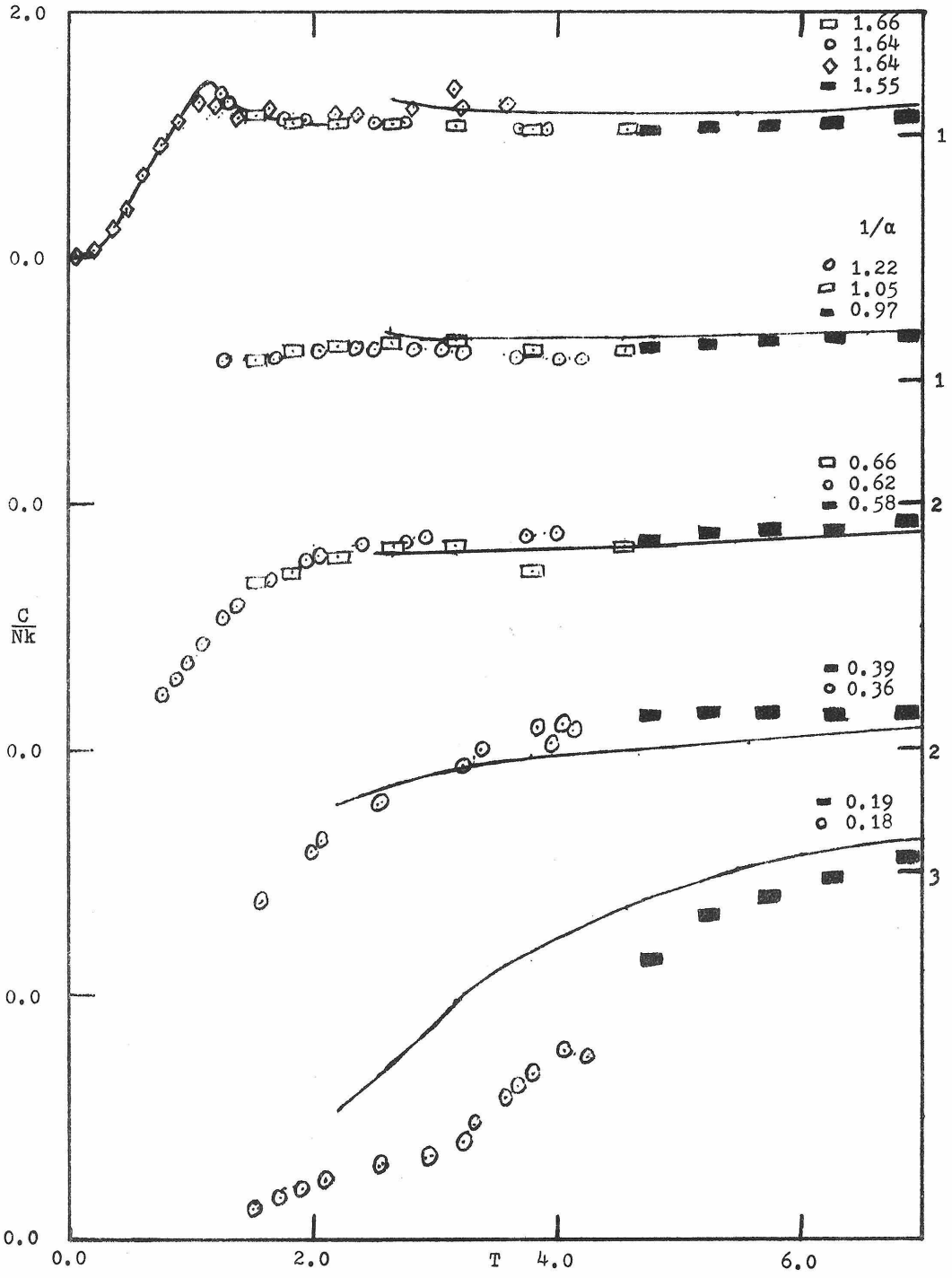

Figure 9 Inhomogeneity Compressed Region

The resulting heat capacity may exceed the ideal gas value (C/Nk = 1) by more than a factor of three, as shown by the lowest coverage in Fig. 9. Combining the substrate energy distribution as found in chapter 3 with a van der Waals' approximation to the equation of state as derived from high temperature virial coefficients gives the lines shown above 2 K in Fig. 9 without any adjustable parameters.

The remainder of the phase diagram is gas. Below 8 K the heat capacity is generally slightly below the ideal gas value. This is quantitatively explained by use of a quantum mechanical calculation of the two-dimensional second virial coefficient (Siddon & Schick 1973). Larger heat capacities above 8 K are due to progressive excitation of a state of oscillation perpendicular to the surface. This state has an energy of 55 K.

A general property shown in Fig. 2 is the existence of at least one transition line between high and low temperatures at any density. This is expected since a classical gas cannot have zero entropy at 0 K as required by Nernst's theorem. The gas must therefore make one or more transitions to reach a state that may have zero entropy. In the bulk, these states are hcp crystalline solid, superfluid He II, and

vacuum (8).

The corresponding information on two-dimensional phases is still incomplete. The low temperature forms triangular crystalline solid, triangular ordered lattice gas, and a bose condensed fluid of uncertain order have been located. Several measured coverages do not show any peaks. Those at $1/\alpha = 8.03$ (9) and 8.24 atoms/nm^2 still have a shoulder in the heat capacity that could merely indicate a crossing of of the melting line at a small angle. Those with $1/\alpha < 1$ atom/nm^2 just represent smearing due to inhomogeneity--the actual low temperature phase here is patches of dense solid. This leaves the region $1/\alpha = 7.5 \pm 0.4$ atoms/nm^2 which simply has not been observed below 4.5 K and the homogeneous film with $1/\alpha < 1$ atom/nm^2 which cannot be observed on submonolayer Grafoil. The low temperature phase in these regions is unknown.

---

8. The gas at 28.75 atoms/nm^3 actually crosses 7 transition lines, including two triple "points"! (I/I+hcp/~~3~~/I+bcc/II+bcc/bcc/bcc+hcp/~~3~~/II+hcp/hcp).

9. Bretz et al 1973 list a coverage of 7.5 atoms/nm^2 for their Fig. 22. However, these same points are listed in their data tables as 12.451 Å^2/atom which is 8.03 atoms/nm^2.

CHAPTER 2

Experimental apparatus

The apparatus was originally designed for the study of thick films on sintered copper sponges. Some parts are superfluous for the current submonolayer experiments, but are described because they affect the data reduction. The essential features of the apparatus will be reviewed in chapter 5. A more systematically designed but generally similar apparatus has been used for critical point measurements (Kierstead 1971).

The major components of the calorimeter are shown in Fig. 10. The Grafoil comes in a nominally .015 inch thick sheet (10). Its weight of 0.0370 g/cm^2 is 43% as large as for the same volume of natural graphite. A sheet was cut into 55 disks, slits scored clear through with a razor blade and holes punched as shown actual size in the figure. The result weighed a total of 12.506 g. A sheet of 0.002" shim copper was cut and drilled as shown, into 27 disks weighing 5.32 g. The main body of the calorimeter was machined

---

10. 1 inch = 1" = 0.0254 m.

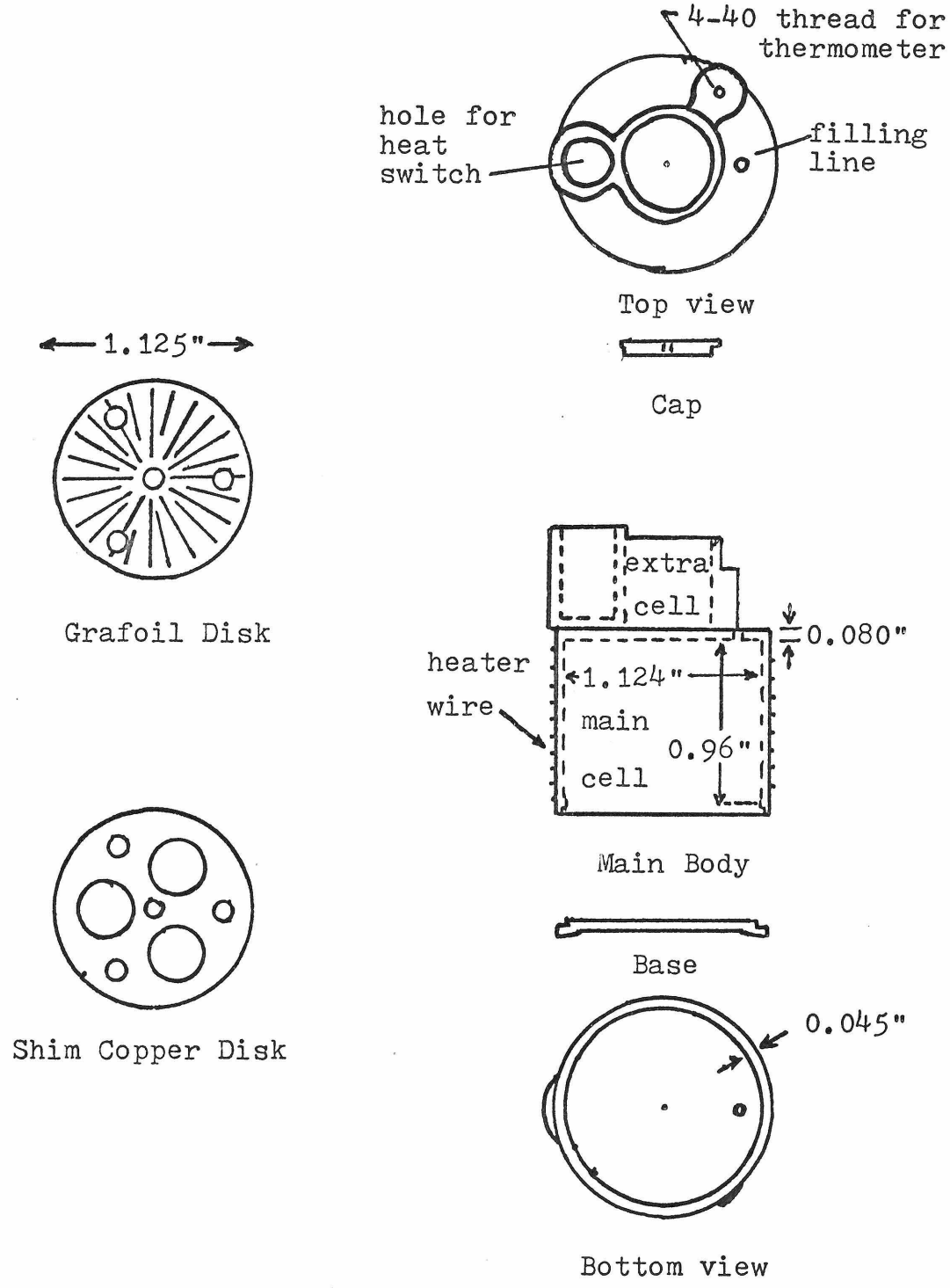

Figure 10 Calorimeter

as one piece from oxygen-free-high-conductivity copper. The base and cap were also made of this OFHC copper.

The Grafoil disks were baked for one hour at about 900°C while being pumped by a liquid-nitrogen-trapped forepump. They were interleaved with the shim copper and handpacked into the main cell with the holes carefully aligned. The base and cap were silver soldered by heating to 650°C in a hydrogen atmosphere. Upon cooling, the calorimeter was soft soldered to the cryostat, 73" of #40 Evanohm (11) heater wire varnished (12) on, and the thermometer (13) attached (14). The complete calorimeter consists of 14 g of Grafoil (partly in the extra cell), 64 g of copper, 3 g of other metals, and less than 0.2 g of other materials. Calculated from its dimensions, the internal volume of the main cell is 15.6 cm^3. Assuming the solid part of the Grafoil has the density of natural graphite (2.25 g/cm^3) and correcting for

---

11. Wilbur B. Driver Co. (Hust 1972).

12. Type 7031 varnish, General Electric Co.

13. Type 107 Germanium thermometer, Texas Instruments (Claiborne, Hardin, & Einspruch 1966).

14. The main cell accidentally leaked to one atmosphere of air during leak testing. After resoldering it was baked for 40 hours at 120°C while under high vacuum. The outgassing rate was then equal to only one monolayer in 500 years.

the shim copper leaves a free volume of 9.5 cm^3. Most of the Grafoil is under no external pressure since the main cell height is 9% larger than the nominal thickness of the Grafoil plus shim.

The calorimeter is suspended from two 1/16" i.d. x 75 cm long Cu-Ni filling lines (15) and a 1/4" i.d. monel tube housing a heat switch consisting of a movable copper cylinder in helium gas (Dash & Siegwarth 1963). A 2" i.d. x 5" long copper isolation can surrounds and extends 2" above the calorimeter. A 7/16" monel tube extends the isolation region to the top of the cryostat. Direct radiation down this tube is blocked by a copper disk held just below it and connected to the isolation can by brass screws. This disk also includes right angle turns in the filling lines and thermally grounds them about 0.5 K above the bath temperature. Six #30 Manganin wires (11) also feed down this tube and are thermally grounded to the isolation can. Two are shorted together for lead corrections, two connect to the heater, and two connect to two 6" #32 copper wires which are varnished (12) in a loop around the calorimeter before connecting to the thermometer.

The gas handling system uses 1/4" copper refrigerator

---

15. 30% Cu, remainder Ni, 0.003" walls, Superior Tube Company.

tubing and bellows valves (16) connected by soft solder. Two capacitive manometers (17) are built into the holding volume which connects the filling lines to the storage cylinders. The other sides of the manometers are connected to an ionization gauge (18) and a 1" copper pipe that leads past the isolation tube to a diffusion pump (19).

The thermometry system compares the germanium resistor to a standard resistance (20) by sending a 100 Hz signal (21) through a homemade Wheatstone bridge and a lock-in amplifier (22) (Wallace & Goodstein 1970) and records the results (23). A battery operated preamplifier (24) reduces the effects of noise in the lock-in power supply.

---

16. Model 4551Q4M Bellows Seal Valve, Hoke Inc.

17. Barocel type 538H-12 (1000 torr full scale) and 538H-11 (100 torr), Datametrics Division, ITE Imperial Corp.

18. Type IG 100P, Carl Herrmann Associates.

19. Speedivac Model E02, Edwards High Vacuum, Inc., using Santovac 5 oil, Monsanto Co.

20. Model 1432-M decade resistor, General Radio Co.

21. Model 200CD oscillator, Hewlett Packard Co.

22. Model RJB, Electronics, Missiles, & Communications, Inc.

23. Model 680 strip chart recorder, Hewlett Packard Co.

24. Transistor amplifier, Infrared Industries, Inc.

Two variable resistances (25) and a manual switch are used to adjust the power supply (26) that provides both the temperature regulation and the heat pulse for calorimetry. The voltages were checked periodically against a standard cell (27) and the drifts found to be negligible. The duration of the heat pulse was found automatically by an interlock with the switch (28).

---

25. Dekastat decade resistors, Models DS1464 & DS464, Electro Scientific Industries.

26. Model 855C programmable power supply, Harrison Laboratories.

27. Model 8687 Volt Potentiometer, Leeds & Northrup Co.

28. Model 1192 counter, General Radio Co.

Methods of data reduction

The coverage. The total helium in the system, N_o, was measured in units of 100 STP cm^3 (29) in the holding volume. The volume was compared by gas manometry to that of a large storage cylinder that had been calibrated by filling it with water. Flexure of the Barocel and valves within the holding volume caused its 18.50 cm^3 volume to increase by 0.4 mm^3 per torr. The temperature was measured by a mercury thermometer graduated to 0.1^oC and imbedded in a heavy aluminum plate to which all the valves were attached. The pressure was measured by the included Barocel. Its claimed accuracy was 0.05%. Calibration against a mercury manometer near $\frac{1}{2}$ atmosphere confirmed the calibration to the 0.1% accuracy to which the mercury manometer could be calibrated. The linearity of the Barocel was checked by a long series of comparisons of relative volumes in the system. Deviations greater than 0.2% were found on the highest scale, but all deviations were reproducible to 0.05%, so all reported data have been corrected by means of a deviation plot.

---

29. 100 STP cm^3 = 1/224.14 mol $\approx$ 10.3 atom/nm^2 $\approx$ 0.85 monolayer.

The absolute accuracy of N_o is limited to 0.2% by the accuracy of the volume calibration, but the reproducibility is limited only by the 0.05% reproducibility of the pressure measurement. The gas was assumed ideal since the pressure never exceeded 500 torr. So, with P in torr and t in ^oC, N_o is given by:

$$100\, N_o = \frac{P}{760}\,(18.50 + 0.0004\, P)/(1 + \frac{t}{273.1})\,.$$

The purity of the helium was insured by evaporating it from a liquid supply (30), passing it slowly through a liquid nitrogen cooled charcoal trap (Kidnay & Hiza 1970), and storing it in a stainless steel beaker with a heliarced top. At the end of the experiment (run D2) the cell was pumped for ½ hour at about 70 K, then sealed and warmed to 300 K. The remaining gas was equal to 20 ppm impurities in the original helium. This is consistent with the measured permeability of the Barocels during the 4 week run. However, the previous run (D1) gave over 1000 ppm impurities by the same test. This was traced to a leak in the solder connection to the storage beaker. Since it is probable that this air condensed in the filling line during the run, the values of N_o were corrected by subtracting 0.12% on all D1 points. This was

---

30. Gardner Cryogenics, Inc.

not completely adequate where the thermal transpiration was large. This probably indicates that the air adsorbed on the filling line changed the transpiration correction.

The temperature. The calorimeter temperature, T, was measured in kelvins by the germanium thermometer. The thermometer was calibrated against T_{58} (van Dijk, Durieux, Clement, & Logan 1960) from 1.5 K to 3.5 K using a saturated helium film in an earlier calorimeter. It was calibrated against a constant volume gas thermometer to an accuracy of 0.2% at a dozen points between 4 K and 25 K in a still earlier thermal transpiration experiment. Interpolation and smoothing was done using heat capacity measurements of a sintered copper sponge in a copper cell. The low temperature data fit well to the formula of Osborne (Osborne, Flotow, & Schreiner 1967) for 5.7 moles of copper if $0.4\,T + 0.055\,T^3$ mJ/K was assumed for the addenda. The scale above 4 K was defined so as to fit this formula. Small adjustments were later made where they improved the thermodynamic consistency of the data. This could be done with confidence because over 1000 items of data depend on only 14 different temperatures. T_{58} is generally agreed to be 0.2% low in the region used here (Cetas & Swenson 1972), and even with much

purer copper and negligible addenda, 0.3% variation in copper heat capacity measurements is common (Holste, Cetas, and Swenson 1972). The temperature scale defined here is believed to be within 0.2% of the true thermodynamic scale at all points. However, the derivative may be in error by 0.5%.

The temperatures used were planned to give 10% intervals, but the experimental definition was in terms of standard values for the resistance of the germanium thermometer plus its leads. These values were 477, 348, 263, 205, 164.5, 135.4, 113.7, 97.2, 84.2, 73.7, 65.1, 57.8, 51.5, and 46.1 Ω. About 13 Ω of this is actually the leads. In run D2 these corresponded to the temperatures 4.570, 5.004, 5.478, 5.999, 6.568, 7.188, 7.870, 8.614, 9.436, 10.34, 11.33, 12.42, 13.62, and 14.90 K respectively, as used in Appendix I. In run D1, the lead resistance was 0.13 Ω larger because of a loose aluminum nut. This meant the actual temperatures used in run D1 were 4.570, 5.004, 5.479, 6.000, 6.570, 7.191, 7.874, 8.619, 9.443, 10.349, 11.342, 12.435, 13.639, and 14.924 K respectively. All the pressure and chemical potential calculations used the temperatures corresponding to the same run as the data.

The pressure. The room temperature pressure, P_w, was measured in torr by the Barocels. The low pressure Barocel allowed readings down to 10^{-5} torr so the accuracy, after correction with the deviation plot and for background, was $\pm 2 \times 10^{-5}$ torr $\pm$ 0.05% (31). Below 11 torr, the pressure at the calorimeter, P, is significantly lower than at room temperature because of thermal transpiration. This must be accurately corrected for because otherwise there will be no overlap at all between heat capacity and pressure measurements (see Fig. 1). Over six months of experimental and literature research on this effect are summarized in Appendix II. The correction procedure adopted is based on empirical corrections to the formula of Weber and Schmidt (1937).

$$a = 4.64 \times 10^4 \, r \, P_w / T_w^{1.147}, \quad b = (1.12 \, T/T_w)^{-1.147}$$

where P is in torr and r is 0.078 cm. Solve for R:

$$\log R = -0.43592 \log b + 0.18131 \log \frac{R a b + 0.1878}{a + 0.1878}$$

$$+ 0.41284 \log \frac{R a b + 1.8311}{a + 1.8311} - 0.15823 \log \frac{R a b + 4.993}{a + 4.993}$$

---

31. A Barocel with ten times greater sensitivity is available, but the limit to accuracy at low pressures is set by the permeation of about 5×10^{-9} STP cm^3/sec of air in the Delrin lining of the Barocels. This caused a background value of 2×10^{-5} torr when the true helium pressure was zero.

Then solve for P:

$$\frac{1}{P_w - P} = \frac{1}{P_w - R P_w} - 3.1 + 0.38 \sin(1.14 \log(11 P_w)) .$$

When the pressure was greater than 3 torr, complete equilibrium within the cell and between the cell and the holding volume took less than 5 minutes. At the lowest measurable pressures, if the calorimeter remained isothermal as additional helium was added, equilibrium took days (Wallace & Goodstein 1970) because the gas would first condense at the mouth of the filling tube and only slowly redistribute. This problem was completely overcome by first raising the temperature until the equilibrium pressure was greater than 3 torr and holding for 5 minutes. The calorimeter was then allowed to cool slowly to the desired final temperature. Completely reproducible equilibrium was always obtained in less than 1 hour using this method.

Run D2 measured all the pressures and heat capacities reported for $N_o > 1.1$. It also measured the pressures for $N_o \approx .04$, .08, .12, .16, .2, .25, .3, .35, .4, .5, .6, .7, .8, .9, 1.0, and 1.1. The remaining heat capacities and pressures were taken in run D1. These were slightly less accurate because the pressure was not always raised above 3 torr after

increasing the coverage and also because of the impurities and lead problems noted above.

The heat capacity. The common technique of applying predetermined heat pulses to the calorimeter and extrapolating the drift rates to the middle of the heating periods (McCormick, Goodstein, & Dash 1968) could not be usefully applied to this system. First, the thermodynamic analysis required only the average heat capacity over 13 temperature intervals and the temperature scale was most accurately defined at the 14 end points of these intervals. So the sampling of the heat capacity over variable temperature intervals would not only require much more data, but would also lower the accuracy. Second, this system had unusually large heat leaks (32) and thermal equilibrium times (33) making conventional drift rate extrapolation inaccurate.

---

32. The heat leak commonly caused a 2% drop in the absolute temperature each minute. Reducing the leak through the filling lines would degrade the manometry but the leak could have been more than halved by lengthening the heat switch.

33. Most of the Grafoil, as well as all the rest of the calorimeter, relaxed with an exponential time constant of <5 seconds. However, about 3% of the Grafoil had a time constant ≈ 1 minute. This was believed to be caused by some tearing during preparation as well as by insufficient pressure between the Grafoil and the walls of the calorimeter.

If sample equilibrium times are long, conventional drift rate extrapolations fail because the sample is no longer near the temperature for which the heat leak is needed by the time the final drift rate can be measured. One solution is to invert the technique. Instead of setting the power input and observing the temperature rise, set the temperature rise and observe the power input. If the thermal conductivity of the calorimeter surface is large and the bath temperature is stable, then the heat leak will be completely independent of the sample. Therefore, subtracting the power input to the empty calorimeter from that to the calorimeter plus sample will correct for the heat leak as well as for the background.

The main drawback to using the inverted technique is the programming. Conventionally, one simply turns on a charge flow for a preset interval. Inverting, one needs to turn on a "temperature flow" for a preset interval. This requires an active temperature regulator interlocked with a ramp generator and a power integrator. Additional complications arise when one considers that the Wheatstone bridge is inaccurate and difficult to calibrate when far from its null position. It was finally found that the procedure could be simulated manually as follows: (i) The heater current was

adjusted until the calorimeter stabilized at the initial temperature. (ii) A larger current was switched on until the calorimeter was within 0.1% of the final temperature. (During the heating period the Wheatstone bridge balance point was shifted to this temperature.) (iii) The large current was switched off and a new small current switched on to stabilize nearly at the final temperature. (iv) Short pulses of the large current were added to compensate for backdrift due to the sample still being cooler than the calorimeter. (v) The heater current was adjusted at half minute intervals until the calorimeter stabilized at the final temperature. (vi) If all went well, the sequence was continued at step (ii) with a new final temperature. Otherwise, the heat switch was closed until the old initial temperature was reached and the process returned to step (i).

Due to the highly systematic method of taking the data, the heating currents could usually be accurately predicted in advance. Points were repeated if step (iii) was delayed by over 0.2 seconds because then the "temperature flow" was not sufficiently similar to the background data to ignore the heat leak. With this precaution, only 2 of the 548 points were clearly inconsistent with the surrounding data.

They are recorded in parentheses.

The heat capacity, C_o, was measured in units of (8.3143 J/mol)(mol/224.14)/K = 37.09 mJ/K for consistency with energy in kelvins and coverage in 100 STP cm^3. The main source of systematic error was a 0.2% uncertainty in the low temperature resistance of the heater wire. The precision is indicated by the comparison of two background calibrations. The 13 pairs of points differed by an average of 0.0014 (x 37.09 mJ/K). The heat leak during step (ii) above ranged up to 0.6 and the total heat capacity ranged up to 6.3. Week to week variations are believed to be about twice this large, mainly due to drifts in the thermometry circuits. The background heat capacity, C_b, for the standard intervals was 0.390, 0.471, 0.583, 0.728, 0.909, 1.138, 1.443, 1.825, 2.337, 2.973, 3.807, 4.879, and 6.310 respectively. For the data on the lattice gas ordering peak: $0.1 < C_b < 0.2$.

The true coverage. The calculation of the helium actually on the Grafoil surface, N, consists of a series of terms. The temperature distribution in the filling line can be approximated by assuming that 4 cm are at the temperature of the copper disk above the calorimeter and the rest are at room

temperature (34). The free volume of the cell as measured by gas expansion at 77 K is 9.6 cm^3 (35). Nonideality corrections are occasionally significant at the higher densities that occur at low temperatures (Grimsrud & Werntz 1967). The total volume at room temperature was 47 cm^3. Finally, at pressures above 11 torr, the 8 cm^3 volume containing the low pressure Barocel was sealed off. The resulting formula is

$$N = N_o - \left[\left(\frac{9.6}{T} \left[1 + \frac{P}{T} \left(\frac{0.0067}{T} - 0.00033 \right) \right] + \frac{0.08}{4.5} \right) P + \frac{39\,P_w + 8\,P'_w}{299} \right] \frac{273.15}{760 \times 100}$$

where P'_w is the last value of P_w that was <11 torr.

---

34. This separation was determined by holding the calorimeter temperature constant while varying the bath temperature. The isolation of the filling line from the bath greatly reduces its contribution to the gas correction and also makes the correction insensitive to the bath height.

35. This is accurate enough for the present data, but see refinements in footnote 36. It was not possible to separate the cell volume from the filling line volume when they were both at room temperature.

CHAPTER 3
Two-dimensional thermodynamics

"Thermodynamics is a collection of useful relations between quantities, every one of which is independently measurable. ... Thermodynamics is useful precisely because some quantities are easier to measure than others, and that is all." (McGlashan 1966) By this definition, thermodynamics is a dynamic field, for new quantities become measurable with every scientific advance. In particular, the unique reproducibility of the helium-Grafoil system allows more detailed comparisons and therefore requires more careful formulations than heretofore.

The system is not well defined thermodynamically until after assembly in the cryostat. The only measurable quantities are then the quantity of helium added, the quantity of heat added, the pressure, and the temperature. The only combinations of these that can be measured in practice are, the changes in pressure on adding helium at constant temperature (adsorption isotherm), the changes in temperature on adding heat without adding helium (total heat capacity), and the changes in temperature on adding helium without

adding heat (heat of adsorption ÷ total heat capacity). The latter cannot be measured accurately on the current apparatus because the filling line is in poor contact with the bath so as to reduce the nonfilm gas correction. It will be shown below that it is redundant anyway.

The purpose of the thermodynamic relations is to generate other combinations that are more useful. In particular, we are not interested in the bulk properties of the Grafoil and helium separately, but only in the film that forms at their interface. The formulation in terms of surface excesses is ideally suitable for this purpose. The bulk contribution from the Grafoil and body of the calorimeter is well defined experimentally; just measure the heat capacity before adding any helium. The bulk contribution from the helium is given by a comparison system having the same pressure, temperature, and free volume, but negligible surface area. In practice, this comparison system is seldom built, because one trusts statistical mechanics and the virial equation of state for low pressure gases in the bulk. However, "free volume" has been defined in several ways. It will be defined here as the entire volume accessible to helium in any form. This may be measured by turning off the adsorption forces, namely, by raising the temperature

until the adsorption becomes negligible (36).

The thermodynamic analysis follows the terminology

---

36. Discussion of this atypical definition follows, ad nauseam.

E. Guggenheim claims that the only well defined free volume is the geometric volume of the cell without the adsorbent (Guggenheim 1967). He was considering adsorption isotherms measured by weighing on a fine balance. By his definition the coverage is merely equal to the weight change on adding the gas. However, even for his case, this paper's definition can be used. The coverage comes out as the weight loss on heating to high temperature at constant gas density. This avoids the negative coverages that will otherwise result at high temperatures.

Terrell Hill (1949) chooses the free volume to be the volume accessible to unadsorbed helium only, claiming this is needed to give a realistic transition to the bulk liquid state. This is inconsistent since the volume of the thin film is undefinable unless one makes the unrealistic assumption that the bulk liquid is incompressible. This is also poorly defined and physically misleading above the critical point, for there the film does not have a surface even in principle, but still exists to multilayers (Ross & Steele 1961).

Actually, below the critical point, the limit of infinite coverage is the bulk liquid at saturation. This paper's definition describes this in an unconventional but very useful manner. Only the density in excess of the vapor density is ascribed to the liquid "film." This is the density term that actually appears in equations for gravity waves, third sound, critical exponents, etc. Above the critical point, in fact for any temperature and pressure that does not destroy the calorimeter, this method is well defined and leads to nonnegative coverages.

William Steele makes the interesting point that this paper's free volume depends on the gas species even in the limit of high temperatures, because the volume within one molecular radius of the walls is not accessible (Steele 1967). It would seem best not to "correct" for this effect because the "radius" is poorly defined and the resulting coverage could become negative.

of Landau and Lifshitz (1958) with modifications to better match the recommendations of the IUPAC (McGlashan 1970). The independent variables are taken as the chemical potential, μ, and the temperature, T, because these are identical in all phases (Widom 1969). The subscript '$_o$' is used for extensive variables referring to all the helium in the experimental system. The subscript '$_g$' is used for extensive variables referring to all the helium in the comparison system. The surface excesses, defined as the differences between the above, are not subscripted. The constants, A and V, and the intensive variables, μ, T, P, ϕ, v, α, B, and e, do not need to be distinguished by subscripts.

Starting with the internal energy, U_g, of the comparison system, we may define in the usual way, the Gibbs' free energy,

$$G_g = U_g - T S_g + PV \qquad [1a]$$

and the Landau potential,

$$\Omega_g = U_g - T S_g - \mu N_g \qquad [1b]$$

so that:

$$dU_g = T\,dS_g - P\,dV + \mu\,dN_g \qquad [2a]$$

$$dG_g = -S_g\,dT + V\,dP + \mu\,dN_g \qquad [2b]$$

$$d\Omega_g = -S_g\,dT - P\,dV - N_g\,d\mu\,. \qquad [2c]$$

Since P depends only on μ and T, we may integrate [2c] at constant μ and T to get,

$$\Omega_g = - P V . \qquad [3]$$

If we now specialize to constant volume, we may drop dV and replace $V\,dP$ with $- d\Omega_g$ so [2] simplifies to:

$$dU_g = T\,dS_g + \mu\,dN_g \qquad [4a]$$

$$dG_g = - S_g\,dT - d\Omega_g + \mu\,dN_g \qquad [4b]$$

$$d\Omega_g = - S_g\,dT - N_g\,d\mu . \qquad [4c]$$

Also, from [1] and [3] we get

$$G_g = \mu N_g . \qquad [4d]$$

Although we assumed a particular form for the external work in the derivation, it has now been subsumed by the Landau potential. So equations [4] apply to any system on which no external work is done. In particular, by replacing every '$_g$' in [4] by '$_o$' we generate 4 more equations (to be referred to as [5]), and dropping all subscripts gives another set of 4 [6].

The experimental data may be converted into a complete thermodynamic description of the film as follows: From pressure isotherms at high temperature we may calculate $\mu(N_o)$ at constant T, using the formula from statistical mechanics (Landau & Lifshitz 1958),

$$\mu = k\,T \log\left[\frac{P}{k\,T}\left(\frac{2\,\pi\hbar^2}{m\,k\,T}\right)^{3/2}\right] + B\,P\,.$$

Explicitly, for ^{4}He with P in torr and μ in kelvins (37),

$$\mu = T \log(0.006419\,P/T^{2.5}) + (0.00033 - 0.0067/T)P\,.$$

We then find Ω_o by integrating [5c] to get the Gibbs-Bangham equation (Hill 1949):

$$\Omega_o = -\int_{N_o=0}^{N_o} N_o\,d\mu\,.$$

Using [5b] and [5d] we find the entropy at a temperature midway between two isotherms by

$$S_o = -\left(\partial\Omega_o/\partial T\right)_{N_o} - N_o\left(\partial\mu/\partial T\right)_{N_o}\,.$$

From the gross heat capacity of the calorimeter, we may find $C_o = \left(\partial U_o/\partial T\right)_{N_o}$ by subtracting the calorimeter background, C_b, which is the gross heat capacity when $N_o = 0$. We then have from [5a] that

$$C_o = T\left(\partial S_o/\partial T\right)_{N_o}\,. \qquad [7]$$

---

37. In both two and three dimensions one may find all thermodynamic functions by measuring the variations along a path connecting to the dilute three-dimensional gas. In three dimensions, one must do work to create the dense phases, so the compressibility is easily measured, but the chemical potential requires an integration. In two dimensions, on a solid surface, the chemical potential may be found directly from the co-existent bulk gas, but one cannot do work, so the compressibility must be found by differentiation. This is why the Landau Potential is more natural than the internal energy in two dimensions.

So the entropy at the upper (+) and lower (-) isotherm is

$$S_o = -(\partial\Omega_o/\partial T)_{N_o} - N_o(\partial\mu/\partial T)_{N_o} \pm \tfrac{1}{2} C_o \Delta T/\overline{T}.$$

Thus we can find the function Ω_o, its proper variables T and μ, and its proper first derivatives $-S_o$ and $-N_o$, at each experimental point on a rectangular N_o, T grid. We may extend S_o to lower temperatures, where the pressure is unmeasurably small at low coverage, by integrating [7]. Taking derivatives of $(G_o + \Omega_o)$ with respect to T and N_o in either order and using [5b] gives the Maxwell Relation:

$$(\partial\mu/\partial T)_{N_o} = -(\partial S_o/\partial N)_T \qquad [8]$$

which allows us to calculate the chemical potential at lower temperatures, given the entropies at adjacent coverages. Then, using [5c] we may extend Ω_o along an isostere. Finally, if it is possible to obtain heat capacity data to low enough temperatures to integrate S_o accurately from absolute zero, the accuracy of the entire analysis increases by an order of magnitude because both proper derivatives of Ω_o are then found by integrations rather than by differentiation. The accuracy at high coverage is also improved if the integration of Ω_o is carried out along a series of isotherm and isostere segments such that N_g is

always small along the isostere segments.

One simply subtracts Ω_g, N_g, and S_g from Ω_o, N_o, and S_o to find Ω, N, and S respectively. For the current case where the comparison system is a dilute gas,

$$N_g = P V(1 - P B/(k T))/(k T) \qquad [9a]$$

$$S_g = 2.5 N_g k + N_g k \log \left[\frac{V}{N_g}\left(\frac{m k T}{2 \pi \hbar^2}\right)^{3/2}\right] - \frac{N_g^2 k}{V}\left(B + T\frac{dB}{dT}\right). \qquad [9b]$$

Given T, N, μ, S, and Ω, the other energy functions follow immediately (38):

Internal energy	$U = \Omega + T S + \mu N$	[10a]
(Helmholtz) free energy	$A = \Omega + \mu N$	[10b]
Gibbs' (free) energy	$G = \mu N$	[10c]
Enthalpy	$H = T S + \mu N$.	[10d]

Other quantities of interest in adsorption studies--the calorimetric (differential) heat of adsorption, q_d, the isosteric heat of adsorption, q_{st}, and the heat capacity at constant spreading pressure, C_ϕ,--will be derived below.

An implicit definition of q_d is given (Steele 1970) by

$$C_o = C + C_g - q_d(\partial N/\partial T)_{N_o}.$$

---

38. Except for [10b], A is always used for area in this paper.

This may be evaluated by considering U as a function of N and T, with N_o, A, and V fixed. Then, with

$$e = U_g/N_g \approx 1.5\,k\,T - N_g\,k\,T(dB/dT)/V$$

$$dU_o = dU + dU_g = (\partial U/\partial N)_T dN + (\partial U/\partial T)_N dT - (\partial U_g/\partial N_g)_T dN + (\partial U_g/\partial T)_{N_g} dT$$

$$(\partial U_g/\partial N_g)_T = e + N_g(\partial e/\partial N_g)_T$$

From [10a] and [5c],

$$(\partial U/\partial N)_T = -N(\partial\mu/\partial N)_T + T(\partial S/\partial N)_T + N(\partial\mu/\partial N)_T + \mu\ .$$

So $q_d = e + (\partial e/\partial \log N_g)_T + T(\partial\mu/\partial T)_N - \mu\ .$

Following Hill (1949), we take the isosteric heat to be defined in direct analogy to the Clausius-Clapeyron equation:

$$(\partial P/\partial T)_N = N_g\,q_{st}/(T\,V)\ .$$

The usual correction for the film volume is zero in this formulation. Using [9a], we get

$$q_{st} = -\left.\frac{\partial(\log P)}{\partial(1/k\,T)}\right|_N (1 + \frac{P\,B}{k\,T})\ .$$

This shows the manner in which q_{st} is usually derived from adsorption isotherms. Alternatively, we may put the constant V inside the partial derivative and then use [3], [4c], and [8] to get Hill's other definition,

$$q_{st} = T S_g/N_g - T(\partial S/\partial N)_T .$$

Using the dilute gas formulae given previously, and [8], we may evaluate these heats of adsorption in terms of the tabulated functions plus a small virial correction:

$$q_{st} = 2.5\, k\, T + T(\partial\mu/\partial T)_N - \mu + N_g\, k\, T(B - T\, dB/dT)/V$$

$$q_d = 1.5 k\, T + T(\partial\mu/\partial T)_N - \mu - 2\, N_g\, k\, T^2(dB/dT)/V .$$

C_ϕ can be calculated only after explicitly allowing the area to vary, since $T = T(N, A, \phi)$. Define generalized functions: $\Omega^* = A\,\Omega$, $S^* = A\,S$, $N^* = A\,N$, and $C^* = A\,C$ for a cell A times larger than the experimental cell (assumed to have unit area). Since, by analogy to P, we define ϕ by $\Omega^* = -\phi A$, it follows that $\phi = -\Omega$. So $d\phi = 0$ is equivalent to

$$d\Omega = 0 = (\partial\Omega/\partial N)_T dN + (\partial\Omega/\partial T)_N dT \quad \text{or}$$

$$(\partial N/\partial T)_\phi = -(\partial\Omega/\partial T)_N/(\partial\Omega/\partial N)_T .$$

Taking S as a function of N and T, and holding N^* constant so that A is a function only of N, gives

$$dS^* = A(\partial S/\partial T)_N dT + (S\, dA/dN + A(\partial S/\partial N)_T)dN$$

$$C_\phi^* = A\, C_A - T(-S\, A/N + A(\partial S/\partial N)_T)(\partial\Omega/\partial T)_N/(\partial\Omega/\partial N)_T$$

$$C_\phi = C + T(S/N - (\partial S/\partial N)_T)(\partial\Omega/\partial T)_N/(\partial\Omega/\partial N)_T .$$

Tabulation of results

The main experimental data from this project are tabulated in the left hand columns of Table I of Appendix I. It lists the room-temperature pressure, P_w, the total helium heat capacity, C_o, the pressure at the cell, P, and the true coverage, N, as a function of the total helium in the system, N_o, and the cell temperature, T, over the range $0.01 < N_o < 2.5$ and $4.57 < T < 14.9$ K. C_o covers the temperature interval between the given temperature and that on the preceding page of the Table. All other entries (including C) refer to the given temperature. These data were taken using cell D and are a composite of the two runs D1 and D2 as explained in chapter 2.

The next step should be to follow the analysis just presented to find Ω_o and S_o and then all the film properties. However, the use of a manometer at room temperature introduces a second major problem in addition to the need to apply a thermal transpiration correction at low pressures. Its use causes approximately 10% of the unadsorbed gas to be external to the calorimeter. This makes it impossible to retain the ability to measure derivatives experimentally without interpo-

lation. In outline, the procedure remains the same, but the film properties must be calculated directly using q_d to correct the heat capacity, rather than waiting until the final step to subtract the comparison system.

Part of the derived results could be found immediately. For $P > 0.001$ torr, μ was found using the formula on page 47 and interpolated to even values of N (39). For $P < 0.001$ torr, C was given by the average value of C_o from the same and following page of the Table. For $P > 0.001$ torr but $N_g < 0.001$, desorption corrections were first applied to C_o using the formulae on pages 49 and 50, before calculating C. The limits to the regions where these methods were applied are shown by short horizontal bars in the Table.

The remainder of the μ and C columns and all the S and Ω values are dependent on more than two items of input data. The value of Ω at $N = 0.01$ and $T = 14.90$ was determined from an earlier survey using cell C. $\int N \, d\mu$ from $N = 0.001$ to 0.01 gave 0.33. As the integral is approximately proportional to N, the extension to $N = 0$ can be expected to give

---

39. The central column in Table I has two purposes. The values of N_o for the experimental data on the left are given as entered. The values of N for the derived results on the right are given by these same entries rounded to the nearest 0.01.

0.36 ± 0.02. Similarly, the value of S at $N = 0.01$ and $T = 14.90$ K was found to be 0.045 ± 0.005 (40).

The reduction procedure given in the thermodynamics section was then followed as given except all the '$_o$' subscripts were dropped and interpolation was used where needed to give isosteric data. This gave all the remaining results shown. The blank areas at the highest coverages are outside the range of the experimental data.

The use of experimental units in the construction of Table I should not detract from its utility. N can be considered a molar quantity by the simple expedient of redefining the size of the substrate. For a substrate made of $(12.506\ g)(224.14) = 2.80$ kg of Grafoil identical to the current sample; N_o, N, C_o, C, and S will be in moles, μ in kelvins, and Ω in kelvin-moles. P_w and P remain in torr. Any other units for energy may easily be inserted by multiplying by the gas constant, R. For S.I. units (McGlashan 1970), $R = 8.3143\ J\ K^{-1}mol^{-1}$ and 760 torr $= 101325$ Pa $= 101325\ N\ m^{-2}$.

The substrate area, unlike the quantities given

---

40. For historical reasons, this is <u>not</u> the value that was used in compiling Table I. However, the uncertainty in integrating S from $N = 0.01$ to $N = 0.10$ is comparable to the 0.01 discrepancy introduced here. So the tabulated low coverage entropy values are probably high, but the other coverages are merely uncertain by ± 0.01.

in Table I, is not measurable in a model-independent manner. However, for convenience in comparison with other experiments, one assumes perfect homogeneity at the lattice gas ordering transition. The ordering occurs at $N = 0.6565 \pm 0.001$, so the total area is $A = 15.3$ acres for molar units or $A = 277$ m^2 for the actual cell D. This makes the coverage $1/\alpha = (N/0.6565) \times (6.366 \text{ atoms/nm}^2) = 9.70\,N \text{ atoms/nm}^2$. Then the spreading pressure, ϕ, is found in dyne/cm by multiplying the tabulated value of Ω by 0.134. For example $\Omega = 2.8$ at the 0 K bulk surface tension of 0.37 dyne/cm.

Table II in Appendix I shows the heat capacity data taken during run D1 to locate the lattice gas ordering transition. The pressure was far too low to be measured directly (see Fig. 1). The derived functions shown in the Table follow directly using the thermodynamics section and starting with S and Ω at 4.57 K as given in Table I: S follows from inverting [7], then μ is found using [8], and then Ω is found using [5c].

The early data taken with cell C are shown in Table III in Appendix I. This cell had an 8% smaller surface area as measured by the lattice gas ordering transition and the melting line. The coverage has been measured in units of 92 STP cm^3 and the heat

capacity scaled accordingly, in order to make the data consistent with Tables I and II. The data points on this run are too sparse to support an accurate, point by point thermodynamic analysis.

An argon isotherm at 63.5 K was also taken on cell C. The temperature regulation was poor in this region, but sharp steps were still seen--see Fig. 11. Note that the pressure at points below a monolayer has been multiplied by 1000. If we analyze multilayer formation in the same manner as was done for helium on page 12, we get a first layer compressed 10% by a pressure of ≈6000 atmospheres. Then scaling areas to volumes as described in footnote 6, and taking the substrate area determined by the lattice gas ordering transistion, gives the layer capacities listed. The agreement appears good, except that even numbered layers have much sharper steps.

The only other thin film data on Grafoil in this laboratory was taken by Stewart, Siegel, & Goodstein (1973) using a residual gas analyzer (RGA). Their extended 4.2 K isotherm is compared with data at 4.57 and 5.00 K from Table I, in Fig. 12. It is interesting to find that their "direct" measurements using the RGA, an ionization gauge, and a thermocouple tend to show more uncertainty than the

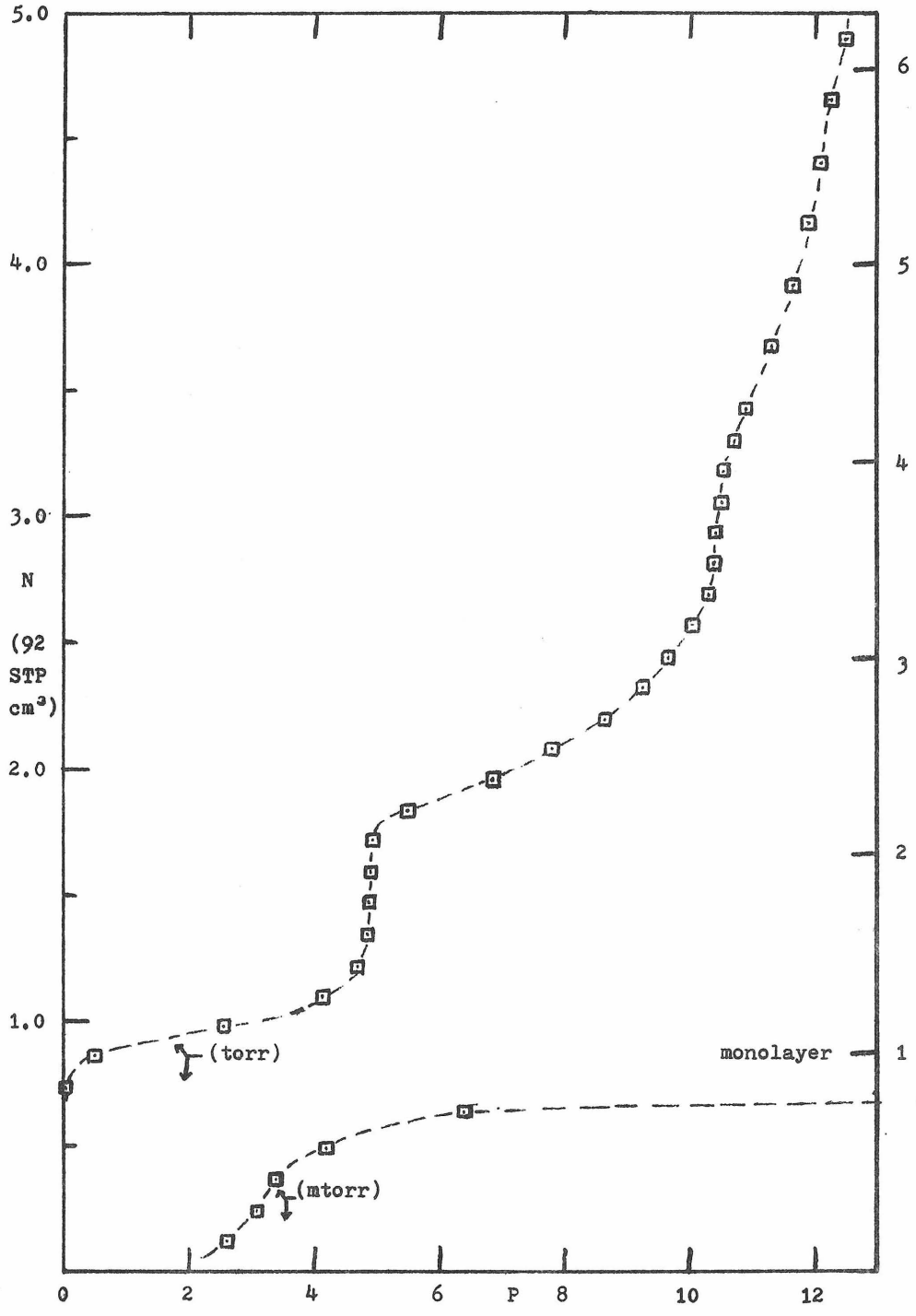

Figure 11 Argon Isotherm at 63.5 K

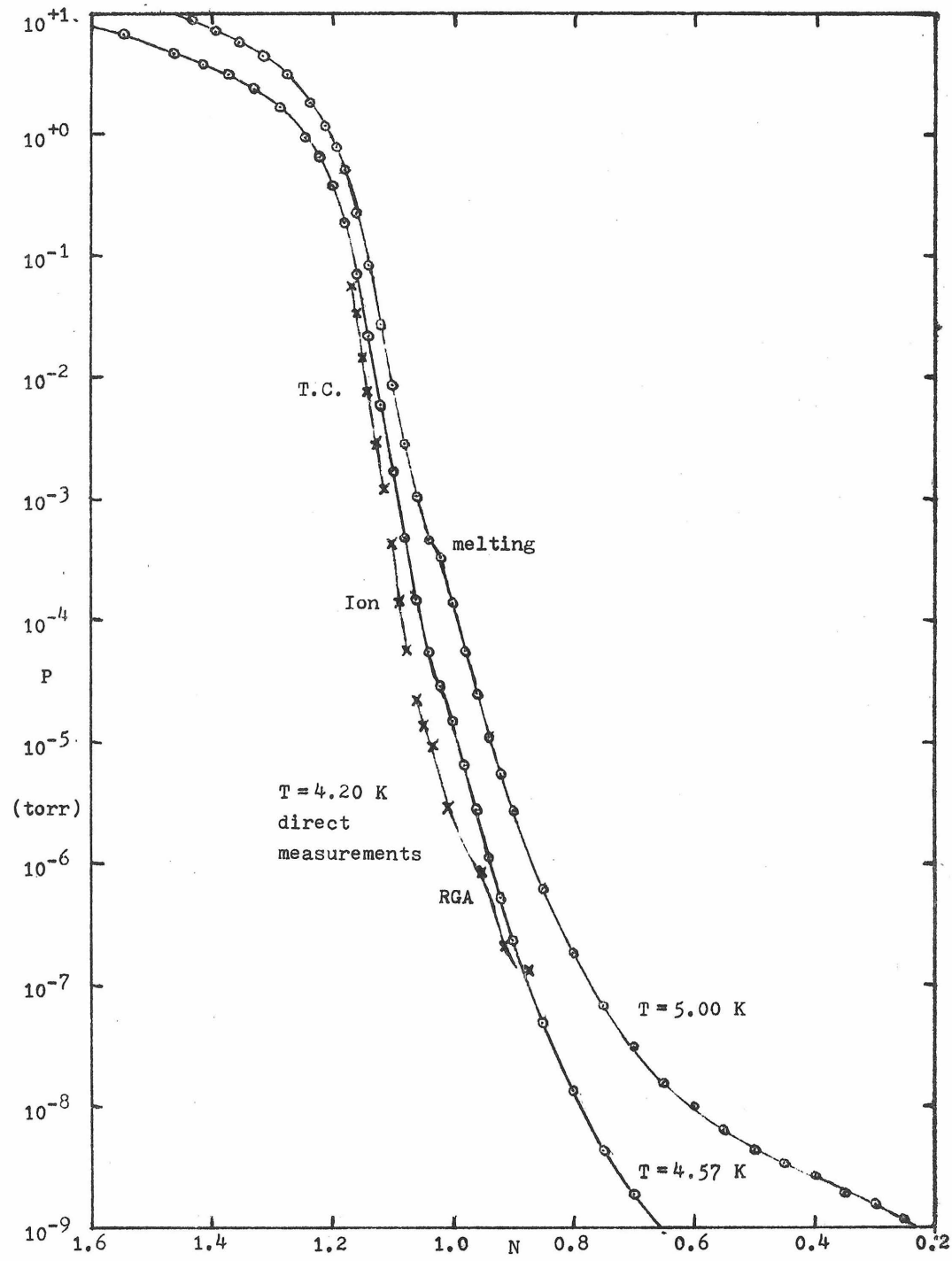

Figure 12 Direct and Indirect Pressures

indirect values calculated from the heat capacity.

A major purpose of this project was to find the chemical potential near the low temperature phase transitions, where direct pressure measurements are impossible. The data reported here are not sufficient for this task. It was shown in chapter 1 that in nearly all cases where these data overlap those taken at the University of Washington (Bretz et al 1973) there is good agreement. Therefore it was possible to carry out the low temperature analysis using the combined data sets. The derivatives using the combined data are less accurate, but they all go to zero at 0 K, so the resulting thermodynamic functions are only slightly less accurate than the higher temperature results from which they are derived. They are given in Table IV of Appendix I.

CHAPTER 4

Subsystem identification

The central problem under investigation is the behavior of simple atoms constrained to move in two dimensions at finite density but otherwise free of external force fields. Only a fraction of the helium in the adsorption cell is even approximately in such a system. The preliminary problem is therefore to identify the contributions of the atoms that are not in this system.

The helium may undergo four different types of motion normal to the graphite planes: uniform, accelerated, oscillatory, and stationary. The helium in uniform motion is just bulk gas. This contribution has already been subtracted off during the data reduction. The helium undergoing acceleration is a more compressed gas. Only part of this has already been accounted for. The oscillating helium is in an excited surface state. It contributes an extra term to the energy, but is still physically located in the first layer (Hagen, Novaco, & Milford 1972). The stationary helium may be in more than one layer, in which case the components

may form two separate two-dimensional systems.

The helium in the first layer is still subject to residual fields. The periodic field due to the crystalline nature of the graphite is negligible except in the region of lattice gas ordering (Hagen, Novaco, & Milford 1972). However, the field energy can double near the regions where two graphite surfaces come into contact. Lattice defects, impurities, and isolated edges seem to be negligible compared to the effects of these contact regions.

The interaction energy between the helium atoms and the substrate is different for each of these modes of behavior. In the bulk gas, it is zero. In the compressed gas region, it varies as the inverse cube of the elevation. It never has a measurable effect on the low pressure data collected here. At coverages where the periodic field is important, it greatly modifies the behavior of the entire film. Because of this collective effect, the energy of interaction with a single atom is neither measurable nor needed. The remaining energies are found below.

The energy of the first excited state, E_1, may be found at intermediate coverages and high temperatures. The number of excited atoms relative to unexcited ones is just given by the Boltzmann factor,

$\exp(-E_1/T)$, so the additional energy per atom is $E_1/(1+\exp(E_1/T))$. Taking the temperature derivative gives $C/N = (\frac{1}{2}E_1/T)^2 \mathrm{sech}^2(\frac{1}{2}E_1/T)$. This is shown added to the two-dimensional ideal gas value $C/N = 1$ in Fig 13. Data points are taken from Table I for $N = 0.4$, 0.5, 0.6, and 0.7 and corrected for the effects of the second virial coefficient (Siddon & Schick 1973). These coverages correspond to bulk densities between that of the critical point and the liquid, so the small remaining discrepancy at low temperatures is not surprising. Ignoring this slight offset, the data clearly fall within the range $E_1 = 55 \pm 3$ K.

The energy of the ground state may be found at intermediate coverages (41) and low temperatures. The ground state calculations of Miller, Woo, and Campbell (1972), give μ within 1 K of the binding energy for $N < 0.5$ and $T = 0$. If we assume that the inhomogeneous region can hold no more than 10% of the monolayer capacity, we find the binding energy as given by the upper band in Fig. 14, using Table IV. Alternatively, if we use the ideal gas law and

---

41. There is a common misconception that an extrapolation to zero coverage will give the binding energy. This will actually give the binding energy of the least typical sites since they strongly bind the first few atoms.

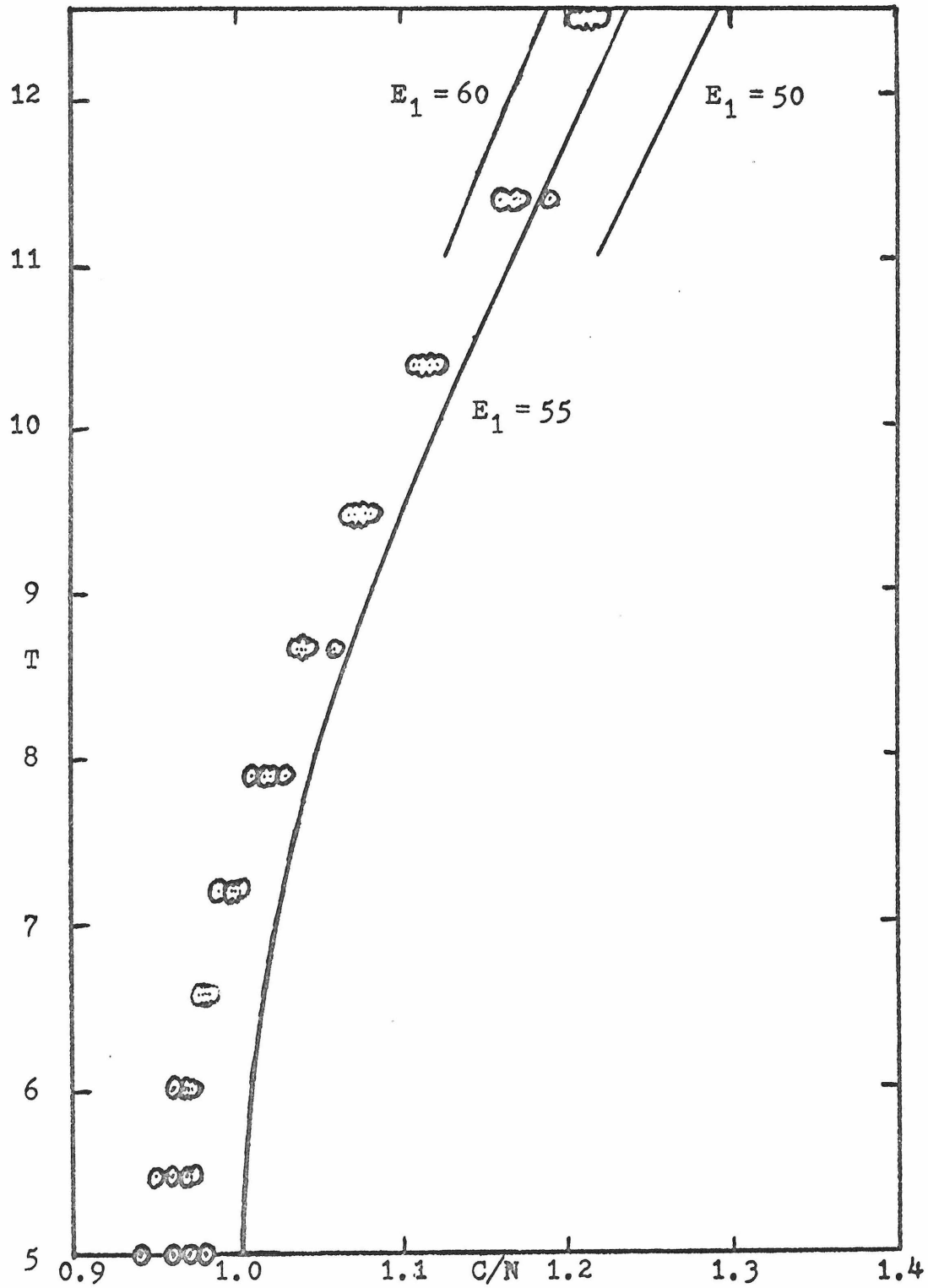

Figure 13 Excited State Energy

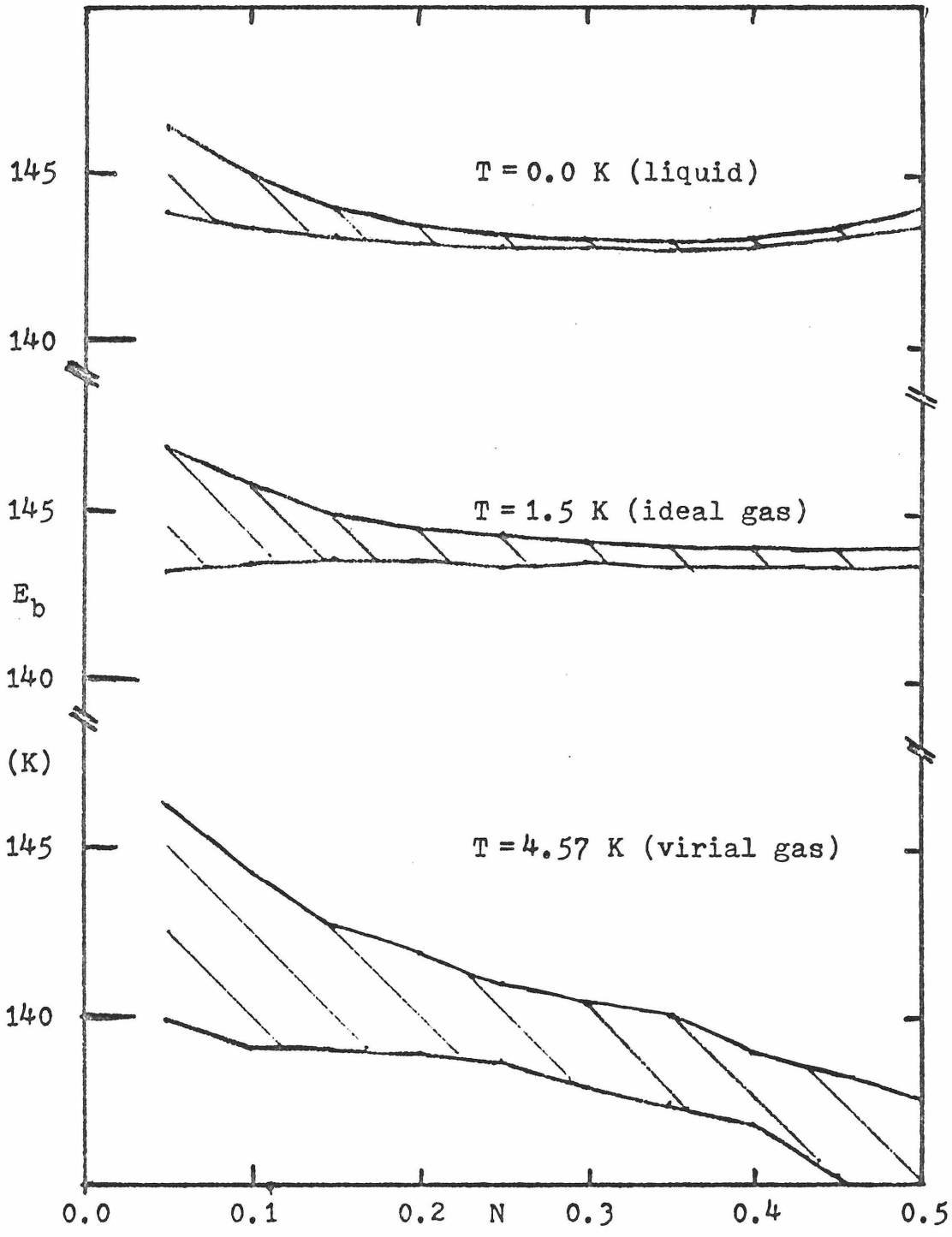

Figure 14 Binding Energy Estimates

the 1.5 K data of Table IV, we get the middle band in Fig. 14. Neither of these models is particularly realistic, but the chemical potential is insensitive to such details near 0 K. Higher temperature data give a poorer fit, as shown by the bottom band. This was calculated using the 4.57 K data of Table I and assuming a virial gas (Siddon & Schick 1973). The low temperature estimates agree within 1 K, but allowing for possible systematic errors in the calculation of Table IV, we get $E_b = 143 \pm 2$ K.

The energy binding the second layer on a complete first layer is outside the range of Table IV. Instead we must use Table I at 4.57 K and assume a virial gas again. Adjusting the monolayer capacity to $N = 1.16$, in reasonable agreement with Fig. 1, all the μ points with $N > 1.18$ fit $E_{b2} = 29 \pm 1.2$ K.

If the variation in binding energy is due to contact at small angles between large flat sheets, then the variation of the excess binding energy in the direction normal to the line of contact is proportional to the variation of the total binding energy in the direction normal to the surface. But this latter function is just the van der Waals' attraction energy, so the only adjustable factor is the average

constant of proportionality. If the adsorption sites are ordered according to their energy and a fraction θ_1 of the sites are within one atomic layer of the second sheet, then the total binding energy is $E = E_b + E_b/(1 + \theta/\theta_1)^3$, $0 < \theta < 1$. This is compared with the values for $-\mu$ at 0 K from Table IV in Fig. 15. μ should approximately equal the binding energy at 0 K because all the other contributions to μ are small. θ_1 was taken to correspond to $N = 0.026$ for the fit shown (42). The binding energy variation is more commonly given by the distribution function: $f(E)\,dE = d\theta$. This follows immediately by differentiation:

$$f(E) = \tfrac{1}{3}\,\theta_1\,E_b^{1/3}(E - E_b)^{-4/3}, \quad E_b(1 + \theta_1^3) < E < 2\,E_b$$

$$\approx 0.045\,(E - 143)^{-4/3}, \quad 143.0025 < E < 286.$$

Although most discussion in the literature concentrates on the strictly two-dimensional system, estimates have been given for the energies just described. The effects of the excited states on the heat capacity were first calculated by H. W. Jackson (1969) for a noble-gas covered copper substrate.

---

42. This does not completely determine θ_1 because the size of an adsorption site depends on the two-dimensional pressure. For the lowest coverage data $E - E_b \approx 50$ K and at $N \approx 1$, $\mu + E_b \approx 50$ K, so $N \approx \theta$.

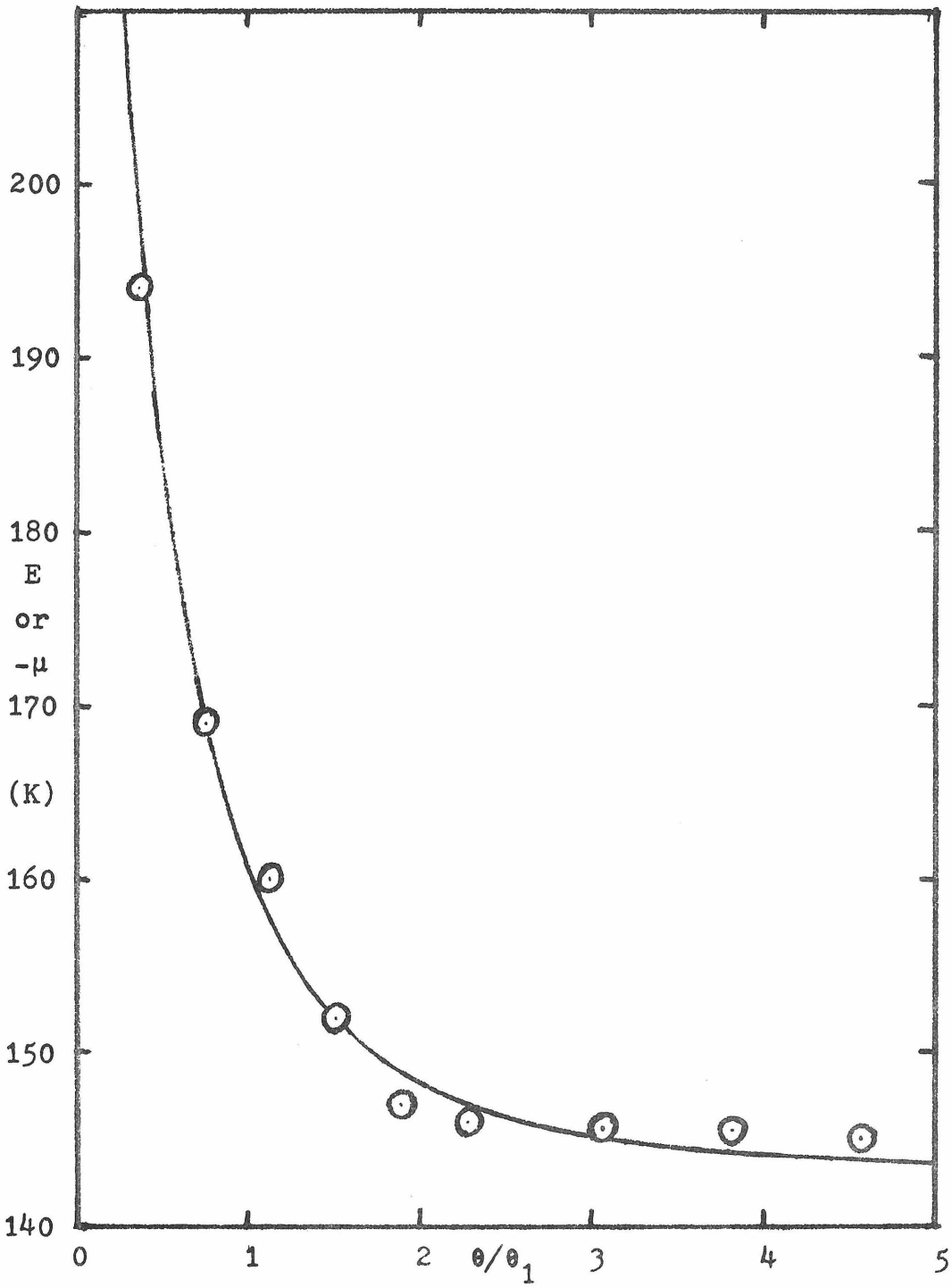

Figure 15 Binding Energy Distribution

The first calculation for a graphite was $E_1 = 80$ to 85 K by Hagen, Novaco, and Milford (1972). They also found the ground state energy to be $E_b = 188.8$ K. The second layer binding energy was calculated by Campbell, Milford, Novaco, and Schick (1972) to be $E_{b2} = 30$ K.

All of these are higher than the experimental values. The most likely cause of the discrepancy is the helium-carbon potential. Novaco (1973) has noted that the rules used for finding the hybrid Lennard-Jones potential between dissimilar atoms have proved inaccurate before. His solution was to reduce the energy parameter in this potential until he fit the experimental value of E_b. Using the WKB approximation it was found that a 20% reduction in this parameter gave the 25% reduction needed in E_b. However, this still left E_1 15% too large. The obvious next step is to adjust the length parameter in the potential until both experimental values are reproduced, but this leaves nothing dependent on the theory! It appears that the helium-graphite potential cannot yet be calculated from first principles.

The distribution functions suggested for Grafoil have been quasi-Gaussian (Novaco 1972) or constant (Campbell, Dash, & Schick 1971) with a maximum energy

variation of order 1 K. This differs by two orders of magnitude from the 143 K estimate given here! However, the models are much closer than this indicates. The central 90% of the sites have an energy spread between 0.5 and 1.0 K in all three models. The literature models were both invented to explain heat capacity data at $T \approx 1$ K and $N > 0.2$. Under these conditions the most energetic sites are covered by a dense solid with negligible heat capacity. At lower coverages the effects are pronounced, as shown in the following model.

Model generation

The simplest interpolation formula between dilute gas and liquid behavior is given by van der Waals (Landau & Lifshitz 1958). This equation is combined with substrate inhomogeneity in the Ross-Oliver model (Ross 1967). Its only assumption in addition to this equation of state and the energy distribution formula is that the substrate energy variation is smooth rather than random. One calculates a state point for the whole system by setting the overall temperature and chemical potential and summing the coverage and entropy at each value of the binding energy. This is usually a four parameter model. However, the two van der Waals' constants may be found from the theoretical high temperature virial coefficient of Siddon and Schick (1973). They are $1/b = 11.51$ atom/nm^2 and $1/a = 1.792$ atom/(nm^2 K) . The energy distribution has also been evaluated independently of this model (43). The resulting heat capacity curves were shown in Fig. 9.

The heat capacity calculations cannot be extended

---

43. θ_1 was set at 0.02 for Fig. 9. The larger estimate given previously would probably make the fit better.

to lower temperatures because one runs into a two-phase region below 1.903 K. While something peculiar does occur in the experimental data in this region, it is certainly not classical condensation to a van der Waals' liquid. It is surprizing that the theory works so well at higher temperatures, for the van der Waals' equation of state gives a very poor representation of the solid phase that must exist on the most energetic sites. A better model will be derived later, but first we must determine the behavior of the solid phase.

It can be seen in Fig. 4 that the high coverage region exhibits a wide range of behavior. There are both constant and T^2 heat capacities at low temperatures, small peaks at intermediate temperatures, and sharp peaks on high plateaus at high temperatures. Figures 1 and 3 show that this region includes multilayer formation and large desorption corrections. We may apply the same general techniques to disentangle these effects as we used to study the combination of a gas and an inhomogeneous substrate.

In this case, rather than a continuum of binding sites, we have only three subsystems: the first layer, the second layer, and the bulk gas (44). The equations

---

44. The continuum of binding sites still exists but may be ignored in first approximation. In the

for the bulk gas have been given previously. The second layer is dilute in the region of interest, so a two-dimensional ideal gas with its chemical potential lowered by the amount E_{b2} will be sufficient. In principle, for a given experimental μ and T, one could subtract the second layer and bulk contributions from N_o, S_o, and Ω_o to determine the first layer properties. However, these thermodynamic quantities are available only on a coarse scale above 4.57 K. Fine structure is available at scattered coverages solely as heat capacities. We are therefore forced to guess the first layer equation of state and adjust it until it reproduces the observed heat capacities.

At the lower coverages and temperatures the first layer is the only occupied subsystem, so the problem is greatly simplified. We need only to find the chemical potential that corresponds to the observed heat capacity. To maintain the precision of the heat capacity data near the peak, in spite of the large breaks in coverage, the analysis was done analytically. The data at 0 K in Table IV over the relevant range of $0.9 < N < 1.15$ could be fit by:

---

44. (cont.) first layer, the energetic sites are always filled with an inert high density solid. The inhomogeneity of the second layer is down by the ratio of the binding energies. Its effects show up only very near to monolayer completion.

$$S(0) = 0$$

$$\mu(0) = -141 + 43.6\,N^5$$

$$U(0) = \Omega + TS + \mu N = -3.5 - 141\,N + 7.27\,N^6 .$$

The Debye temperatures of Bretz, Huff, and Dash (1972) could be fit by $\theta_D = 33\,N^{3.5}$ where the exponent is the two-dimensional Gruneisen constant. The temperature of the melting peak fit $T_m = 4.35\,N^5$ in the range $0.9 < N < 1.05$. The entropy of melting, S_m, is not well defined in two dimensions, since the transition always occurs over a finite temperature interval. However, the choice of the smooth function $3\,N^4/(115\,N^{10}/T^2 + 1)$ for the remainder of the heat capacity left a value, $S_m/N = 0.39 - 0.66/T_m$ or $S_m \approx 0.46 - 0.96/T_m$. The observation that the melting peak rose like T^{11} on the low side and was symmetrical, along with the requirement that the function be integrable, fixed the remaining term. The result was:

$$C = 3\,N^4/(115\,N^{10}/T^2 + 1) + (0.46 - 0.96/T_m)(T/T_m)M$$

where $M = 0.185 \exp\,[9.5(T/T_m - 1)]$ for $T < T_m$

and $M = 0.185 \exp\,[12.5(1 - T/T_m)]$ for $T > T_m$.

μ may next be found from:

$$U = U(0) + \int C\,dT$$

$$S = S(0) + \int C\,d(\log T)$$

$$\mu = [\partial(U - TS)/\partial N]_T \quad (45).$$

Although these equations were derived using data where only the first layer is occupied, they have been carefully chosen to be physically reasonable at nearby coverages and temperatures (46). Putting it all together to find $S_o(N,T)$ and differentiating numerically gives the solid lines of Fig. 4. The inset in that figure shows the contribution to the heat capacity from the first layer (1.) and the two layers interacting (2.), as well as for the total system, at the highest coverage. This model was also used to correct the melting points in Fig. 5 for second layer formation. So we have found that the qualitative changes found in Fig. 4 are not intrinsic parts of the two-dimensional solid. On the contrary, the behavior of the solid is qualitatively the same for all coverages greater than $N = 0.88$ ($1/\alpha = 9.1$ atom/nm^2).

---

45. It was not possible to find μ by use of [8] because that would require a second integration. The differentiation given here was complicated enough!

46. The heat capacity rises to the unreasonable value of $3N^4$ or about 3 in the high temperature limit. This resulted from forcing such a simple equation to fit both the low and intermediate temperature data. Ultimately one should use the theoretical heat capacity of a triangular solid, which, unlike that for a square or cubic lattice, is unique in shape.

We may now construct a more realistic equation of state. At intermediate coverages, the experimental data from Table I may be used, since the effects of the inhomogeneity are small. At high coverages, the melting model just described gives the proper two-dimensional equation (47). At low coverage, a two term virial equation of state should be adequate. The second virial coefficients have been calculated for a two-dimensional bose gas from the Lenard-Jones potential by R. L. Siddon and M. Schick (1973). This is in essence a careful scaling of three-dimensional virial data to two dimensions, since the Lenard-Jones parameters were found from a quantum mechanical analysis of the three-dimensional helium virial data (de Boer & Michels 1938).

If we put this combined equation of state in a Ross-Oliver type of analysis we find the total entropy shown by the solid lines in Fig. 16 (48). The points

---

47. The reason for dropping the second layer at high coverages is that the difference between the first and second layer binding energies rises as the first layer energy does. This means the second layer will form at a larger coverage on the inhomogeneities.

48. The energy distribution actually used in this computation was $f(E) = 0.015/(E - 143)$. This formula provided nearly as close a fit in a graph like Fig. 15 as the formula given earlier so the results with either will be similar.

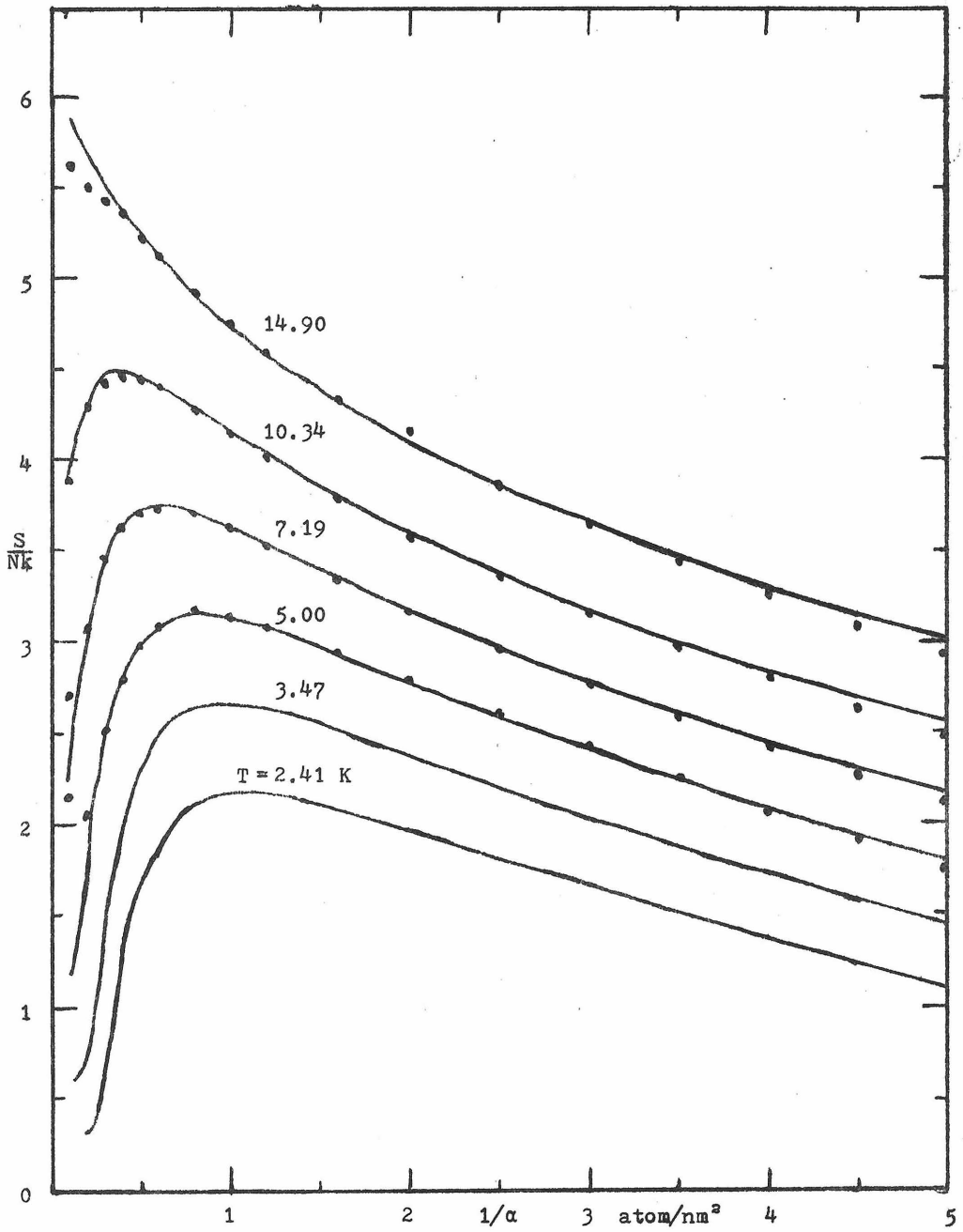

Figure 16 Fit to Virial Gas + Inhomogeneity

give experimental data from Table I. The close agreement is strong evidence for the accuracy of all the underlying assumptions. In particular, is shows that substrate-mediated helium-helium interactions are unimportant, the area calibration by lattice gas ordering is accurate, and the energetic binding sites occur in clusters.

There is a small erratic scatter in the theoretical values caused by the interpolation of experimental data and the joining of the three pieces of the equation of state. This makes heat capacity calculations inaccurate. However, Fig. 16 suggests the mechanism behind the large heat capacities found at low coverage; it is simply the two-dimensional heat of vaporization from the small solid entropy found at low temperatures to the large near-ideal gas entropy found at high temperatures. Calculations below 2 K are again impossible because the virial equation of state becomes double valued (in the sense of two coverages for the same chemical potential) before the density becomes large enough to use experimental data.

Combining the experimental data, the thermodynamic analysis, and the models gives a nearly complete picture of the helium-Grafoil system. Typical pressure isotherms are given in Fig. 17. The data above 10 torr were measured directly. Between 0.001 and 10 torr

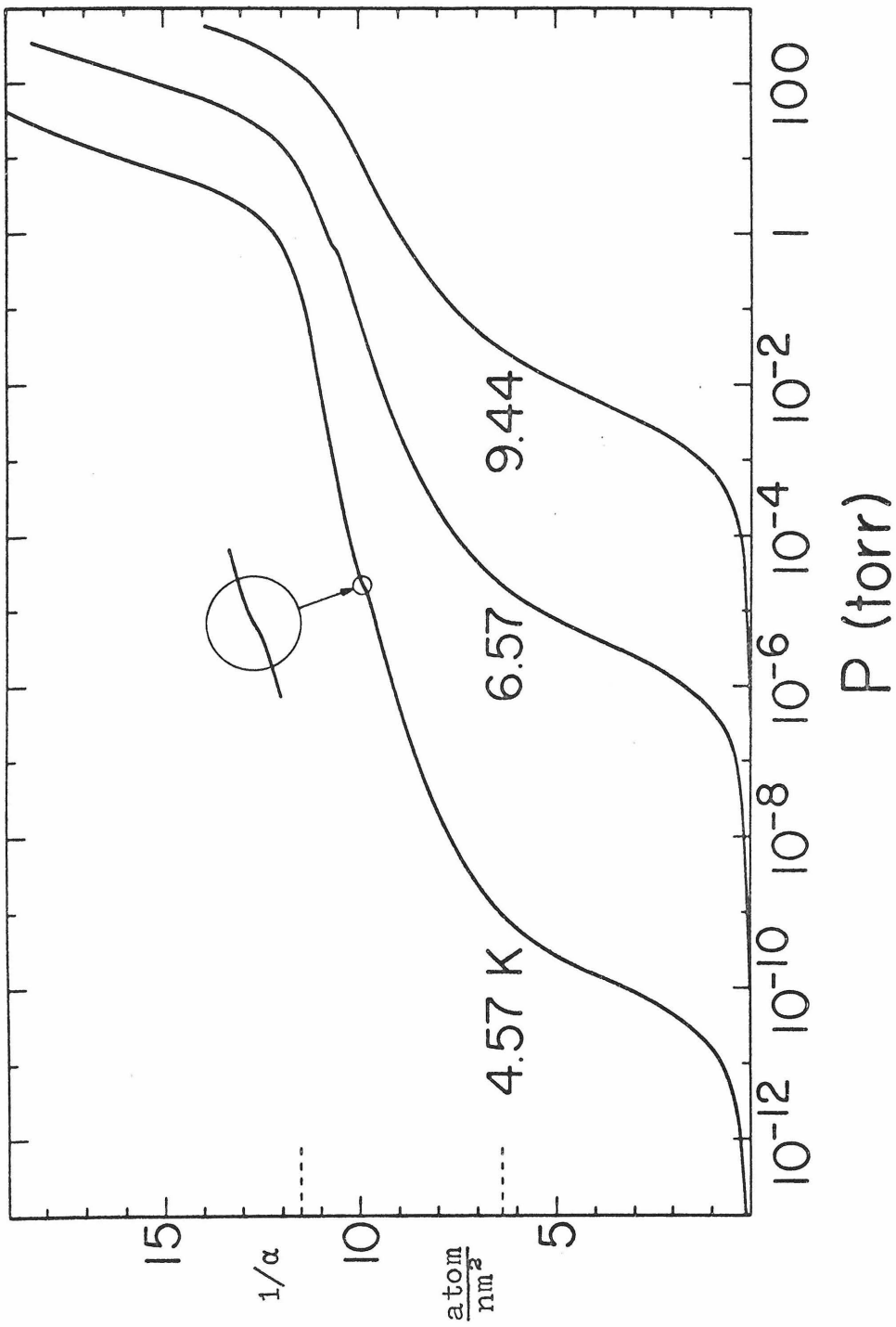

Figure 17 Pressure Isotherms

the data were corrected for thermal transpiration. The lower pressures were calculated from the thermodynamically derived chemical potential. The small glitches near 10^{-5} torr at 4.57 K and near 1 torr at 6.57 K were drawn using the melting model. Isosteric heats are usually found at some average temperature where desorption is small but the pressure is easily measured. Here we find much more detail, as shown in Fig. 18. The upper two curves have been calculated from the chemical potentials given in Table I. For 0.0 K, q_{st} is identical to the $-\mu$ given by Table IV. The bump in the middle of the 0.0 K curve indicates the ordered lattice gas. The sharp peak on the 5.0 K curve indicates melting.

One can make further use of the models to study first layer behavior alone. Fig. 19 shows P-V-T data for bulk helium at relatively high pressures (Dugdale & Frank 1964; Ahlers 1970; McCarty 1972). If one makes the corresponding two-dimensional ϕ-A-T plot using Table I, the highest coverage curves bunch together and have a negative slope. However, the first layer alone looks much more like the bulk, as shown by Fig. 20. The heavy dashed lines indicate the multilayer effects. The coverages of Fig. 20 correspond to the densities used in Fig. 19.

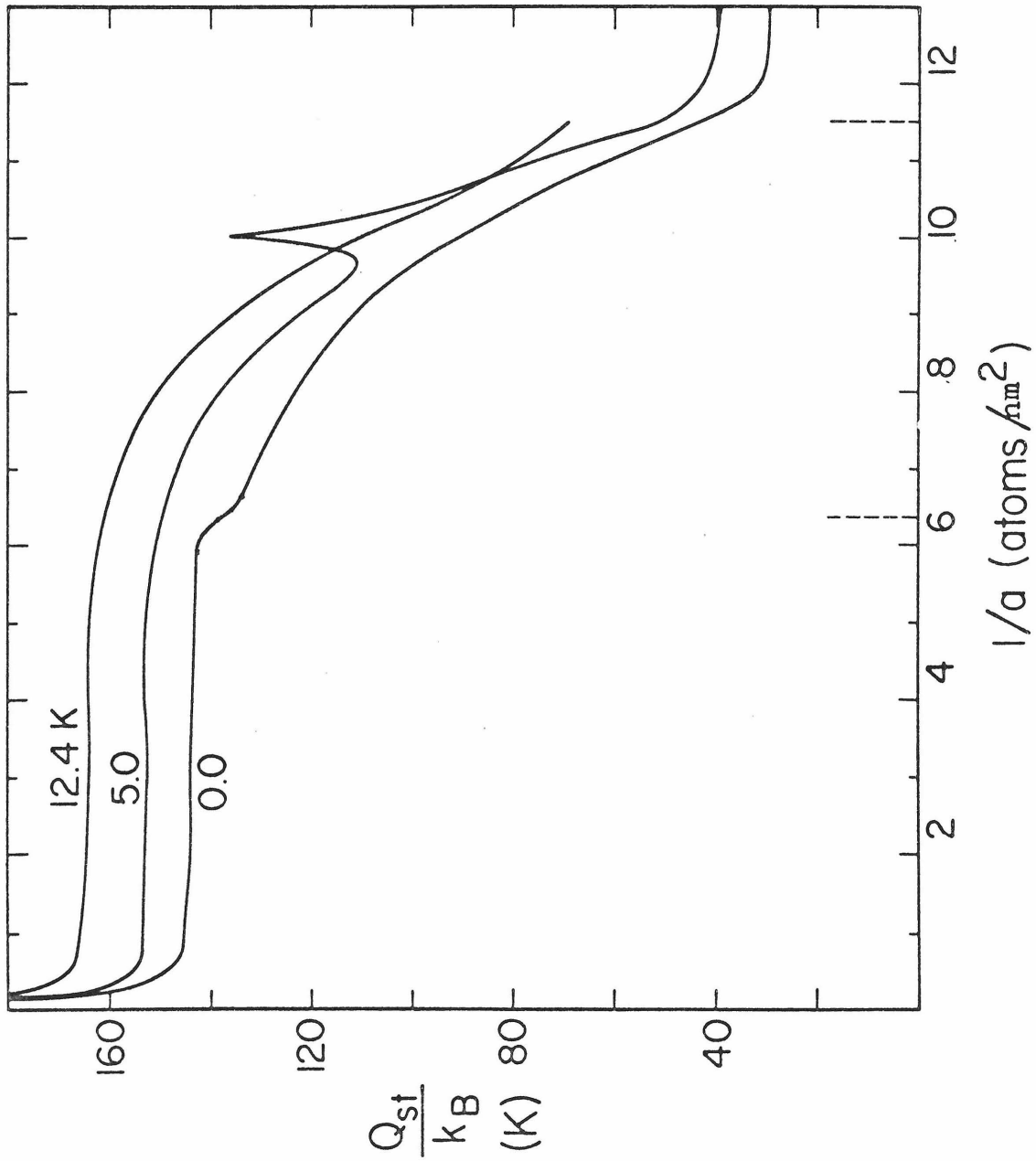

Figure 18 Isosteric Heat

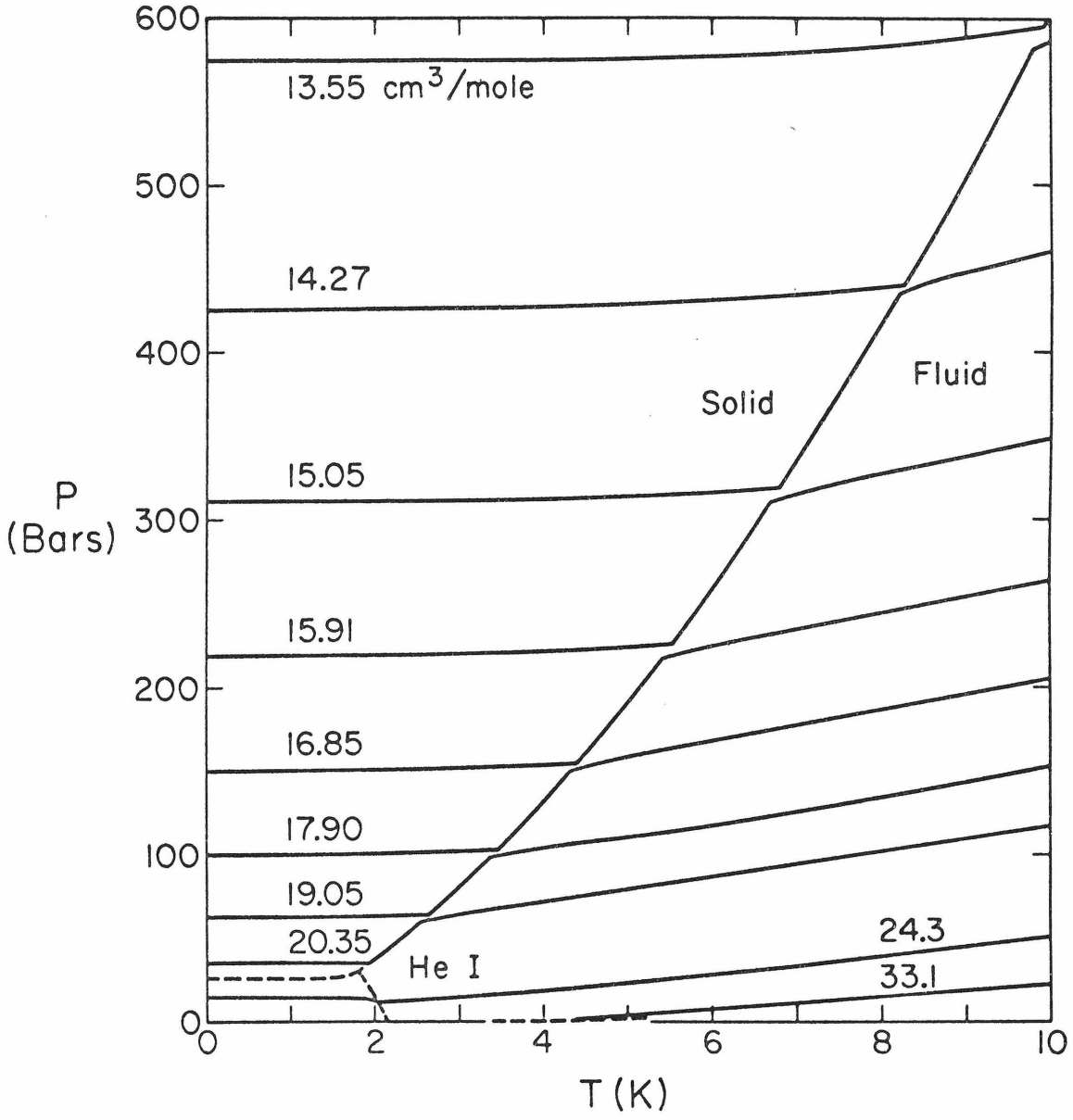

Figure 19 Bulk P-V-T Diagram

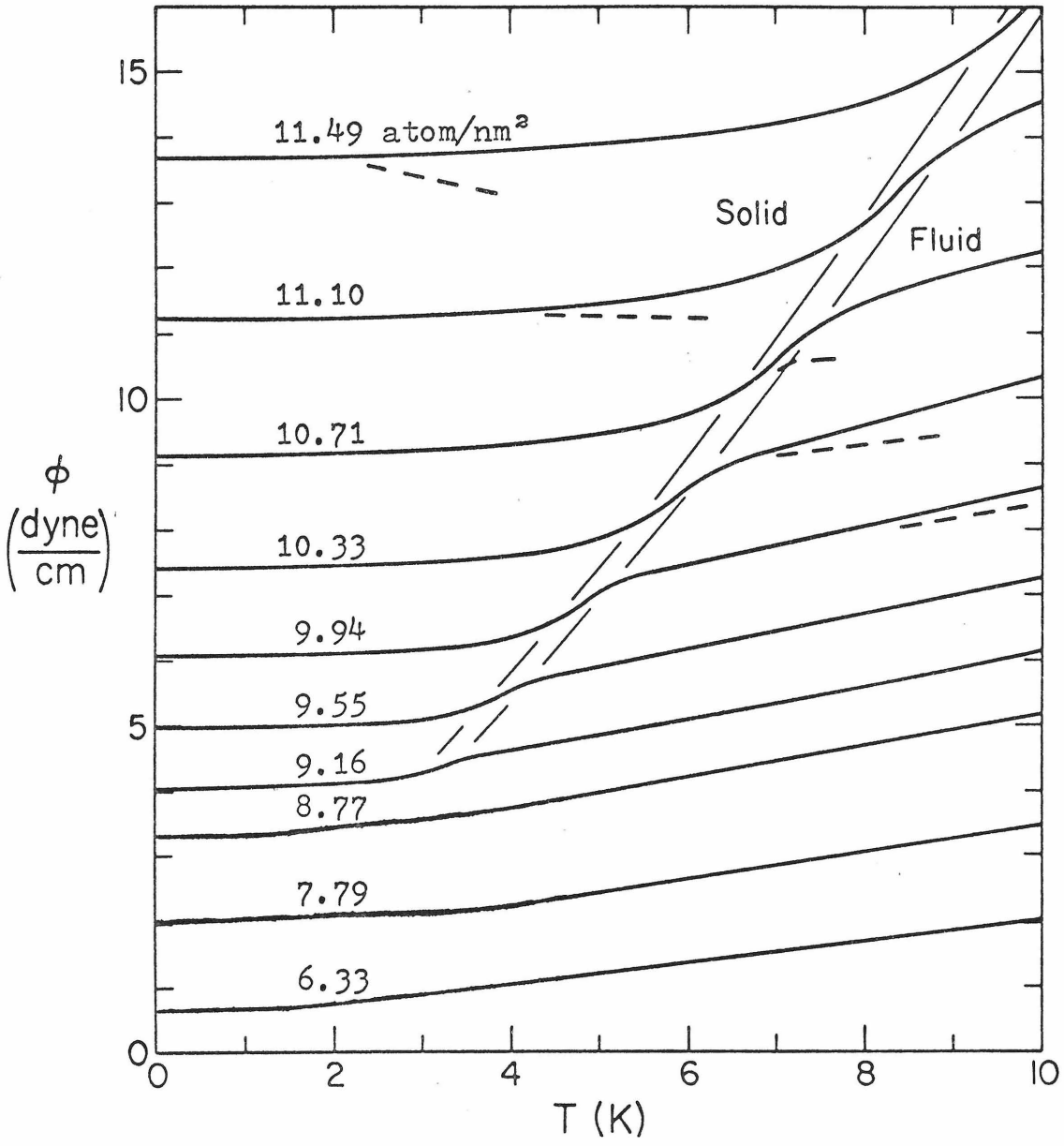

Figure 20 Film ø-A-T Diagram

The sharp peaks in the heat capacity at high coverage in Fig. 4 can now be explained. Fig. 20 shows that the film tries to expand on melting, just as in the bulk case. At the lower coverages, the adsorption forces hold the film at constant density, so the pressure rises instead. However, at higher coverages the process of melting overcomes the adsorption forces enough to promote some helium to the second layer. This narrows the melting region (see dashed line at $1/\alpha = 10.71$ in Fig. 20)and also does work against the adsorption forces. The result is larger heat capacitites over a narrower temperature range.

The correction of the low density, high temperature data to the first layer on a homogeneous substrate is not interesting. The close fit in Fig. 16 shows that one would just recover the virial gas that one started with. The low temperature region shows very interesting effects, but cannot be analyzed definitively. The current hypotheses are analyzed in the next section. Extrapolating the model of page 75 does show that the inhomogeneity raises the helium adsorbed at the ordering peak by $1.7 \pm 0.3\%$. To avoid complicating interlaboratory comparisons, this correction has been ignored.

Model analysis

In this section, the various phases shown in Fig. 3 will be analyzed by reviewing the current helium-Grafoil literature in the light of this project. Some of the discussion is definitive. In the other regions, reasons for the remaining uncertainty and possible methods of resolution will be discussed.

Theoreticians have a particular fondness for the low density limit, for obvious reasons (Lai, Woo, & Wu 1970). Unfortunately, this region is totally dominated by the effects of inhomogeneity if the maximum energy variation is large compared to the temperature as it is here. In fact, since any substrate made of packed material should show inhomogeneity due to touching surfaces, and no energy distribution in the literature is compatible with this mechanism, no low density theory for such systems has ever worked before.

A. Widom and J. B. Sokoloff (1972) presented a virial model for the bose compressed region. Since it assumed that the range of binding energies was small compared to the temperature, its virial terms did not fit over any reasonable range of the data. They also made the unphysical assumption of a tunneling

band. It has been shown by Hagen, Novaco, and Milford (1972) that the tunneling band is so wide that it is meaningless. Specifically, localization about a single lattice site would, at best, create a zero point energy over four times larger than the decrease in the potential energy.

J. G. Dash speculated that a low density solid formed at $1/\alpha \approx 0.5$ atom/nm^2 on the basis of heat capacities below 4 K that fit a two-dimensional Debye solid formula in both the first and second layer (J. G. Dash 1973). Fig. 9 and Table I show that the experimental data actually fit this hypothesis up to at least 15 K. However, the data at nearby coverage have high temperature heat capacities ranging from one half to twice the Debye limit without any special stability shown where the theory suddenly fits. The Ross-Oliver treatment, on the other hand, explains the entire range of data nearly from first principles. Ironically, the helium <u>is</u> mostly solid at low temperatures at this coverage, but it is in isolated patches of ordinary high density solid compressed by the inhomogeneity. (This is the same problem that vexed experimenters with copper substrates.)

C. E. Campbell, J. G. Dash, and M. Schick (1971)

also presented a model for the bose compressed region based on a small inhomogeneity. Unlike Widom's, it does not purport to apply at very low density, so the omission of the more energetic sites may be irrelevant. However, their choice of $f(E) = 1$, $0 < E - E_b < 1$ for the energy distribution is not as "physically reasonable" as they suggest. The heat capacity peak they find occurs precisely where the chemical potential crosses the sharp edge of this distribution. As all physically reasonable distributions have a tail on the energetic side, the sharp peak is an artifact of their choice for $f(E)$.

The other two theories look for the cause of the bose compressed region in the helium-helium potential rather than in the helium-graphite potential. Their interpretations are divergent, but their methods are generally complementary. R. L. Siddon and M. Schick (1973) start from the virial coefficients of a low density gas. A. D. Novaco (1972) starts with a liquid state at 0 K. Neither a two-term virial gas nor an entropyless liquid are an accurate representation in the region of the heat capacity peaks so it is not surprising that both find only qualitative agreement.

The virial coefficients have been confirmed experimentally, at least above 4 K. This was shown

in Fig. 16. There is no experimental evidence for the existence of the low density liquid state hypothesized by Novaco. However, this may be more a reflection on the experiments than on the theory. Data exist at only three coverages in this region and only one run both extends to temperatures well below the peaks and is consistent with other high temperature data ($1/\alpha = 2.79$ in Fig. 8). In principle, one could determine the liquid state (or whatever it is) by successive approximation as was done to find the intrinsic properties of the solid. The binding energy distribution was given previously, the low density state should be accurately describable by the virial coefficients, and a first approximation to the dense state is given by Novaco. Such a procedure will go nowhere without more data, especially at temperatures below the peaks.

M. Bretz and J. G. Dash (1971b) suggest that the nonreproducibility of the intermediate region is due to interplay between two different ordered lattice gases at three-fourths the density of the triangular ordered lattice gas. The main evidence for this is some misleadingly drawn lines on a phase diagram. It was already argued in chapter 1 that the lower temperature peaks in this region are the true equilibrium state and lie on a smooth curve connecting

the peaks at higher and lower coverages. The high temperature peaks occur at a temperature suspiciously close to that of the triangular lattice gas peak. The phase diagram of Bretz et al (1973) implies that the temperatures of all three sets of peaks are distinct and practically independent of coverage.

One of these two hypothesized structures has never been observed in any atomic system and the other has been calculated to be unstable (Novaco 1973). The 1.5 K entropy of Table IV provides additional information. It dips to small values near the triangular lattice gas ($N = 0.656$) and the solid ($N > 0.9$). At the coverage of interest here ($N = 0.492$) there is no dip at all. On the contrary, the plunge to the triangular lattice value has just started.

The lack of any special structures in the intermediate region does not imply it is simple. The transition between an essentially classical ordered lattice gas and a yet-to-be-explained bose-ordered fluid should keep theoreticians perplexed for years.

Campbell and Schick (1972) have provided a detailed model of the triangular lattice gas transitions. They calculate not only the heat capacity at the coverage of maximum ordering, but also find an entire phase diagram, including the chemical potential at

the boundaries. Rather surprisingly, they predict the heat capacity will peak at 5.5 K, nearly twice the experimental value of 2.925 K.

They evaluated the nearest neighbor energy (corresponding to the bulk solid under 20,000 atmospheres of pressure) from the Lenard-Jones potential (derived from the virial coefficients of the bulk gas). Sposito (1970) claims the repulsive term is given more realistically by the Morse-V_{DD} potential. This gives a 28% smaller nearest neighbor energy. Campbell and Schick's article implies that the data scale with this parameter. However, their choice of the ratio of the nearest neighbor energy to the next nearest neighbor energy is also inconsistent with the Morse-V_{DD} potential. Correcting this should lower the transition temperature further, but the exact amount cannot be determined without reworking the original analysis.

Even with this uncertainty, it is still interesting to scale the calculations to give the experimental peak temperature and compare the other predictions. Fig. 21 shows their calculation of the phase diagram. The circles show observed heat capacity peaks taken from Fig. 3. The vertical lines indicate the region where the experimental chemical potential takes on the values they claim are associated with the phase boundary.

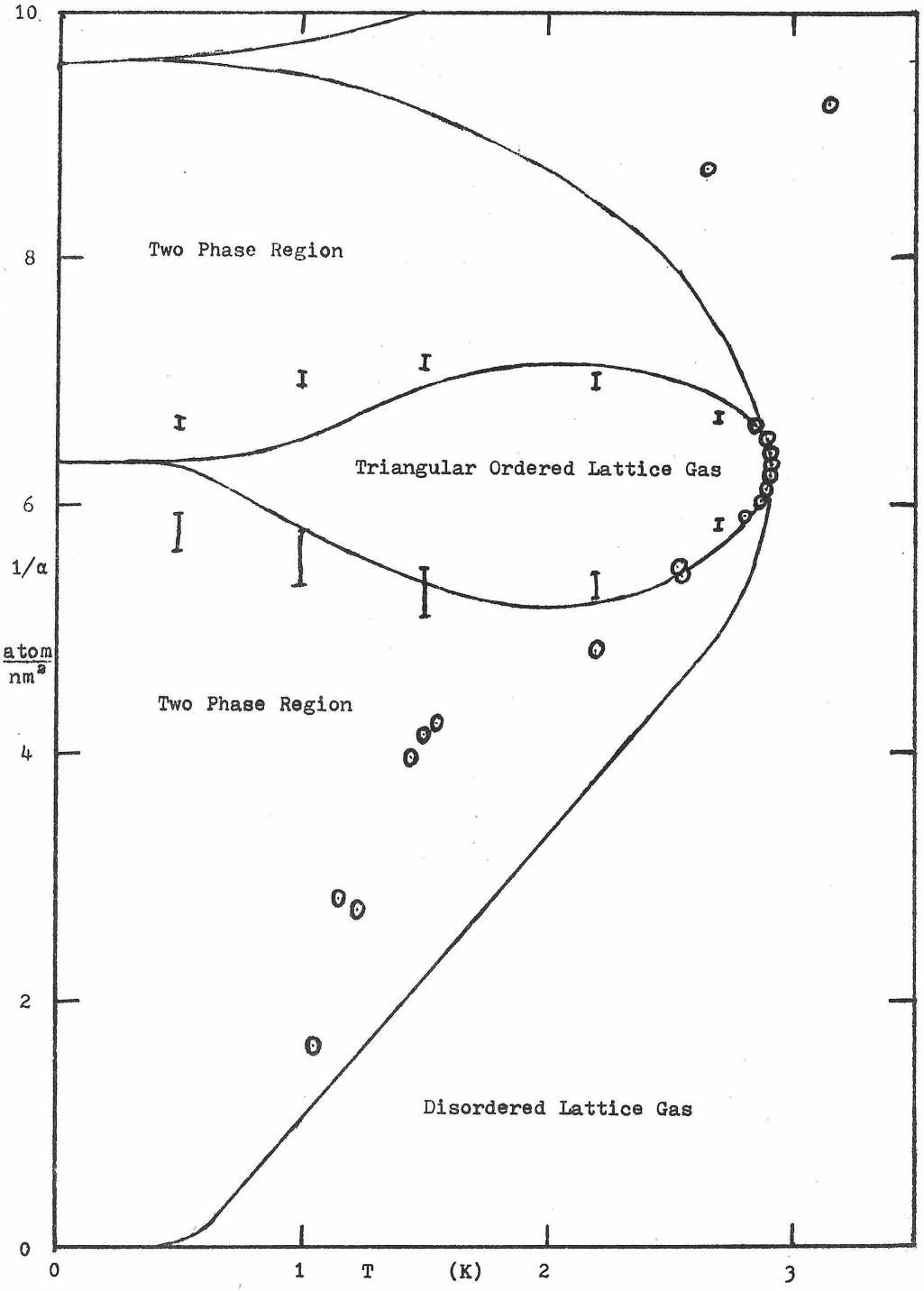

Figure 21 Lattice Gas Phases

One sees quantitative agreement on the shape of the high temperature boundary of the ordered phase and much of the chemical potential, and qualitative agreement on the lower coverage phase boundary. With a little imagination, one can even see a shoulder at about 1.3 K on the lowest curve in Fig. 7 corresponding to crossing the low temperature boundary of the ordered region.

There are still many problems with the model. The phase transitions are predicted to be first order. The entire two-phase region should have the same chemical potential, rather than just the ordered phase boundary. There is no agreement at coverages significantly larger than ordering. While the lattice gas approximation clearly must break down somewhere, the significance of the current disagreements is unclear. For example, second order phase transitions are possible in the model, but were unstable with the old choice of the ratio of interatomic potentials. A reanalysis with the Morse-V_{DD} potential should be very useful.

A. D. Novaco (1973) calculates that this ordered lattice gas is stable relative to a fluid at the same density but not relative to a low density gas. This is easy to check using the spreading pressure derived from Ω in Tables I and IV and shown in Fig. 22.

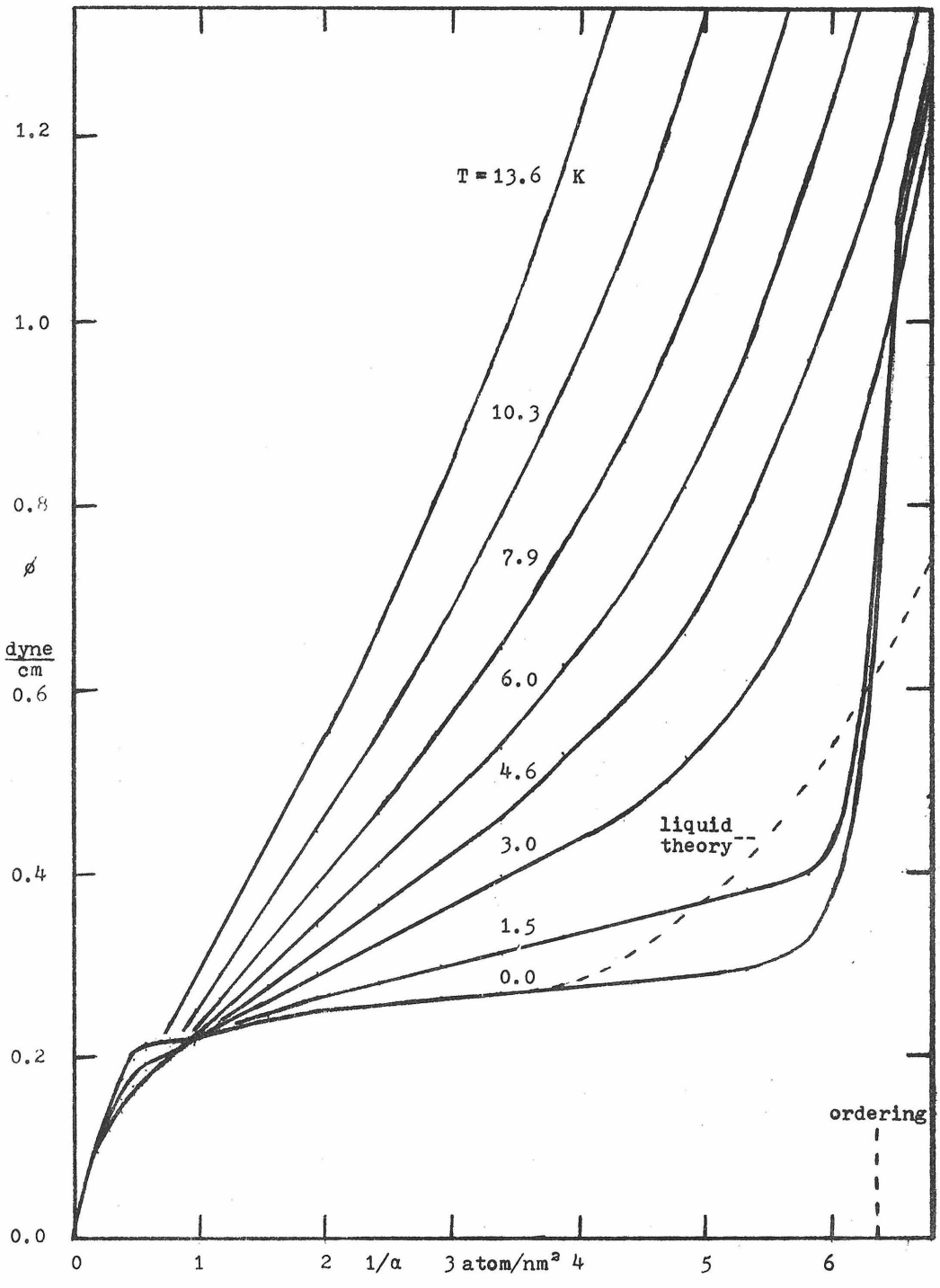

Figure 22 Spreading Pressure

Since gas always flows toward lower pressures, the most stable phase must have the lowest pressure. The dashed line shows the pressure expected for the liquid state at 0 K (Miller, Woo, & Campbell 1972). The system clearly has found a more stable state for overall coverages in the range $3.5 < 1/\alpha < 6.2$. Presumably this is the ordered state. If the ordered state were more stable than the low density gas, isolated ordered regions would form at low overall density and the pressure would remain constant until they filled the entire surface. This test cannot be applied at 0 K, because if the ideal gas were more stable, the pressure would still remain constant (see below). However, at 1.5 K the two cases do lead to different results. It can be seen that the pressure rises with coverage, as expected if the gas is the more stable state.

Two peculiarities of this plot deserve comment. The expected ideal gas behavior of ϕ is ϕ proportional to $T(1/\alpha)$. This is approximately true for $1 < 1/\alpha < 4$ atom/nm^2. The initial rise in ϕ at low coverage is due to the inhomogeneity. Relative to a homogeneous substrate, this is a negative pressure region, since the energetic sites "suck" the helium to themselves. As a first approximation to the homogeneous system

one may readjust the zero on both axes to ignore this region. The pressure falls when the temperature rises in two regions of this graph. While this behavior is unusual it is perfectly possible. As a three-dimensional example, consider ice under pressure on being warmed through the melting temperature.

The strong evidence in favor of the existence of a two-dimensional solid has already been shown in figures 4, 5, 6, 19, and 20. It has long been known that conventional long range order cannot exist in two dimensions, but this is irrelevant to the question of whether a two-dimensional fluid may crystallize. Two dimensional crystals can have all the properties of bulk crystals to experimental accuracy at finite temperature without long range order (Hohenberg 1967; Mermin 1968).

J. G. Dash and M. Bretz (1972) explicitly use the lack of long range order to explain the lack of a first order melting transition. As the temperature rises, the crystal becomes disordered at progressively shorter wavelengths. Their model was solved in the limit $T_m >> \theta_D$ and gave peaks reflecting the unphysically sharp cutoff used in the Debye approximation, but comparable in width to experiment. A better fit to experimental data will require numerical solution

with $T_m \approx 0.15\,\theta_D$ as well as use of the actual frequency spectrum for a triangular lattice.

J. M. Kosterlitz and D. J. Thouless (1972) give a topological definition of long range order that can exist in two dimensions. They predict a first order phase transition at which the resistance to shear disappears. R. P. Feynman (1973) has corrected an error in their derivation. This results in the transition temperature depending on only the coverage and the Debye temperature:

$$T_m = (1/8)\,m\,k\,\alpha\,(\theta_D/h)^2 = 0.026\,\alpha\,\theta_D^2 .$$

Using θ_D from Fig. 6 gives melting temperatures 20% to 40% below the experimental values.

The heat capacities are measured at constant area but this is not necessarily the easiest form to analyze. Only at constant pressure will the latent heat be self-evident (Dash, May 1973). With the aid of the melting model, one can find any thermodynamic relationship in this region. The shape of C_ϕ for a melting temperature of 4 K in shown in Fig. 23 along with the nearest experimental data (49).

---

49. Since N varies when ϕ is held constant (see Fig. 20) the value of C_ϕ was normalized by dividing by the value of N at the center of the peak. The lack of rounding on the C_ϕ peak is an artifact.

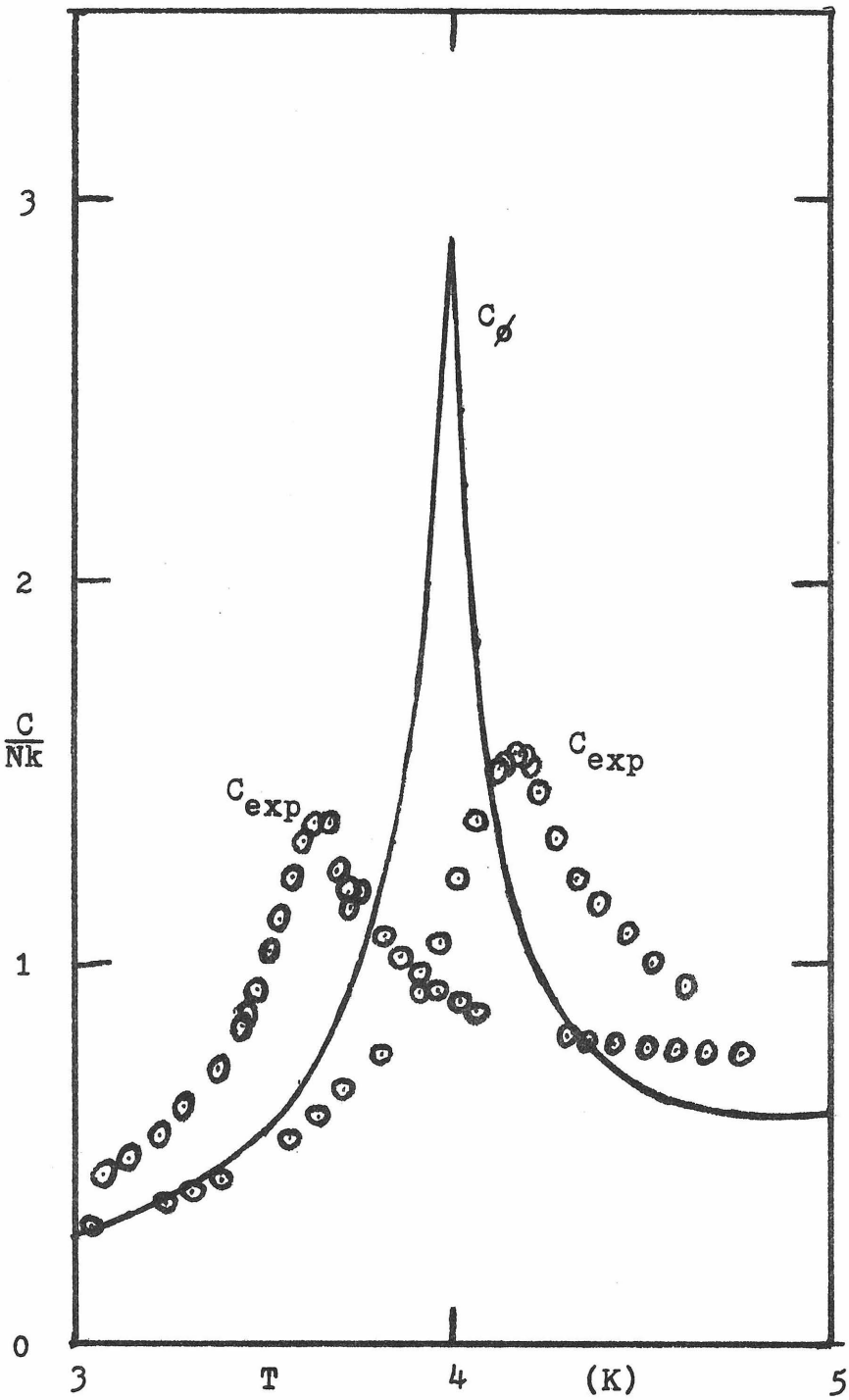

Figure 23 Constant Pressure Heat Capacity

The C_ϕ peak is only one third as wide as, but otherwise similar to, the ones at constant area. If one changes S_m (see page 73), the width varies as $S_m(\text{bulk}) - 2S_m$. A negative width would give a first order phase transition. This raises the possibility that the order of the transition may depend on the details of the solid phase and not just on the dimensionality.

C. E. Campbell, F. J. Milford, A. D. Novaco, and M. Schick (1972) have performed a detailed theoretical analysis of monolayer completion at 0 K. Their second layer binding energy was given earlier, where it was found to be only marginally larger than the semi-experimental value. Their Debye temperature, 67 K, is 15% above experiment while their compressibility is 0.0053 cm^2/erg. This latter can be found from the chemical potential in Table IV. The experimental value is 0.019 cm^2/erg at 95% of a monolayer. Using the melting model lowers this to 0.013 cm^2/erg at a full monolayer.

Most of the discrepancies above can be traced to the use of $E_b = 188$ K for the ground state energy. The use of the experimental value $E_b = 143$ K would lower the Debye temperature and raise the compressibility. The experimental value for the compressibility has also been raised somewhat by inhomogeneity in the second

layer. The melting model attempted to correct for a homogeneous second layer, so the few atoms adsorbed in energetic sites of the second layer before apparent monolayer completion will raise the apparent compressibility of the first layer. The helium-helium potential in their model somehow used a combination of the Lenard-Jones potential plus an adjustible hard core. It would be useful to try the Morse-V_{DD} potential instead.

In the above model system the point of monolayer completion was uniquely defined by the first atom to enter the second layer. At finite temperatures or in the presence of substrate inhomogeneity, completion may occur at different points depending on the criterion. The melting model allows both experimental and theoretical criteria to be compared with the following results.

The two most common experimental methods, the Langmuir and the B.E.T. isotherms, give meaningless results at sufficiently low temperatures where the pressure varies exponentially with coverage. This exponential variation occurs when either the inhomogeneity energy or the interparticle interaction energies become large compared to the temperature. This occurs over the entire temperature range of the present experiment.

George Jura and Terrell Hill (1952) in heats of immersion studies suggested the entropy minimum as a more sound criterion for monolayer completion. This criterion was also used by Bretz et al (1973) by integrating their heat capacities from 0 K. It does not seem to have been noticed that essentially the same criterion may be applied using only pressure isotherms near the monolayer. The trick is to plot the data in the form of a chemical potential (see page 47) versus the coverage. These lines will cross where the partial molar entropy is zero [8]. This quantity is negative for a solid and positive for a gas, so every other crossing should indicate the completion of a layer (50). When the lines cease crossing (or if they never cross!), the gas is no longer condensing into distinct layers. This monolayer criterion thus contains a built in test for homogeneity (51). Fig. 17 is replotted in μ form as Fig. 24.

In the present case, the second derivative of the chemical potential with density is positive for

---

50. The other crossings indicate the transition from dilute to dense fluid within a single layer. Below the critical temperature, plotting $T \log (P_o/P)$, where P_o is the vapor pressure in the bulk, should give the more sensitive test of whether the partial entropy is above the bulk value.

51. An experiment in this laboratory using helium on oxidized copper gave no crossings for $T > 4$ K.

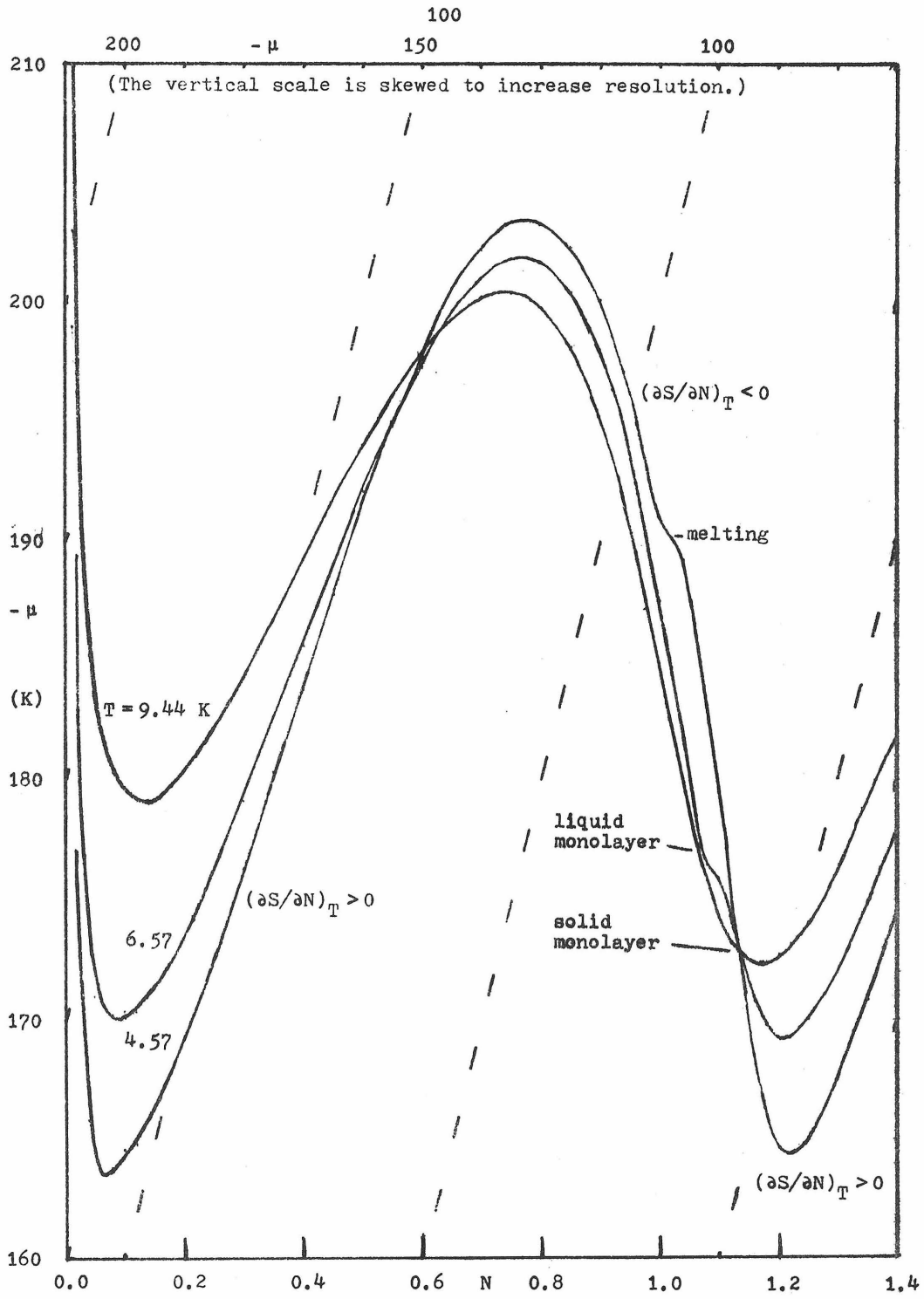

Figure 24 Chemical Potential Plot

the solid. This should be true for all other helium experiments, but it is not known whether it is true in general. When it is true the point of inflection in a plot of μ vs T (or simply log P vs T) using a single isotherm will indicate the monolayer. Both the inflection and crossing criteria give essentially the same monolayer capacities in the present experiment. This drops about 1% for each 1 K rise in T with an extra 4% drop on crossing the melting line (see Fig. 1). The simple theoretical criterion that the next atom added has an equal probability of going into either layer gives the same capacity at 0 K but only half the temperature dependence.

The second layer structures were not shown on Fig. 3. This does not imply a lack of interesting behavior, only a lack of enough published data to determine any phase boundaries. In many ways the second layer should be more ideal than the first. If the inhomogeneity model presented here is correct, the surface area will be reduced by only $2\,\theta_1 \approx 5\%$ while the importance of the inhomogeneity will be reduced by the factor $E_b/E_{b2} \approx 5$. The possibility of a substrate ordered lattice gas is greatly reduced because the substrate is now solid helium. The application of the thermodynamic reduction techniques

given in chapter 3 should be considerably more accurate because the pressure is measurable down to 2 K (see Fig. 1 and Table III). On the other hand, since all phase boundaries except melting will probably be below 2 K, desorption will still not be a problem. Indeed, the study of helium adsorbed on helium precoated Grafoil may be the next major advance in the experimental pursuit of two dimensional matter.

CHAPTER 5

Conclusions

The helium-Grafoil system has led to a qualitative advance in the understanding of two-dimensional matter. Positive identification has been made of a virial gas, an ordered lattice gas, and a crystalline solid, all in two dimensions. Deviations caused by desorption, multilayer formation, excited states, and substrate inhomogeneity have been analyzed quantitatively.

Theoretical calculations of the helium-graphite potential are not consistent with the data, perhaps indicating that the top graphite layer has an anomalous separation. The virial calculations are highly successful when inhomogeneity is taken into account. The lattice gas and monolayer completion calculations are generally successful but suffer from inaccurate choices of potentials. The melting transition is well characterized experimentally, but the theories are still semi-quantitative. Possible ordering in both low and high density fluid states at low temperatures is poorly understood, mainly because of a scarcity of experimental data. Data from the second layer might be more clear-cut.

Two innovations made major contributions to the experimental accuracy. The practice of always heating the sample to the multitorr range and cooling slowly after each change in coverage gave complete equilibrium in a fraction of an hour, whereas isothermal equilibrium sometimes takes weeks. The inverted heat capacity technique allowed background corrections to better than 0.1% and heat leak corrections to better than 1%, giving useful data below 1% of a monolayer even at high temperatures.

The measurement of pressures at room temperature in precision adsorption experiments is obsolete. There seems little hope of calculating thermal transpiration corrections to better than 1% even with extensive calibration because the effect is sensitive to tube aging and the intermediate temperature profile. Having part of the gas at a different temperature also adds to the complexity and reduces the accuracy of the heat capacity analysis. In situ capacitive manometry (Gonano, Roland, & Adams 1970) can measure pressures over four orders of magnitude to 0.1% accuracy. The inverted heat capacity technique is well suited for correcting the large background and heat leak additions the manometer will cause.

The film has been well defined thermodynamically.

Methods of combining the data into a coherent and complete whole have been developed and, most important, have actually been shown to work. In particular, high temperature measurements of the pressure of the three-dimensional gas have been transformed to give the two-dimensional pressure and compressibility at all temperatures.

The complete coverage of the high temperature data is both the strength and weakness of this project. Analysis of the interesting regions where there is fine structure always requires the use of data from other laboratories. On the other hand, as new structures are discovered, their analysis should also be aided by the pre-existing high temperature data at the same coverage. The high reproducibility of the Grafoil data, especially at high temperatures, should continue to make these combined analyses dependable.

APPENDIX I TABLE I

ORIGINAL DATA AND DERIVED THERMODYNAMIC QUANTITIES FOR HELIUM 4 ON GRAFOIL

Robert L. Elgin experimenter, David L. Goodstein adviser.
Department of Physics, California Institute of Technology, Pasadena, Ca 91109

Cell characteristics: 12.50 g. Grafoil, 64 g. copper; 9.7 cc free volume + 47 cc at 299 K; 65.65 ± .10 cc STP of helium at lattice gas transition.

The directly measured quantities were:

N_o the total helium in the system in units of 100 cc STP.

P_w the pressure at room temperature in torr.

C_o- the heat capacity over the preceding temperature interval.

Corrections for thermal transpiration in the 1/16 inch i.d. Cu-Ni filling tube and for gas in the free volume give:

P the pressure in the cell.

N the helium adsorbed.

The last 4 columns on each page give the derived quantities interpolated to constant film density. (Numerically given by rounding N_p to hundredths.)

μ the chemical potential in kelvins.

C the film heat capacity interpolated to the given temperature.

S the entropy.

Ω the Landau potential in kelvins.

The values of μ below the short bar were derived solely from the P column. The values of C and the differences in S above the bar were derived from the C_o column with desorption corrections. The remaining entries were derived from these by use of the thermodynamic identities:

$$(\partial\mu/\partial T)_N = -(\partial S/\partial N)_T, \quad C = T(\partial S/\partial T)_N, \quad d\Omega = -N\,d\mu - S\,dT, \quad \Omega = S = 0 \text{ at } N = 0$$

Using Boltzmann's constant, k, we may transform to conventional atomic units:

Heat capacity at constant area kC/N Entropy kS/N

Three dimensional pressure $155.8\ T^{2.5} \exp(\mu/T)$ torr

Internal energy $k(\mu + \Omega/N + TS/N)$ Free energy $k(\mu + \Omega/N)$

Gibbs potential $k\mu$ Enthalpy $k(\mu + TS/N)$

Landau potential $k\Omega/N$

Based on the lattice gas ordering transition, the best value for the area per atom is given by $0.1014\ nm^2/N$. From this we get:

Two dimensional pressure $-k\Omega/0.1014\ nm^2 = -0.1362\,\Omega$ dyne/cm.

HELIUM 4 ON GRAFOIL AT T = 4.570 K

P_w	P	N	N_o	$-\mu$	S	$-\Omega$
0.			.009988	198	.0217	.42
			.019966	173.6	.0373	.80
			.02996	166.6	.0691	.97
			.03999	161.8	.1041	1.14
			.04992	159.70	.1413	1.24
			.05992	157.18	.1767	1.38
			.07997	155.93	.2444	1.47
			.09984	154.56	.3033	1.59
			.11993	152.85	.3584	1.78
			.15988	150.81	.4576	2.06
			.19986	149.32	.5424	2.33
			.2499	147.60	.6337	2.71
			.3001	146.30	.7073	3.07
			.3502	145.33	.7641	3.38
			.4002	143.81	.8062	3.95
			.4499	142.80	.8364	4.38
			.5002	141.69	.8502	4.91
			.5494	139.78	.8498	5.91
			.6001	137.64	.8378	7.14
			.6493	135.53	.8153	8.45
			.7001	132.14	.7860	10.74
			.7492	128.42	.7447	13.44
			.8000	123.25	.7039	17.44
			.8490	117.29	.6602	22.36
0.			.9000	110.05	.6099	28.70
.00002	.000003		.9189	106.55	.5872	31.89
.00003	.000004		.9389	103.13	.5614	35.06
.00003	.000004		.9589	98.92	.5326	39.06
.00005	.000007		.9788	95.03	.4984	42.83
.00010	.000013		1.0000	91.07	.4450	46.76
.00019	.000025		1.0188	88.15	.3342	49.7
.00042	.000056		1.0388	85.19	.272	52.8
.00102	.000141		1.0587	80.57	.240	57.6
.00293	.000444		1.0787	75.25	.21	63.3
.00907	.00167	1.09998	1.1000	69.68	.19	69.4
.02341	.00596	1.11994	1.1200	63.78	.17	75.9
.05479	.0213	1.13981	1.1400	57.98	.16	82.5
.1212	.0692	1.15940	1.1600	52.52	.16	88.8
.2427	.1796	1.17850	1.1800	48.02	.18	94.0
.4207	.3575	1.19704	1.2000	44.70	.22	98.0
.6349	.5774	1.21525	1.2200	42.46	.27	100.7
1.005	.9575	1.24214	1.2500	40.13	.35	103.6
1.689	1.654	1.2865	1.3000	37.55	.47	106.8
2.416	2.389	1.3304	1.3500	35.84	.59	109.1
3.171	3.149	1.3741	1.400	34.54	.68	110.9
3.960	3.942	1.4177	1.450			
4.794	4.779	1.4609	1.500			
6.700	6.689	1.5452	1.600			
9.034	9.026	1.6260	1.700			
12.06		1.7022	1.800			
16.11		1.769	1.900			
21.25		1.828	2.000			
27.48		1.877	2.100			
42.26		1.956	2.301			
58.78		2.019	2.501			

HELIUM 4 ON GRAFOIL AT T = 5.004 K

P_w	C_o -	P	N	N_o	$-\mu$	C	S	$-\Omega$
0.	.008			.009988	199	.008	.0225	.42
	.046			.019966	174.9	.049	.0415	.79
	.076			.02996	168.2	.076	.0760	.96
	.091			.03999	163.4	.091	.1124	1.13
	.10			.04992	161.29	.099	.1503	1.22
	.10			.05992	158.78	.104	.1861	1.36
	.115			.07997	157.26	.116	.2548	1.47
	.127			.09984	155.79	.128	.3148	1.60
	.139			.11993	154.05	.140	.3710	1.79
	.165			.15988	151.79	.166	.4725	2.10
	.194			.19986	150.20	.196	.5600	2.39
	.231			.2499	148.33	.233	.6547	2.81
	.27			.3001	146.87	.273	.7318	3.21
	.314			.3502	145.75	.316	.7926	3.57
	.358			.4002	144.17	.360	.8387	4.17
	.405			.4499	143.00	.407	.8732	4.66
	.453			.5002	141.73	.455	.8913	5.27
	.504			.5494	139.77	.504	.8955	6.29
	.554			.6001	137.51	.553	.8881	7.59
	.602			.6493	135.26	.600	.8699	9.00
0.	.637			.7001	131.87	.637	.8437	11.28
.00001	.65	.000001		.7492	128.02	.658	.8041	14.07
.000005	.66	.000001		.8000	122.95	.663	.7633	18.00
.00001	.653	.000001		.8490	116.84	.664	.7194	23.05
.00002	.656	.000003		.9000	109.61	.666	.6694	29.37
.00004	.66	.000005		.9189	106.02	.672	.6472	32.64
.00011	.676	.000015		.9389	102.56	.683	.6227	35.86
.00018	.704	.000025		.9589	98.33	.705	.5965	39.88
.00038	.762	.000053		.9788	94.24	.750	.5675	43.84
.00091	.943	.000131		1.0000	89.94	.874	.5305	48.10
.00177	1.532	.000266		1.0188	85.58	1.28	.4731	52.50
.00284	.902	.000445		1.0388	83.78	1.30	.355	54.36
.00564	.583	.000972	1.05869	1.0587	79.76	.78	.292	58.6
.01249	.459	.00257	1.07868	1.0787	74.75	.55	.25	63.9
.02936	.399	.00840	1.09993	1.1000	69.28	.46	.23	69.9
.06245	.385	.0260	1.11978	1.1200	63.52	.42	.21	76.3
.1322	.429	.0785	1.13938	1.1400	57.95	.42	.21	82.6
.2724	.530	.2086	1.15840	1.1600	52.92	.55	.22	88.4
.5109	.645	.4496	1.17658	1.1800	48.77	.60	.25	93.2
.8465	.745	.7946	1.19399	1.2000	45.73	.63	.29	96.8
1.245		1.203	1.21093	1.2200	43.56	.64	.34	99.5
1.927		1.895	1.2357	1.2500	41.23	.61	.42	102.3
3.179	1.270	3.158	1.2762	1.3000	38.55	.56	.53	105.8
4.505		4.489	1.3162	1.3500	36.73	.53	.64	108.1
5.880		5.868	1.3557	1.400	35.32	.53	.74	110.1
7.311		7.301	1.3949	1.450				
8.802	2.62	8.794	1.4337	1.500				
12.09	3.36		1.5100	1.600				
15.85	4.15		1.582	1.700				
20.27			1.649	1.800				
25.62			1.709	1.900				
31.88			1.762	2.000				
39.06			1.808	2.100				
55.65			1.883	2.301				
74.16	6.28		1.942	2.501				

HELIUM 4 ON GRAFOIL AT T = 5.478 K

P_w	C_o-	P	N	N_o	$-\mu$	C	S	$-\Omega$
0.	.009			.009988	200	.010	.0233	.42
	.053			.019966	176.6	.054	.0463	.78
	.077			.02996	170.0	.078	.0830	.94
	.092			.03999	165.2	.092	.1207	1.11
	.10			.04992	163.01	.098	.1592	1.21
	.11			.05992	160.57	.106	.1956	1.34
	.117			.07997	158.73	.118	.2654	1.47
	.130			.09984	157.18	.131	.3266	1.61
	.141			.11993	155.36	.142	.3838	1.81
	.168			.15988	152.91	.170	.4877	2.15
	.198			.19986	151.18	.200	.5779	2.46
	.235			.2499	149.18	.237	.6759	2.91
	.276			.3001	147.52	.279	.7568	3.37
	.319			.3502	146.27	.322	.8214	3.77
	.363			.4002	144.58	.366	.8716	4.41
	.410			.4499	143.29	.412	.9103	4.96
0.	.457			.5002	141.79	.459	.9327	5.67
.00001	.505	.000001		.5494	139.81	.507	.9412	6.70
.00000	.553	.000000		.6001	137.39	.555	.9381	8.10
.00002	.599	.000003		.6493	135.04	.600	.9241	9.57
.00000	.637	.000000		.7001	131.56	.638	.9014	11.91
.00003	.662	.000004		.7492	127.66	.666	.8640	14.74
.000005	.671	.000001		.8000	122.55	.679	.8240	18.70
.00003	.675	.000004		.8490	116.43	.685	.7805	23.75
.00017	.677	.000025		.9000	109.04	.689	.7306	30.22
.00030	.68	.000044		.9189	105.55	.692	.7089	33.39
.00065	.690	.000096		.9389	101.88	.700	.6851	36.81
.00120	.706	.000183		.9583	97.81	.713	.6603	40.67
.00244	.739	.000391		.9788	93.44	.739	.6343	44.91
.00527	.807	.000928	.99999	1.0000	89.16	.790	.6034	49.14
.00990	1.040	.00197	1.01878	1.0188	84.21	.947	.5668	54.15
.01768	1.698	.00416	1.03877	1.0388	80.73	1.41	.508	57.73
.02450	.995	.00653	1.05864	1.0587	78.16	1.43	.381	60.43
.04085	.666	.0138	1.07859	1.0787	73.95	.92	.32	64.9
.08064	.561	.0383	1.09971	1.1000	68.74	.65	.28	70.6
.1579	.556	.1007	1.11927	1.1200	63.31	.57	.26	76.6
.3155	.637	.2513	1.13822	1.1400	58.03	.60	.26	82.6
.6068	.775	.5481	1.15617	1.1600	53.48	.63	.27	87.8
1.057	.907	1.011	1.17298	1.1800	49.70	.64	.30	92.3
1.647	1.023	1.611	1.1888	1.2000	46.87	.63	.35	95.6
2.324		2.296	1.2041	1.2200	44.78	.62	.40	98.2
3.460		3.440	1.2262	1.2500	42.35	.61	.53	101.2
5.522	1.623	5.509	1.2618	1.3000	39.63	.60	.59	104.6
7.697		7.687	1.2967	1.3500	37.67	.60	.75	107.2
9.946		9.939	1.3310	1.400	36.21	.61	.80	109.2
12.32			1.3656	1.450				
14.73	3.11		1.3992	1.500				
19.83	3.92		1.464	1.600				
25.39	4.71		1.526	1.700				
31.48			1.584	1.800				
38.33			1.637	1.900				
45.88			1.685	2.000				
54.16			1.727	2.100				
72.65			1.799	2.301				
93.03	6.95		1.864	2.501				

HELIUM 4 ON GRAFOIL AT T = 5.999 K

P_w	C_o	P	N	N_o	$-\mu$	C	S	$-\Omega$
0.	.012			.009988	201	.013	.0244	.42
	.056			.019966	178.6	.057	.0514	.76
	.079			.02996	172.0	.078	.0901	.93
	.092			.03999	167.3	.091	.1290	1.09
	.10			.04992	164.91	.099	.1681	1.20
	.108			.05992	162.59	.107	.2054	1.33
	.119			.07997	160.38	.119	.2762	1.48
	.132			.09984	158.74	.133	.3386	1.63
	.144			.11993	156.82	.145	.3969	1.84
	.172			.15988	154.21	.174	.5033	2.20
	.203			.19986	152.27	.205	.5964	2.55
	.240			.2499	150.17	.243	.6977	3.02
0.	.282			.3001	148.27	.284	.7824	3.55
.000005	.326	.000001		.3502	146.90	.329	.8510	3.99
.00000	.370	.000000		.4002	145.06	.374	.9052	4.68
.00001	.415	.000002		.4499	143.66	.419	.9479	5.28
.00000	.462	.000000		.5002	141.92	.465	.9746	6.10
.00003	.510	.000005		.5494	139.89	.512	.9876	7.16
.00002	.557	.000003		.6001	137.31	.559	.9887	8.65
.00003	.602	.000005		.6493	134.82	.605	.9787	10.20
.00003	.640	.000005		.7001	131.27	.644	.9595	12.60
.00011	.670	.000017		.7492	127.27	.676	.9248	15.50
.00013	.688	.000020		.8000	122.12	.696	.8865	19.49
.00023	.696	.000035		.8490	115.96	.707	.8437	24.57
.00124	.702	.000197		.9000	108.46	.715	.7943	31.14
.00200	.703	.000328		.9189	105.00	.717	.7727	34.29
.00363	.712	.000630	.93889	.9389	101.22	.725	.7497	37.79
.00640	.723	.00120	.95889	.9589	97.20	.734	.7258	41.62
.01159	.744	.00246	.97878	.9788	92.75	.750	.7015	45.94
.02139	.782	.00548	.99996	1.0000	88.34	.779	.6738	50.30
.03523	.871	.0112	1.01871	1.0188	83.38	.844	.6447	55.31
.06018	1.159	.0248	1.03862	1.0388	79.02	1.03	.610	59.80
.09818	1.95	.0512	1.05835	1.0587	74.77	1.55	.552	64.26
.1309	1.262	.0774	1.07818	1.0787	72.19	1.48	.430	67.03
.2220	.911	.1601	1.09894	1.1000	67.90	1.25	.355	71.70
.4069	.888	.3435	1.11777	1.1200	62.99	.99	.32	77.1
.7547	1.000	.7003	1.13550	1.1400	58.29	.84	.32	82.5
1.316	1.145	1.275	1.15185	1.1600	54.09	.79	.33	87.3
2.087	1.273	2.057	1.1669	1.1800	50.70	.77	.36	91.2
3.023	1.386	3.000	1.1808	1.2000	48.11	.74	.41	94.3
4.060		4.043	1.1942	1.2200	46.00	.71	.45	96.9
5.771		5.759	1.2132	1.2500	43.64	.69	.52	99.8
8.848	1.97	8.840	1.2435	1.3000	40.82	.66	.64	103.4
12.16			1.2735	1.3500	38.80	.63	.75	106.1
15.51			1.3023	1.400	37.16	.61	.85	108.3
18.96			1.3305	1.450				
22.49	3.41		1.3584	1.500				
29.81	4.18		1.412	1.600				
37.50	4.92		1.463	1.700				
45.57			1.512	1.800				
54.21			1.557	1.900				
63.33			1.599	2.000				
73.00			1.638	2.100				
93.79			1.705	2.301				
116.2	7.51		1.760	2.501				

HELIUM 4 ON GRAFOIL AT T = 6.568 K

P_w	C_o-	P	N	N_o	-μ	C	S	-Ω
0.	.015			.009988	202	.018	.0257	.42
	.059			.019966	180.9	.060	.0567	.75
	.077			.02996	174.2	.078	.0971	.91
	.091			.03999	169.7	.091	.1373	1.07
	.100			.04992	166.99	.099	.1772	1.19
	.107			.05992	164.83	.108	.2151	1.31
	.119			.07997	162.22	.120	.2840	1.50
	.134			.09984	160.47	.136	.3507	1.65
0.	.147			.11993	158.45	.149	.4102	1.87
.000005	.176	.000001		.15988	155.65	.179	.5193	2.26
.00001	.207	.000002		.19986	153.51	.210	.6151	2.65
.00001	.246	.000002		.2499	151.27	.250	.7200	3.15
.00001	.287	.000002		.3001	149.14	.293	.8084	3.74
.00002	.332	.000003		.3502	147.62	.337	.8811	4.23
.00003	.38	.000004		.4002	145.64	.384	.9395	4.97
.00004	.423	.000006		.4499	144.08	.428	.9863	5.63
.00005	.469	.000008		.5002	142.14	.474	1.0171	6.56
.00008	.514	.000013		.5494	139.99	.520	1.0341	7.68
.00010	.562	.000016		.6001	137.31	.567	1.0396	9.22
.00017	.61	.000027		.6493	134.60	.614	1.0339	10.92
.00024	.648	.000038		.7001	131.01	.655	1.0182	13.34
.00050	.682	.000080		.7492	126.85	.691	.9866	16.36
.00096	.705	.000157		.8000	121.68	.717	.9503	20.36
.00223	.719	.000383		.8490	115.43	.733	.9088	25.52
.00661	.730	.00129	.89999	.9000	107.87	.746	.8603	32.13
.01003	.74	.00211	.91888	.9189	104.35	.750	.8390	35.34
.01584	.74	.00374	.93887	.9389	100.59	.758	.8166	38.83
.02477	.754	.00682	.95885	.9589	96.49	.766	.7934	42.73
.03905	.774	.0131	.97671	.9788	92.11	.779	.7704	46.98
.06478	.810	.0277	.99982	1.0000	87.49	.800	.7448	51.56
.1017	.877	.0540	1.01845	1.0188	82.72	.844	.7200	56.37
.1719	1.020	.1134	1.03810	1.0388	77.85	.924	.694	61.39
.2994	1.41	.2354	1.05728	1.0587	72.93	1.26	.663	66.55
.5126	2.56	.4515	1.07602	1.0787	68.49	1.68	.588	71.31
.7579	2.38	.7038	1.09593	1.1000	65.94	1.90	.506	74.08
1.108	1.716	1.063	1.11373	1.1200	62.43	1.83	.441	77.98
1.766	1.690	1.732	1.1298	1.1400	58.42	1.65	.411	82.51
2.699	1.755	2.674	1.1443	1.1600	54.78	1.46	.42	86.7
3.859	1.829	3.841	1.1574	1.1800	51.79	1.28	.44	90.2
5.196	1.900	5.182	1.1695	1.2000	49.33	1.12	.48	93.1
6.645		6.634	1.1810	1.2200	47.36	1.01	.53	95.5
8.995		8.987	1.1971	1.2500	45.02	.90	.59	98.4
13.29	2.32		1.2230	1.3000	42.09	.80	.71	102.1
17.74			1.2472	1.3500	39.95	.73	.81	105.0
22.32			1.2705	1.400	38.20	.68	.91	107.4
27.00			1.2933	1.450				
31.77	3.55		1.3157	1.500				
41.53	4.21		1.3588	1.600				
51.58	4.85		1.400	1.700				
61.89			1.440	1.800				
72.61			1.477	1.900				
83.62			1.513	2.000				
95.01			1.546	2.100				
118.8			1.606	2.301				
143.8	7.78		1.657	2.501				

HELIUM 4 ON GRAFOIL AT T = 7.188 K

P_w	C_o -	P	N	N_o	$-\mu$	C	S	$-\Omega$
0.	.022			.009988	204	.023	.0277	.42
	.062			.019966	183.6	.063	.0623	.73
0.	.080			.02996	176.7	.079	.1043	.90
.000005	.092	.000001		.03999	172.4	.092	.1456	1.05
.00001	.098	.000002		.04992	169.32	.099	.1860	1.19
.00000	.110	.000000		.05992	167.30	.110	.2250	1.30
.000015	.122	.000002		.07997	164.28	.122	.2980	1.51
.00002	.138	.000003		.09984	162.40	.139	.3631	1.68
.000025	.152	.000004		.11993	160.26	.153	.4239	1.91
.000035	.183	.000006		.15988	157.28	.185	.5358	2.33
.00005	.213	.000008		.19986	154.91	.216	.6343	2.75
.00008	.254	.000013		.2499	152.50	.257	.7429	3.29
.00010	.299	.000016		.3001	150.17	.302	.8353	3.94
.00014	.341	.000023		.3502	148.43	.347	.9119	4.50
.00018	.39	.000030		.4002	146.34	.393	.9746	5.29
.00024	.433	.000040		.4499	144.58	.439	1.0253	6.04
.00032	.480	.000053		.5002	142.45	.486	1.0604	7.04
.00048	.527	.000080		.5494	140.13	.533	1.0816	8.26
.00064	.573	.000108		.6001	137.38	.579	1.0913	9.84
.00103	.619	.000176		.6493	134.41	.625	1.0897	11.70
.00156	.662	.000272		.7001	130.76	.670	1.0740	14.16
.00278	.700	.000506		.7492	126.45	.709	1.0497	17.29
.00525	.731	.00102	.79999	.8000	121.21	.742	1.0161	21.35
.01097	.751	.00242	.84898	.8490	114.89	.764	.9763	26.56
.02558	.772	.00721	.89995	.9000	107.22	.784	.9292	33.27
.03523	.779	.0113	.91883	.9189	103.69	.788	.9082	36.48
.05048	.795	.0192	.93878	.9389	99.89	.800	.8867	40.02
.07361	.813	.0336	.95870	.9589	95.80	.810	.8642	43.90
.1109	.846	.0612	.97844	.9788	91.42	.823	.8424	48.16
.1796	.903	.1204	.99931	1.0000	86.79	.847	.8184	52.74
.2830	1.002	.2193	1.01757	1.0188	81.98	.88	.7974	57.60
.4824	1.174	.4207	1.03648	1.0388	77.05	.95	.777	62.68
.8390	1.464	.7870	1.05440	1.0587	72.08	1.11	.756	67.89
1.424	1.978	1.385	1.07117	1.0787	67.37	1.44	.734	72.94
2.353	3.28	2.326	1.0874	1.1000	63.10	1.90	.699	77.59
3.473	4.70	3.453	1.1013	1.1200	59.87	2.30	.653	81.17
4.743	5.08	4.728	1.1143	1.1400	57.85	2.45	.614	83.45
5.916	4.51	5.904	1.1279	1.1600	55.23	2.40	.597	86.47
7.108	3.54	7.098	1.1415	1.1800	52.72	2.25	.596	89.40
8.693	3.15	8.684	1.1528	1.2000	50.56	2.09	.609	91.98
10.49		10.48	1.1631	1.2200	48.70	1.92	.635	94.23
13.57			1.1776	1.2500	46.37	1.70	.69	97.1
18.89	2.96		1.1991	1.3000	43.41	1.39	.78	100.9
24.52			1.2190	1.3500	41.16	1.14	.88	103.8
30.32			1.2379	1.400	39.31	.92	.96	106.4
36.24			1.2562	1.450				
42.27	3.72		1.2740	1.500				
54.52	4.21		1.3081	1.600				
67.04	4.71		1.3408	1.700				
79.71			1.3726	1.800				
92.71			1.402	1.900				
105.9			1.431	2.000				
119.3			1.459	2.100				
146.8			1.509	2.301				
175.1	7.64		1.555	2.501				

HELIUM 4 ON GRAFOIL AT T = 7.870 K

P_w	C_o-	P	N	N_o	-μ	C	S	-Ω
0.	.024			.009988	206	.030	.0299	.42
0.	.064			.019966	186.7	.064	.0681	.71
.00003	.079	.000005		.02996	179.5	.079	.1115	.89
.00003	.092	.000005		.03999	175.3	.092	.1539	1.03
.00006	.100	.000010		.04992	171.94	.101	.1951	1.19
.00008	.110	.000014		.05992	170.05	.109	.2350	1.29
.00010	.122	.000017		.07997	166.60	.121	.3091	1.53
.00013	.140	.000021		.09984	164.56	.140	.3758	1.71
.00018	.155	.000031		.11993	162.29	.156	.4380	1.96
.00025	.187	.000043		.15988	159.11	.188	.5527	2.41
.00035	.220	.000061		.19986	156.50	.223	.6543	2.87
.00048	.261	.000084		.2499	153.91	.265	.7666	3.46
.00065	.306	.000115		.3001	151.35	.308	.8630	4.16
.00086	.353	.000153		.3502	149.39	.358	.9438	4.80
.00111	.40	.000199		.4002	147.17	.405	1.0106	5.63
.00144	.445	.000261		.4499	145.18	.451	1.0656	6.48
.00192	.493	.000354		.5002	142.86	.499	1.1050	7.58
.00265	.540	.000500		.5494	140.34	.547	1.1305	8.90
.00361	.586	.000699	.60009	.6001	137.49	.595	1.1443	10.54
.00539	.633	.00109	.64929	.6493	134.30	.642	1.1469	12.54
.00794	.680	.00170	.70009	.7001	130.51	.689	1.1354	15.09
.01278	.723	.00294	.74918	.7492	126.09	.733	1.1149	18.30
.02166	.760	.00587	.79996	.8000	120.71	.769	1.0844	22.47
.03841	.793	.0131	.84892	.8490	114.32	.801	1.0470	27.74
.07689	.831	.0358	.89980	.9000	106.53	.827	1.0020	34.55
.1025	.850	.0546	.91860	.9189	102.98	.832	.9816	37.78
.1432	.883	.0880	.93843	.9389	99.16	.848	.9611	41.34
.2074	.931	.1462	.95813	.9589	95.06	.863	.9398	45.23
.3134	.999	.2493	.97751	.9788	90.69	.88	.9192	49.47
.5100	1.115	.4489	.99780	1.0000	86.09	.90	.8981	54.03
.8050	1.296	.7522	1.01500	1.0188	81.32	.94	.880	58.84
1.325	1.553	1.284	1.03235	1.0388	76.44	1.01	.864	63.87
2.132	1.875	2.102	1.0482	1.0587	71.62	1.11	.853	68.93
3.260	2.23	3.239	1.0625	1.0787	67.05	1.26	.848	73.82
4.813	2.59	4.798	1.0759	1.1000	63.01	1.53	.851	78.22
6.544	3.01	6.533	1.0873	1.1200	59.53	1.90	.856	82.08
8.483	3.52	8.474	1.0975	1.1400	56.57	2.24	.856	85.43
10.60	4.59	10.59	1.1069	1.1600	54.12	2.50	.852	88.25
12.99	5.83		1.1161	1.1800	52.17	2.67	.853	90.53
15.36	6.42		1.1244	1.2000	50.53	2.75	.861	92.48
17.84			1.1322	1.2200	49.44	2.75	.874	93.81
21.68			1.1433	1.2500	47.50	2.62	.902	96.19
28.26	7.23		1.1608	1.3000	44.69	2.34	.959	99.77
35.02			1.1775	1.3500	42.37	2.06	1.017	102.83
41.80			1.1939	1.400	40.37	1.82	1.073	105.59
48.27			1.2120	1.450				
54.93	5.35		1.2292	1.500				
69.24	5.05		1.2583	1.600				
84.08	5.18		1.2846	1.700				
99.06			1.3104	1.800				
114.4			1.3340	1.900				
129.8			1.3573	2.000				
145.6			1.3785	2.100				
177.3			1.420	2.301				
209.5	7.42		1.458	2.501				

HELIUM 4 ON GRAFOIL AT T = 8.614 K

P_w	C_o	P	N	N_o	$-\mu$	C	S	$-\Omega$
0.	.04			.009988	209	.034	.0331	.41
.00004	.064	.000007		.019966	190.3	.066	.0739	.69
.00014	.080	.000025		.02996	182.7	.080	.1187	.88
.00017	.092	.000031		.03999	178.5	.091	.1622	1.02
.00027	.102	.000049		.04992	174.96	.101	.2043	1.18
.00039	.108	.000071		.05992	173.02	.108	.2447	1.29
.00052	.121	.000095		.07997	169.24	.123	.3200	1.56
.00071	.141	.000131		.09984	166.96	.143	.3885	1.76
.00091	.158	.000169		.11993	164.59	.160	.4522	2.02
.00131	.189	.000247		.15988	161.15	.192	.5698	2.50
.00179	.226	.000343		.19986	158.32	.229	.6746	3.00
.00245	.269	.000479		.2499	155.47	.274	.7908	3.65
.00326	.312	.000651		.3001	152.74	.318	.8911	4.40
.00421	.365	.000863	.35019	.3502	150.47	.369	.9767	5.14
.00539	.41	.00113	.40019	.4002	148.15	.418	1.0479	6.01
.00691	.458	.00150	.44989	.4499	145.88	.464	1.1068	6.97
.00891	.507	.00201	.50019	.5002	143.39	.511	1.1506	8.15
.01180	.558	.00281	.54938	.5494	140.63	.56	1.1806	9.60
.01554	.608	.00392	.60007	.6001	137.67	.613	1.1988	11.30
.02152	.657	.00595	.64926	.6493	134.24	.662	1.2058	13.45
.02966	.709	.00913	.70005	.7001	130.31	.713	1.1987	16.10
.04315	.760	.0155	.74911	.7492	125.74	.762	1.1823	19.41
.06701	.807	.0294	.79984	.8000	120.28	.802	1.1552	23.64
.1119	.863	.0620	.84869	.8490	113.67	.843	1.1212	29.10
.2180	.947	.1560	.89924	.9000	105.82	.879	1.0788	35.96
.2932	.988	.2292	.91780	.9189	102.23	.86	1.0587	39.23
.4150	1.068	.3518	.93724	.9389	98.40	.87	1.0402	42.79
.6078	1.175	.5494	.95632	.9589	94.29	.89	1.0203	46.70
.9184	1.339	.8684	.97475	.9788	89.95	.92	1.001	50.91
1.447	1.549	1.408	.99363	1.0000	85.39	.96	.984	55.43
2.159	1.827	2.130	1.00892	1.0188	80.74	1.01	.969	60.12
3.227	2.13	3.206	1.0239	1.0388	76.07	1.07	.960	64.94
4.638	2.43	4.622	1.0373	1.0587	71.51	1.15	.957	69.71
6.368	2.70	6.357	1.0493	1.0787	67.32	1.23	.963	74.20
8.525	2.92	8.516	1.0605	1.1000	63.54	1.31	.976	78.32
10.80	3.08		1.0700	1.1200	60.31	1.40	.997	81.91
13.41			1.0791	1.1400	57.51	1.55	1.022	85.07
16.07			1.0871	1.1600	55.15	1.74	1.051	87.79
18.87			1.0943	1.1800	53.11	1.90	1.080	90.17
21.75	3.56		1.1012	1.2000	51.36	2.03	1.108	92.26
24.74			1.1076	1.2200	49.82	2.13	1.133	94.12
29.33			1.1167	1.2500	47.83	2.23	1.163	96.57
37.21	4.14		1.1309	1.3000	45.05	2.33	1.212	100.12
45.33			1.1439	1.3500	42.77	2.39	1.259	103.13
53.62			1.1560	1.400	40.83	2.46	1.304	105.80
62.05			1.1676	1.450				
70.57	7.3		1.1789	1.500				
87.78	8.18		1.2001	1.600				
105.2	8.70		1.2202	1.700				
122.7			1.2402	1.800				
140.6			1.2582	1.900				
158.4			1.2764	2.000				
176.3			1.2940	2.100				
212.6			1.3267	2.301				
249.1	10.92		1.3576	2.501				

HELIUM 4 ON GRAFOIL AT T = 9.436 K

P_w	C_o-	P	N	N_o	-μ	C	S	-Ω
.00002	.032	.000004		.009988	213	.031	.0361	.41
.00026	.068	.000049		.019966	194.2	.067	.0800	.67
.00059	.081	.000113		.02996	186.4	.079	.1261	.87
.00089	.091	.000173		.03999	182.1	.092	.1705	1.02
.00128	.101	.000251		.04992	178.41	.101	.2134	1.18
.00169	.108	.000336		.05992	176.26	.111	.2545	1.30
.00238	.125	.000483		.07997	172.28	.126	.3313	1.58
.00322	.145	.000669		.09984	169.65	.147	.4017	1.81
.00400	.162	.000846		.11993	167.20	.165	.4669	2.08
.00575	.197	.00126	.15987	.15988	163.45	.200	.5876	2.61
.00758	.235	.00173	.19985	.19986	160.42	.239	.6959	3.15
.01016	.282	.00243	.24988	.2499	157.25	.286	.8163	3.86
.01312	.328	.00329	.30008	.3001	154.34	.334	.9208	4.66
.01651	.378	.00436	.35017	.3502	151.75	.383	1.0108	5.50
.02045	.427	.00569	.40017	.4002	149.28	.430	1.0864	6.43
.02527	.478	.00751	.44986	.4499	146.77	.484	1.1498	7.50
.03132	.526	.0100	.50015	.5002	144.01	.532	1.1978	8.81
.03945	(.63)	.0138	.54933	.5494	141.07	.58	1.233	10.35
.04986	.635	.0192	.60000	.6001	137.89	.635	1.2555	12.18
.06576	.691	.0288	.64916	.6493	134.32	.686	1.2670	14.14
.08740	.752	.0435	.69989	.7001	130.19	.740	1.2647	17.20
.1239	.820	.0719	.74886	.7492	125.40	.796	1.2530	20.67
.1906	.894	.1305	.79941	.8000	119.74	.844	1.2300	25.06
.3256	1.001	.2613	.84785	.8490	113.08	.84	1.195	30.55
.6525	1.188	.5949	.89744	.9000	105.06	.88	1.155	37.57
.8906	1.306	.8398	.91528	.9189	101.47	.89	1.137	40.83
1.254	1.468	1.212	.93369	.9389	97.63	.91	1.119	44.41
1.791	1.675	1.757	.95136	.9589	93.55	.94	1.102	48.28
2.560	1.930	2.534	.9680	.9788	89.26	.98	1.085	52.45
3.687	2.22	3.668	.9843	1.0000	84.81	1.02	1.072	56.85
5.013	2.53	4.999	.9974	1.0188	80.34	1.07	1.063	61.37
6.741	2.80	6.730	1.0099	1.0388	75.95	1.12	1.059	65.89
8.791	3.03	8.783	1.0211	1.0587	71.73	1.17	1.062	70.31
11.17	3.2		1.0313	1.0787	67.84	1.19	1.072	74.48
14.04	3.32		1.0412	1.1000	64.38	1.21	1.089	78.25
16.87			1.0493	1.1200	61.38	1.20	1.112	81.58
19.85			1.0568	1.1400	58.72	1.19	1.139	84.58
23.00			1.0636	1.1600	56.45	1.18	1.168	87.20
26.28			1.0699	1.1800	54.46	1.17	1.198	89.52
29.61	3.66		1.0759	1.2000	52.72	1.15	1.230	91.60
33.07			1.0813	1.2200	51.16	1.15	1.261	93.49
38.36			1.0891	1.2500	49.07	1.23	1.308	96.06
47.40	3.88		1.1011	1.3000	46.23	1.38	1.382	99.68
56.69			1.1121	1.3500	43.83			102.8
66.18			1.1221	1.400	41.74			105.7
75.80			1.1316	1.450				
85.54	4.33		1.1408	1.500				
105.2	4.58		1.1579	1.600				
125.2	4.86		1.1733	1.700				
145.1			1.1894	1.800				
165.4			1.2034	1.900				
185.7			1.2175	2.000				
206.2			1.2305	2.100				
247.1			1.2568	2.301				
288.4	7.26		1.2806	2.501				

HELIUM 4 ON GRAFOIL AT T = 10.34 K

P_w	C_o-	P	N	N_o	-μ	C	S	-Ω
.00018	.031	.000036		.009988	217	.036	.0389	.40
.00124	.066	.000254	.019965	.019966	198.7	.063	.0861	.66
.00253	.078	.000537	.02996	.02996	190.5	.076	.1332	.86
.00375	.094	.000821	.03999	.03999	186.2	.094	.1790	1.01
.00515	.103	.00116	.04991	.04992	182.34	.099	.2228	1.18
.00661	.115	.00153	.05991	.05992	179.86	.114	.2649	1.32
.00912	.130	.00221	.07996	.07997	175.72	.132	.3430	1.61
.01192	.152	.00302	.09982	.09984	172.71	.149	.4154	1.88
.01455	.171	.00383	.11991	.11993	170.14	.170	.4823	2.16
.02001	.209	.00567	.15985	.15988	166.08	.207	.6064	2.73
.02549	.249	.00775	.19982	.19986	162.80	.247	.7182	3.31
.03279	.299	.0108	.24985	.2499	159.31	.298	.8430	4.10
.04083	.351	.0147	.30003	.3001	156.16	.348	.9521	4.97
.04972	.402	.0194	.35011	.3502	153.29	.400	1.0466	5.90
.05995	.453	.0253	.40008	.4002	150.56	.446	1.1265	6.92
.07271	.514	.0335	.44975	.4499	147.80	.504	1.1952	8.09
.08839	.570	.0444	.50000	.5002	144.85	.556	1.2477	9.49
.1103	.629	.0610	.54913	.5494	141.63	.608	1.287	11.19
.1384	.692	.0840	.59974	.6001	138.24	.661	1.3148	13.13
.1819	.763	.1226	.64878	.6493	134.46	.714	1.3311	15.50
.2470	.845	.1840	.69934	.7001	130.07	.771	1.3338	18.46
.3612	.957	.2972	.74798	.7492	125.07	.83	1.324	22.08
.5716	1.099	.5120	.79793	.8000	119.25	.89	1.305	26.59
1.016	1.326	.9682	.84514	.8490	112.42	.95	1.276	32.23
1.993	1.714	1.962	.89223	.9000	104.30	1.00	1.238	39.33
2.642	1.928	2.617	.9085	.9189	100.69	1.03	1.222	42.62
3.531	2.19	3.511	.9250	.9389	96.85	1.06	1.206	46.19
4.683	2.48	4.668	.9404	.9589	92.80	1.10	1.192	50.03
6.142	2.78	6.130	.9545	.9788	88.67	1.13	1.179	54.05
8.014	3.06	8.005	.9683	1.0000	84.41	1.17	1.170	58.26
10.08	3.28	10.07	.979	1.0188	80.16	1.20	1.165	62.56
12.47	3.48		.9899	1.0388	76.01	1.22	1.165	66.83
15.16	3.64		.9993	1.0587	72.08	1.24	1.170	70.95
18.14	3.75		1.0080	1.0787	68.51	1.24	1.181	74.78
21.55	3.84		1.0166	1.1000	65.29	1.22	1.197	78.28
24.90			1.0237	1.1200	62.46	1.20	1.217	81.42
28.35			1.0303	1.1400	59.96	1.18	1.240	84.25
31.97			1.0363	1.1600	57.75	1.16	1.266	86.80
35.72			1.0418	1.1800	55.79	1.14	1.294	89.08
39.49	4.02		1.0471	1.2000	54.06	1.13	1.318	91.15
43.41			1.0519	1.2200	52.53	1.11	1.342	93.00
49.39			1.0587	1.2500	50.5	1.08	1.387	95.53
59.54	4.13		1.0693	1.3000	47.53			99.3
69.94			1.0790	1.3500				
80.57			1.0876	1.400				
91.38			1.0956	1.450				
102.3	4.38		1.1034	1.500				
124.3	4.53		1.1176	1.600				
146.6	4.7		1.1307	1.700				
169.1			1.1432	1.800				
191.8			1.1546	1.900				
214.4			1.1663	2.000				
237.4			1.1763	2.100				
283.2			1.1970	2.301				
329.4	6.28		1.2155	2.501				

HELIUM 4 ON GRAFOIL AT T = 11.33 K

P_w	C_o-	P	N	N_o	-μ	C	S	-Ω
.00099	.04	.000210	.009987	.009988	222.2	.045	.0427	.38
.00476	.062	.00111	.019960	.019966	203.30	.064	.0917	.66
.00888	.076	.00222	.02995	.02996	195.42	.086	.1400	.85
.01280	.096	.00339	.03997	.03999	190.48	.093	.1876	1.02
.01698	.098	.00476	.04990	.04992	186.78	.102	.2315	1.19
.02094	.117	.00616	.05989	.05992	183.87	.114	.2753	1.35
.02779	.14	.00886	.07993	.07997	179.54	.140	.3554	1.65
.03502	.155	.0120	.09978	.09984	176.16	.153	.4290	1.95
.04146	.179	.0152	.11986	.11993	173.41	.174	.4979	2.25
.05466	.220	.0223	.15978	.15988	169.03	.210	.6255	2.86
.06789	.264	.0305	.19973	.19986	165.48	.254	.7411	3.50
.08568	.321	.0426	.24973	.2499	161.65	.309	.8708	4.36
.1058	.380	.0577	.29986	.3001	158.22	.363	.9845	5.30
.1285	.442	.0760	.34989	.3502	155.08	.417	1.0839	6.32
.1558	.496	.0992	.39980	.4002	152.05	.467	1.1679	7.46
.1918	.570	.1319	.44938	.4499	149.01	.524	1.2421	8.75
.2359	.638	.1734	.49953	.5002	145.83	.576	1.2995	10.26
.3003	.717	.2363	.54850	.5494	142.39	.64	1.344	12.07
.3866	.804	.3227	.59888	.6001	138.70	.70	1.3763	14.19
.5223	.910	.4615	.64757	.6493	134.66	.77	1.3975	16.72
.735	1.053	.680	.6976	.7001	130.08	.83	1.407	19.81
1.117	1.257	1.072	.74524	.7492	124.82	.90	1.405	23.62
1.776	1.533	1.742	.79333	.8000	118.86	.97	1.391	28.24
3.059	1.969	3.037	.8379	.8490	111.77	1.03	1.368	34.09
5.362	2.59	5.348	.8804	.9000	103.55	1.11	1.338	41.28
6.704	2.87	6.693	.8944	.9189	99.94	1.14	1.326	44.56
8.334	3.16	8.325	.9083	.9389	96.17	1.17	1.313	48.07
10.25	3.44	10.24	.9213	.9589	92.27	1.20	1.302	51.77
12.53	3.7		.9335	.9788	88.19	1.22	1.293	55.74
15.24	3.86		.9455	1.0000	84.14	1.23	1.286	59.75
17.90	4.04		.954	1.0188	80.10	1.24	1.283	63.82
20.95	4.17		.9632	1.0388	76.19	1.24	1.284	67.86
24.23	4.28		.9713	1.0587	72.47	1.24	1.289	71.75
27.75	4.35		.9789	1.0787	69.11	1.25	1.299	75.35
31.65	4.40		.9867	1.1000	66.10	1.25	1.314	78.63
35.45			.9931	1.1200	63.41	1.26	1.333	81.62
39.39			.9990	1.1400	61.09	1.25	1.355	84.24
43.46			1.0045	1.1600	59.01	1.25	1.380	86.64
47.66			1.0094	1.1800	57.15	1.24	1.408	88.80
51.86	4.48		1.0143	1.2000				
56.24			1.0186	1.2200	53.96			92.6
62.86			1.0248	1.2500	52.0			95.0
74.10	4.53		1.0345	1.3000				
85.55			1.0435	1.3500				
97.34			1.0511	1.400				
109.3			1.0582	1.450				
121.4	4.66		1.0648	1.500				
145.7	4.74		1.0773	1.600				
170.4	4.86		1.0884	1.700				
195.1			1.0997	1.800				
220.3			1.1088	1.900				
245.3			1.1186	2.000				
270.7			1.1269	2.100				
321.3			1.1441	2.301				
372.4	6.0		1.1589	2.501				

HELIUM 4 ON GRAFOIL AT T = 12.42 K

P_w	C_o-	P	N	N_o	$-\mu$	C	S	$-\Omega$
.00398	.049	.000947	.009983	.009988	227.7	.051	.0472	.38
.01528	.069	.00431	.019945	.019966	208.82	.068	.0978	.65
.02602	.10	.00830	.02992	.02996	200.68	.092	.1489	.85
.03511	.098	.0123	.03994	.03999	195.53	.095	.1961	1.03
.04518	.116	.0173	.04985	.04992	191.60	.107	.2415	1.21
.05399	.124	.0222	.05982	.05992	188.49	.12	.2859	1.38
.06945	.157	.0317	.07984	.07997	183.76	.138	.3686	1.70
.08617	.174	.0432	.09967	.09984	180.14	.159	.4435	2.03
.1009	.197	.0540	.11972	.11993	177.15	.182	.5142	2.36
.1324	.238	.0793	.15958	.15988	172.38	.215	.6448	3.02
.1656	.295	.1082	.19946	.19986	168.51	.261	.7647	3.71
.2124	.368	.1513	.24935	.2499	164.33	.322	.8996	4.66
.2677	.440	.2044	.29937	.3001	160.61	.38	1.0185	5.68
.3331	.515	.2693	.34923	.3502	157.15	.429	1.1229	6.80
.4133	.599	.3500	.39896	.4002	153.86	.49	1.2120	8.04
.5270	.690	.4665	.44828	.4499	150.48	.54	1.2912	9.47
.6628	.792	.6059	.49807	.5002	146.95	.61	1.354	11.15
.8721	.915	.8209	.54658	.5494	143.30	.67	1.405	13.07
1.153	1.066	1.108	.59628	.6001	139.38	.73	1.444	15.32
1.594	1.254	1.557	.64398	.6493	135.05	.79	1.471	18.03
2.257	1.515	2.228	.69243	.7001	130.23	.85	1.486	21.28
3.381	1.877	3.360	.7377	.7492	124.71	.91	1.489	25.28
5.008	2.37	5.074	.7827	.8000	118.50	1.0	1.482	30.09
7.964	3.00	7.955	.8220	.8490	111.28	1.0	1.465	36.05
12.26	3.7		.8595	.9000	102.98	1.1	1.442	43.31
14.40	3.89		.8707	.9189	99.39	1.1	1.432	46.58
16.87	4.15		.8823	.9389	95.62	1.1	1.422	50.08
19.57	4.37		.8932	.9589	91.76	1.1	1.412	53.75
22.63	4.55		.9034	.9788	87.80	1.1	1.403	57.60
26.00	4.67		.9139	1.0000	83.86	1.1	1.396	61.50
29.31	4.80		.921	1.0188	80.01	1.1	1.392	65.38
32.94	4.90		.9291	1.0388	76.31	1.1	1.393	69.20
				1.06	72.87	1.2	1.399	72.80
				1.08	69.81	1.2	1.410	76.08
45.16	5.1		.9504	1.1000	67.04	1.2	1.427	79.10
49.49			.9561	1.1200	64.63			81.8
53.81			.9618	1.1400	62.42			84.3
58.33			.9668	1.1600	60.49			86.5
62.98			.9714	1.1800	58.87			88.4
67.61	5.07		.9761	1.2000				
72.42			.9800	1.2200				
79.68			.9859	1.2500				
91.97	5.06		.9951	1.3000				
104.5			1.0035	1.3500				
117.4			1.0108	1.400				
130.5			1.0172	1.450				
143.7	5.10		1.0235	1.500				
170.2	5.14		1.0353	1.600				
197.3	5.22		1.0451	1.700				
224.4			1.0551	1.800				
251.9			1.0635	1.900				
279.4			1.0719	2.000				
307.1			1.0795	2.100				
362.7			1.0940	2.301				
418.9	6.10		1.1061	2.501				

HELIUM 4 ON GRAFOIL AT T = 13.62 K

P_w	C_o-	P	N	N_o	-μ	C	S	-Ω
.01314	.055	.00372	.009971	.009988	234.10	.052	.0521	.37
.04011	.075	.0149	.019905	.019966	215.14	.067	.1042	.64
.06302	.10	.0278	.02985	.02996	206.65	.075	.1570	.85
.08308	.111	.0412	.03983	.03999	201.08	.096	.2051	1.05
.1041	.124	.0567	.04971	.04992	196.94	.105	.2513	1.23
.1233	(.35)	.0720	.05966	.05992	193.66	.12	.297	1.41
.1590	.160	.1025	.07961	.07997	188.64	.131	.3807	1.76
	.195		.0994	.09984	184.65	.155	.4583	2.12
.2360	.235	.1737	.11935	.11993	181.39	.186	.5315	2.48
.3183	.290	.2544	.15904	.15988	176.15	.230	.6651	3.21
.4090	.359	.3461	.19873	.19986	171.94	.271	.7891	3.96
.5431	.462	.4831	.24832	.2499	167.40	.39	.9301	4.98
.7067	.57	.6511	.29799	.3001	163.31	.45	1.0546	6.11
.9066	.667	.8565	.34742	.3502	159.56	.49	1.164	7.33
1.156	.795	1.111	.39661	.4002	155.92	.52	1.259	8.69
1.517	.948	1.479	.44521	.4499	152.21	.58	1.341	10.27
1.930	1.124	1.898	.49408	.5002	148.43	.63	1.411	12.06
2.572	1.326	2.546	.54135	.5494	144.46	.67	1.468	14.15
3.293	1.594	3.272	.5897	.6001	140.22	.73	1.512	16.58
4.623	1.921	4.607	.6347	.6493	135.61	.79	1.544	19.47
6.308	2.37	6.296	.6801	.7001	130.48	.85	1.564	22.93
8.925	2.93	8.917	.7210	.7492	124.78	.89	1.572	27.06
12.44	3.50		.7619	.8000	118.26	.92	1.57	32.11
17.38	4.24		.795	.8490	110.80	1.0	1.56	38.27
23.91	4.77		.8268	.9000	102.42	1.0	1.54	45.60
26.91	4.95		.8359	.9189	98.77	1.0	1.53	48.92
30.17	5.14		.8457	.9389	95.01	1.0	1.52	52.42
				.96	91.15	1.0	1.51	56.08
37.34	5.41		.8639	.9788	87.24	1.0	1.50	59.88
41.26	5.51		.8735	1.0000	83.52	1.1	1.49	63.56
45.22	5.56		.879	1.0188	79.92	1.1	1.49	67.20
49.41	5.64		.8867	1.0388	76.49	1.2	1.49	70.74
				1.06	73.48			73.9
				1.08	70.78			76.8
63.00	5.74		.9067	1.1000	68.29			79.5
67.82			.9120	1.1200				
72.53			.9175	1.1400				
77.49			.9223	1.1600				
82.64			.9267	1.1800				
87.64	5.7		.9311	1.2000				
92.89			.9349	1.2200				
100.8			.9407	1.2500				
114.1	5.67		.9497	1.3000				
127.7			.9580	1.3500				
141.7			.9649	1.400				
155.8			.9715	1.450				
170.2	5.64		.9775	1.500				
199.0	5.67		.9887	1.600				
228.5	5.71		.9978	1.700				
257.7			1.0082	1.800				
287.6			1.0160	1.900				
317.5			1.0239	2.000				
347.7			1.0307	2.100				
408.3			1.0438	2.301				
469.6	6.33		1.0544	2.501				

HELIUM 4 ON GRAFOIL AT T = 14.90 K

P_w	C_o - P	N	N_o	$-\mu$	S	$-\Omega$
.03506	.055 .0127	.009938	.009988	241.15	.0566	.37
.08861	.076 .0454	.019808	.019966	222.18	.1099	.64
.1353	.083 .0821	.02969	.02996	213.31	.1626	.86
.1786	.123 .1202	.03960	.03999	207.38	.2136	1.06
.2260	.141 .1643	.04940	.04992	202.94	.2605	1.26
.2714	.178 .2081	.05927	.05992	199.44	.308	1.45
.3572	.198 .2937	.07906	.07997	193.92	.3925	1.84
.4600	.242 .3979	.09864	.09984	189.63	.4717	2.22
.5537	.295 .4938	.11842	.11993	186.11	.5498	2.61
.7768	.400 .7231	.15769	.15988	180.40	.6867	3.40
1.028	.492 .9809	.19689	.19986	175.80	.8140	4.23
1.405	.640 1.366	.24579	.2499	170.84	.961	5.34
1.867	.794 1.834	.29460	.3001	166.35	1.091	6.58
2.427	.982 2.400	.34300	.3502	162.20	1.206	7.93
3.117	1.184 3.095	.39089	.4002	158.23	1.305	9.42
4.106	1.441 4.089	.4378	.4499	154.23	1.391	11.12
5.168	1.733 5.154	.4850	.5002	150.10	1.467	13.07
6.796	2.08 6.785	.5295	.5494	145.82	1.53	15.33
8.708	2.49 8.699	.5745	.6001	141.28	1.58	17.93
11.44	3.00	.616	.6493	136.33	1.62	21.03
14.90	3.59	.6576	.7001	130.90	1.64	24.70
19.67	4.16	.6924	.7492	124.90	1.65	29.04
25.30	4.79	.7280	.8000	118.08	1.66	34.33
32.55	5.34	.756	.8490	110.48	1.65	40.60
41.01	5.81	.7833	.9000	101.76	1.63	48.23
44.86	5.94	.7907	.9189	98.06	1.62	51.59
48.81	6.06	.7993	.9389	94.26	1.61	55.13
			.96	90.54	1.60	58.66
57.24	6.24	.8154	.9788	86.92	1.59	62.18
61.59	6.35	.8246	1.0000	83.40		65.7
66.24	6.36	.829	1.0188	79.99		69.1
70.93	6.40	.8363	1.0388	77.29		71.9
85.75	6.48	.8556	1.1000			
90.99		.8608	1.1200			
96.09		.8663	1.1400			
101.5		.8709	1.1600			
107.0		.8751	1.1800			
112.5	6.4	.8795	1.2000			
118.1		.8834	1.2200			
126.6		.8891	1.2500			
141.0	6.38	.8980	1.3000			
155.6		.9064	1.3500			
170.7		.9133	1.400			
185.9		.9199	1.450			
201.3	6.31	.9262	1.500			
232.3	6.30	.9375	1.600			
264.0	6.32	.9469	1.700			
295.3		.9577	1.800			
327.6		.9654	1.900			
359.9		.9731	2.000			
392.4		.9801	2.100			
457.9		.9928	2.301			
524.3	6.71	1.0027	2.501			

TABLE II. HELIUM 4 ON GRAFOIL NEAR ORDERING

N_o=N=	.6093	.6193	.6293	.6393	.6493	.6593	.6693	.6792
T				C_o=C				
2.4113								
2.5237	.746	.689	.642	.597	.573	.571	.599	.643
2.6414	1.025	.938	.868	.803	.777	.784	.827	.887
2.7646	1.502	1.362	1.241	1.124	1.087	1.099	1.161	1.260
2.8283	1.884	1.916	1.811	1.622	1.543	1.549	1.641	1.861
2.8935	1.651	2.060	2.271	2.371	2.195	2.177	2.364	2.499
2.8935								
2.9602	1.352	1.750	2.270	2.916	3.369	3.556	3.374	2.418
3.0285	1.133	1.332	1.576	1.843	2.115	2.183	1.969	1.645
3.1697	.951	1.046	1.144	1.249	1.328	1.359	1.330	1.242
3.3175	.828	.879	.927	.977	1.013	1.036	1.039	1.017
3.4722	.708	.739	.768	.797	.820	.837	.845	.842
3.6341	.683	.706	.729	.750	.767	.782	.791	.794
				S				
2.4113	.2638	.2369	.2115	.1861	.1645	.1464	.1356	.1450
2.5237	.2978	.2683	.2407	.2133	.1907	.1724	.1629	.1743
2.6414	.3445	.3110	.2803	.2500	.2261	.2082	.2006	.2147
2.7646	.4130	.3731	.3369	.3012	.2756	.2582	.2536	.2722
2.8283	.4559	.4168	.3782	.3382	.3108	.2935	.2910	.3146
2.8935	.4935	.4637	.4299	.3922	.3608	.3431	.3448	.3715
2.9602	.5244	.5036	.4816	.4586	.4376	.4242	.4217	.4266
3.0285	.5502	.5340	.5176	.5007	.4858	.4740	.4666	.4641
3.1697	.5935	.5816	.5697	.5576	.5464	.5359	.5272	.5207
3.3175	.6313	.6217	.6120	.6022	.5925	.5831	.5745	.5671
3.4722	.6636	.6554	.6470	.6385	.6299	.6212	.6130	.6055
3.6341	.6947	.6876	.6802	.6726	.6649	.6569	.6491	.6417
				$-\mu$				
2.357		140.31	139.57	138.90	137.93	136.74	135.03	
2.467		139.76	139.29	138.64	137.71	136.58	135.02	
2.582		139.43	138.97	138.35	137.48	136.42	135.03	
2.713		139.01	138.58	138.00	137.21	136.25	135.08	
2.796		138.69	138.28	137.74	137.02	136.16	135.13	
2.861		138.44	138.02	137.52	136.88	136.10	135.20	
2.927		138.23	137.79	137.29	136.72	136.04	135.30	
2.994		138.09	137.64	137.15	136.60	135.99	135.30	
3.087		137.94	137.48	137.00	136.48	135.90	135.26	
3.243		137.75	137.29	136.81	136.31	135.75	135.14	
3.394		137.60	137.14	136.67	136.17	135.62	135.02	
3.552		137.47	137.01	136.53	136.03	135.48	134.90	
3.718		137.35	136.89	136.40	135.90	135.35	134.87	
				$-\Omega$				
2.357		4.42	4.72	5.15	5.77	6.55	7.68	
2.467		4.62	4.92	5.34	5.93	6.67	7.70	
2.582		4.86	5.15	5.55	6.11	6.80	7.71	
2.713		5.16	5.44	5.81	6.31	6.93	7.71	
2.796		5.39	5.65	6.00	6.46	7.02	7.69	
2.861		5.57	5.84	6.16	6.57	7.08	7.66	
2.927		5.73	6.02	6.33	6.70	7.13	7.62	
2.994		5.85	6.14	6.45	6.80	7.20	7.65	
3.087		6.00	6.29	6.60	6.93	7.30	7.72	
3.243		6.20	6.50	6.80	7.13	7.48	7.88	
3.394		6.39	6.68	6.98	7.31	7.66	8.05	
3.552		6.57	6.87	7.17	7.50	7.85	8.23	
3.718		6.76	7.06	7.37	7.69	8.04	8.35	

$P_w \approx P \approx 0.$

TABLE III. HELIUM 4 ON GRAFOIL - SURVEY

P_w	C_o-	P	N	- μ
		T = 1.395		
0.			.0273	
			.0683	
			.1084	
			.1718	
			.2726	
			.4325	
			.6862	
0.			1.088	
.00006		.00000	1.738	
.08105		.039	2.748	12.7
		T = 1.674		
0.	.015		.0273	
	.093		.0683	
	.127		.1084	
	.200		.1718	
	.325		.2726	
	.557		.4325	
	.088		.6862	
0.	.034		1.088	
.00042	.447	.00003	1.738	27.9
.3337	1.13	.269	2.742	12.8
		T = 2.009		
0.	.012		.0273	
	.098		.0683	
	.133		.1084	
	.189		.1718	
	.277		.2726	
	.526		.4325	
	.173		.6862	
0.	.045		1.088	
.00583	.444	.00074	1.738	28.1
1.429	2.34	1.390	2.717	13.0
		T = 2.411		
0.	.017		.0273	
	.107		.0683	
	.139		.1084	
	.188		.1718	
	.262		.2726	
	.444		.4325	
	.393		.6862	
0.	.067		1.088	
.03876	.486	.0126	1.738	28.0
5.368	4.47	5.355	2.645	13.4
		T = 2.894		
0.	.028		.0273	
	.112		.0683	
	.141		.1084	
	.187		.1718	
	.258		.2726	
	.408		.4325	
	1.279		.6862	
0.	.100		1.088	
.1995	.662	.1379	1.736	28.0
15.18	6.50		2.501	14.5

P_w	P	N	- μ
	T = 8.619		
0.		.00434	
		.00686	
0.		.01088	
.00004	.000007	.01723	192
.00011	.000020	.0273	183
.00021	.000038	.0432	178
.00043	.000079	.0683	171.4
.00083	.000154	.1084	165.6
.00145	.000275	.1718	160.6
.00265	.000521	.2726	155.1
.00627	.00135	.4325	146.9
.02676	.00796	.6861	131.6
6.584	6.573	1.050	73.9
91.28		1.208	51.2
237.8		1.357	43.0
	T = 10.35		
.00004	.000008	.00686	234
.00025	.000050	.01088	215.3
.00087	.000177	.01723	202.2
.00203	.000427	.0273	193.1
.00395	.000870	.0432	185.7
.00733	.00173	.0683	178.6
.01267	.00326	.1083	172.0
.02112	.00610	.1718	165.5
.03584	.0122	.2725	158.3
.06724	.0299	.4323	149.1
.2256	.1637	.6853	131.5
17.08		1.004	83.6
125.1		1.121	63.0
309.1		1.216	53.6
	T = 12.43		
0.		.00109	
0.		.00173	
.00004	.000009	.00274	286
.00017	.000037	.00434	268
.00105	.000234	.00685	245.1
.00453	.00109	.01087	225.9
.01154	.00311	.01721	212.9
.02244	.00691	.0272	203.0
.03742	.0134	.0431	194.7
.05908	.0252	.0682	186.9
.09072	.0466	.1081	179.3
.1408	.0867	.1714	171.5
.2359	.1737	.2718	162.9
.4810	.4195	.4307	151.9
2.038	2.007	.6775	132.5
36.44		.9354	96.5
167.1		1.035	77.6
389.3		1.106	67.1

HELIUM 4 ON GRAFOIL - SURVEY

P_w	C_o -	P	N	- μ
		T = 3.472		
0.	.043		.0274	
	.112		.0683	
	.142		.1084	
	.186		.1718	
	.258		.2726	
	.401		.4325	
0.	1.10		.6862	
.00006	.153	.00001	1.088	
1.067	1.28	1.021	1.724	28.3
32.05	7.34		2.308	16.4
		T = 4.167		
0.	.058		.0274	
	.098		.0683	
	.134		.1084	
	.178		.1718	
	.253		.2726	
	.396		.4325	
0.	.719		.6862	
.00113	.232	.00014	1.088	72.8
4.989	2.79	4.975	1.681	29.2
53.62	6.75		2.129	19.4
		T = 5.004		
0.	.070		.0274	
	.113		.0683	
	.133		.1084	
	.177		.1718	
	.253		.2726	
	.396		.4325	
0.	.650		.6862	
.01964	.379	.0047	1.088	72.1
15.85	4.71		1.586	31.6
80.75	6.86		1.964	23.5
		T = 6.000		
0.	.077		.0274	
	.116		.0683	
	.148		.1084	
	.190		.1718	
	.267		.2726	
0.	.408		.4325	
.00006	.646	.00001	.6862	
.1662	.837	.108	1.087	70.5
35.24	5.56		1.452	35.8
119.2	8.06		1.772	28.6
		T = 7.191		
0.	.078		.0274	
0.	.115		.0683	
	.171		.1084	
.00009	.203	.000015	.1718	152
.00013	.267	.000021	.2726	149
.00026	.425	.000043	.4325	144
.00139	.425	.000242	.6862	131.7
1.741	2.77	1.707	1.077	68.0
60.10	5.14		1.326	42.4
172.2			1.557	34.9

P_w	P	N	- μ
	T = 14.92		
.00037	.000089	.00109	315
.00076	.000184	.00173	304.6
.00173	.000428	.00274	291.9
.00493	.00130	.00433	275.4
.01574	.00477	.00683	256.0
.03862	.0145	.01081	239.3
.07262	.0344	.01708	226.5
.1208	.0704	.0270	215.8
.1895	.1303	.0427	206.6
.3017	.2382	.0674	197.6
.4928	.4319	.1067	188.7
.8457	.7943	.1688	179.6
1.604	1.568	.2668	169.5
3.668	3.649	.4190	156.9
13.27		.6385	137.6
70.18		.8361	112.8
223.1		.9353	95.6
484.3		1.003	84.0
	T = 17.92		
.00896	.00270	.00108	325.8
.01601	.00519	.00171	314.0
.02923	.0106	.00269	301.2
.05456	.0238	.00424	286.7
.1015	.0558	.00665	271.5
.1835	.1255	.01044	257.0
.3209	.2579	.01637	244.0
.5499	.4906	.0257	232.5
.9235	.8742	.0404	222.2
1.590	1.554	.0634	211.9
2.780	2.756	.0995	201.6
4.957	4.943	.1560	191.1
9.332	9.323	.2428	179.8
19.52		.3722	166.5
47.96		.5379	150.4
127.8		.6933	132.8
303.7		.7990	117.3
605.4		.8752	105.0

TABLE IV

HELIUM 4 ON GRAFOIL, PRELIMINARY LOW TEMPERATURE COMPOSITE

	3.00 K			1.50 K			0.00 K	
N	$-\mu$	S	$-\Omega$	$-\mu$	S	$-\Omega$	$-\mu$	$-\Omega$
.01	196	.01	.4	194	.01	.4	194	.4
.02	170	.02	.8	169	.01	.8	169	.8
.03	162	.04	1.0	160	.02	1.0	160	1.1
.04	157	.07	1.2	153	.03	1.3	152	1.3
.05	154	.10	1.3	149	.05	1.4	147	1.5
.06	152.0	.14	1.43	147.9	.07	1.53	146.0	1.60
.08	151.2	.20	1.50	147.5	.12	1.57	145.7	1.62
.10	150.3	.25	1.59	146.9	.16	1.61	145.5	1.64
.12	149.1	.29	1.73	146.1	.19	1.70	145.1	1.69
.16	147.8	.38	1.92	145.1	.26	1.84	144.3	1.80
.20	146.5	.46	2.17	144.5	.31	1.97	144.0	1.86
.25	145.5	.53	2.40	144.0	.35	2.08	143.8	1.90
.30	144.5	.58	2.69	143.5	.37	2.22	143.6	1.96
.35	143.7	.62	2.96	143.2	.37	2.31	143.5	2.00
.40	143.1	.64	3.18	142.9	.36	2.44	143.4	2.04
.45	142.6	.65	3.40	142.6	.32	2.58	143.3	2.08
.50	141.5	.62	3.92	142.4	.27	2.73	143.2	2.13
.55	140.3	.59	4.55	142.2	.21	2.85	143.1	2.19
.60	139.1	.54	5.24	142.0	.15	2.97	142.7	2.44
.62	138.1	.52	5.85	141.6	.090	3.24	142.1	2.85
.64	137.1	.48	6.48	140.3	.070	4.14	140.8	3.75
.65	136.6	.46	6.80	139.1	.062	4.97	139.5	4.65
.66	136.0	.45	7.19	137.6	.054	6.00	138.0	5.69
.67	135.3	.44	7.66	135.2	.049	7.60	135.2	7.55
.70	133.3	.44	9.05	132.5	.10	9.45	132.2	9.60
.75	129.3	.44	12.0	129.1	.11	11.9	128.9	12.0
.80	124.6	.42	15.7	124.8	.12	15.2	125.2	14.9
.85	118.8	.38	20.5	120.0	.10	19.2	120.3	18.9
.87	116.5	.36	22.5	117.8	.090	21.1	118.1	20.8
.931	107.9	.25	30.2	109.7	.044	28.4	109.8	28.2
.980	99.8	.14	38.0	100.7	.032	37.0	100.8	36.8
1.028	89.6	.10	48.2	90.2	.024	47.5	90.2	47.5
1.086	74.8	.071	63.8	75.1	.018	63.5	75.1	63.4
1.135	59.5	.058	80.8	59.7	.014	80.6	59.7	80.5
1.172	48.6	.055	93.4	48.6	.012	93.4	48.7	93.2

APPENDIX II

Thermal transpiration

Thermal transpiration, also known as the thermomolecular effect, is simple in outline, but hopelessly complicated in detail. It occurs whenever there is a temperature gradient and the mean free path is not negligible compared with the dimensions of the apparatus. Indeed, Osborne Reynolds (1880) used it to prove that gases <u>have</u> a mean free path! If the mean free path is long, the gas ideal, and the velocity distribution Maxwellian, then a balance in the mass flows between two different temperature regions requires that $P_c/P_w = \sqrt{T_c/T_w}$. If the mean free path is negligible, mass will flow unless $P_c/P_w = 1$. The former regime will always dominate close to a surface, so molecules always creep along a surface in the direction of the thermal gradient.

It is the corrections for nonequilibrium velocity distribution under conditions of both mass and heat flow that makes the theory unwieldy. Surface roughness, nonuniformity, and contamination make the experiments unrepeatable. Fortunately, very few gases exist below

50 K and few solids exist above 2000 K. Within these limits, the maximum transpiration correction to the room temperature pressure is seldom more than a factor of two and many approximations may be tolerated in interpolation formulae (Bennett & Tompkins 1957; Liang 1951, 1955; Takaishi & Sensui 1963).

In helium manometry, on the other hand, the temperature ranges over three orders of magnitude, so the relative error in the cold pressure can be 30 times larger than that in the pressure difference (Watkins, Taylor, & Haubach 1967). The explicit formulae developed in the references above become inconsistent over these large ranges. The sum of the pressure drops calculated for the two halves of a tube is not equal to that calculated for the whole! Instead, one must use the implicit formulae first developed semi-empirically at Leiden (Weber, Keesom, & Schmidt 1937; Roberts & Sydoriak 1956; McConville 1969).

Recent work has shown that there are more independent variables than these formulae imply (Edmonds & Hobson 1965; Hobson 1969, 1970; McConville 1969). In particular, rough surfaces seem to be more reproducible but to require larger pressure corrections than the smooth Pyrex surfaces for which the equations were originally derived. Readjusting the constants in these

equations requires tedious multiple solutions of a cubic equation followed by multiple iterations (McConville 1969). An alternative procedure has been found that is much simpler but gives essentially identical results.

The tube is calibrated as follows. Measure the temperatures T_w and T_c, and the pressures P_w and P_c, at the warm and cold ends, respectively, of the tube (radius r). Use the equation of Weber and Schmidt with <u>their</u> constants to calculate the theoretical cold pressure P_{WS} from the measured values of T_w, T_c, P_w, and r. Calculate the quantity

$$D = (P_w - P_{WS})^{-1} - (P_w - P_c)^{-1} .$$

This quantity is almost completely independent of T_c and P_w. It varied by no more than 25% for $T_c = 1.6$, 4.2, and 77 K, and $0.002 < P_w < 2$ torr, in the experiments done here. (Outside this pressure range it still remained constant within the larger experimental uncertainty.) Therefore, just one calibration point can give a four-fold improvement over using P_{WS} directly, without calibration.

At higher precision, D depends on everything, but is still of tremendous value as an interpolation parameter, since it varies much less than P_c/P_{WS}. For a preliminary data reduction, it was assumed that

$D = 3$ for this experiment's filling line. In the virial gas region of the film, it was found that the entropy calculated from the pressure differed from that found from the heat capacity by an oscillatory term of amplitude ≈ 0.01. This term did not correlate with T or N, but it did correlate with P_w. This seemed to be strong evidence that it was an artifact of the transpiration correction rather than an error in the temperature calibration or a real property of the film. The systematic oscillations were eliminated by using $D = 3.1 - 0.38 \sin(1.14 \log(11 P_w))$. This is the basis of the formula given on page 36.

This still left some nonoscillatory deviation, especially at the lowest pressures. Although the small barocel leaks or systematic errors in the zero correction might have been the cause, a 6% increase in the low pressure limit solved the problem. Nonideal low pressure limits are common if the thermal gradient is steep (Hobson 1969) as it was at the base of the filling line used here. This is the source of the factor "1.12" in the formula for "b" on page 35. The remainder of this formula is identical to that used by Weber and Schmidt.

The effect of varying D is similar to the effect of varying k_2, the surface roughness parameter in

Weber and Schmidt's original derivation. So there probably is a theoretical basis for D being nearly constant. However, the fine tuning given in the preceding two paragraphs is totally empirical and probably unique to the apparatus used. In general, thermal transpiration corrections are a major source of uncertainty and are best avoided by redesign of the system. If this is out of the question, then the interpolation technique given above is recommended. If it is not possible to measure even a single calibration point directly, take a measurement from the literature on a "similar" tube and cross your fingers.

BIBLIOGRAPHY

Ahlers, Guenter, "Thermodynamic Properties of hcp He^4," Phys. Rev. A 2, 1505-26 (1970).

Baskin, Y. and L. Meyer, "Lattice Constants of Graphite at Low Temperatures," Phys. Rev. 100, 544 (1955).

Bennett, M. J. and F. C. Tompkins, "Thermal Transpiration: Application of Liang's Equation," Trans. Faraday Soc. 53, 185-92 (1957).

Bretz, Michael and J. G. Dash, "Quasiclassical and Quantum Degenerate Helium Monolayers," Phys. Rev. Letters 26, 963-65 (1971a).

--- and ---, "Ordering Transitions in Helium Monolayers," Phys. Rev. Letters 27, 647-50 (1971b).

---, G. B. Huff, and J. G. Dash, "Solid Phase of He^4 Monolayers: Debye Temperatures and 'Melting' Anomalies," Phys. Rev. Letters 28, 729-31 (1972).

---, J. G. Dash, D. C. Hickernell, E. O. McLean, and O. E. Vilches, "Phases of He^3 and He^4 Monolayer Films Adsorbed on Basal Plane Graphite," Phys. Rev. A to be published (1973).

--- et al (1973) see above.

Brunauer, Stephen, P. H. Emmett, and Edward Teller, "Adsorption of Gases in Multimolecular Layers," J. Am. Chem. Soc. 60, 309-19 (1938).

Campbell, C. E., J. G. Dash, and M. Schick, "Effects of Lateral Substrate Fields on Helium Monolayers," Phys. Rev. Letters 26, 966-68 (1971).

--- and M. Schick, "Triangular Lattice Gas," Phys. Rev. A 5, 1919-25 (1972).

---, F. J. Milford, A. D. Novaco, and M. Schick, Helium-Monolayer Completion on Graphite," Phys. Rev. A 6, 1648-52 (1972).

Cetas, T. C. and C. A. Swenson, "A Paramagnetic Salt Temperature Scale 0.9 to 18 K," Metrologia 8, 46-64 (1972).

Claiborne, L. T., W. R. Hardin, and N. G. Einspruch, "Ga-Doped Ge Low Temperature Thermometers," Ann. Acad. Sci. Fenn. Ser. A6 No. 210, 49-52 (1966).

Dacey, J. R., "Active Carbon," 995-1024, see (Flood 1967).

Dash, J. G. and J. Siegwarth, "Simple Heat Switch for Low Temperature Use," Rev. Sci. Instr. 34, 1276-77 (1963).

--- and Michael Bretz, "Statistical Mechanics of Monolayers of Bose and Fermi Atoms Adsorbed on Crystalline Surfaces," Phys. Rev. 174, 247-55 (1968).

---, "Theory of T^2 Heat Capacities of Monolayer Helium Films," J. Low Temp. Phys. 1, 173-88 (1969).

---, "Liquid and Solid Monolayers," J. Low Temp. Phys. 3, 301-05 (1970)

---, "Isotherms of Mobile and Localized Ideal Quantum Gases Adsorbed on Crystalline Substrates," Phys. Rev. A 1, 7-14 (1970).

---, R. E. Peierls, and G. A. Stewart, "Desorption, Vapor Pressure, and Absolute Entropy of Adsorbed Films: Application to He^3," Phys. Rev. A 2, 932-36 (1970).

--- and M. Bretz, "Short-Range Order and Melting Anomalies in Thin Films," J. Low Temp. Phys. 9, 291-306 (1972).

---, "Phase Diagram of Helium Monolayers," Proc. 13th Int. Conf. Low Temp. Phys., Boulder Colo. 1972, (1973).

---, "Two Dimensional Matter," Sci. Am. 228, 5, 30-40 (May 1973).

Daunt, J. G. and E. Lerner, "Adsorption of He^4 on Bare and on Argon Coated Exfoliated Graphite at Low Temperatures," J. Low Temp. Phys. 10, 299- (1973).

de Boer, J. and A. Michels, "Contribution to the quantum-mechanical theory of the equation of state and the law of corresponding states. Determination of the law of force for helium." Physica 5, 945-57 (1938).

Dugdale, J. S. and J. P. Frank, "The Thermodynamic Properties of Solid and Fluid Helium-3 and Helium-4 above 3° K at High Densities," Phil. Trans. Roy. Soc. 257, 1-29 (1964).

Duval, Xavier and Andre Thomy, "Isotherms d'adsorption de krypton sur differents graphites exfolies," Compt. Rend. 259, 4007-09 (1964).

Edmonds, T. and J. P. Hobson, "A Study of Thermal Transpiration Using Ultrahigh-Vacuum Techniques," J. Vac. Sci. Technol. 2, 182-97 (1965).

Elgin, R. L. and D. L. Goodstein, "Latent Heat of the Superfluidity Transition in Unsaturated Helium Films," (abstract) Bull. Am. Phys. Soc. 13, 1669 (1968).

--- and ---, "Thermodynamic Functions for Helium 4 Submonolayers," Proc. 13th Int. Conf. Low Temp. Phys., Boulder Colo. 1972, (1973).

Feynman, R. P. private communication (1973).

Flood, E. Alison, ed. The Solid-Gas Interface, Marcel Dekker, Inc. New York (1967).

Frederikse, H. P. R., "On the Specific Heat of Adsorbed Helium," Physica 15, 860-62 (1949).

Glassford, A. P. M. and J. L. Smith, Jr., "Pressure-Volume-Temperature and Internal Energy Data for Helium from 4.2 to 20° K Between 100 and 1300 atm," Cryogenics 6, 193-206 (1966).

Gonano, Roland and E. D. Adams, "In Situ Vapor Pressure Measurements for Low Temperature Thermometry," Rev. Sci. Instr. 41, 716-19 (1970).

Goodstein, D. L., J. G. Dash, and W. D. McCormick, "Phase Change in Adsorbed Helium at Low Temperature," Phys. Rev. Letters 15, 447-49 (1965).

---, W. D. McCormick, and J. G. Dash, "Sintered Copper Sponges for Use at Low Temperatures," Cryogenics 6, 167-68 (1966).

---, David L. and Robert L. Elgin, "Superfluidity without Superflow in Unsaturated Helium Films," Phys. Rev. Letters 22, 383-85 (1969).

Grimsrud, D. T. and James H. Werntz, Jr., "Measurements of the Velocity of Sound in He^3 and He^4 Gas at Low Temperatures with Implications for the Temperature Scale," Phys. Rev. 157, 181-90 (1967).

Guggenheim, E. A., Thermodynamics, 5th ed., North Holland, Amsterdam (1967).

Hagen, Donald E., Anthony D. Novaco, and Frederick J. Milford, "Quantum States and Heat Capacity of Helium Adsorbed on Graphite," Proc. 2nd Int. Symp. on Adsorption-Desorption Phenomena, Florence Italy 1971, Academic Press, N. Y. (1972).

Halsey, G. D. Jr., "A Commentary," 503-14, see (Flood 1967).

Herb, J. A. and J. G. Dash, "Mass Transport of He^4 Films Adsorbed on Graphite," Phys. Rev. Letters 29, 846-48 (1972).

Hickernell, D. C., E. O. McLean, and O. E. Vilches, "Very Low-Temperature Specific Heat of Submonolayer Helium Films," Phys. Rev. Letters 28, 789-92 (1972).

Hill, Terrell L., "Statistical Mechanics of Adsorption. V. Thermodynamics and Heat of Adsorption," J. Chem. Phys. 17, 520-35 (1949).

Hobson, J. P., "Surface Smoothness in Thermal Transpiration at Very Low Pressures," J. Vac. Sci. Technol. 6, 257-59 (1969).

---, "Accommodation Pumping--A New Principle for Low Pressures," J. Vac. Sci. Technol. 7, 351-57 (1970).

Hohenberg, P. C., "Existence of Long-Range Order in One and Two Dimensions," Phys. Rev. 158, 383-86 (1967).

Holste, J. C., T. C. Cetas, and C. A. Swenson, "Effects of Temperature Scale Differences on the Analysis of Heat Capacity Data: The Specific Heat of Copper from 1 - 30 K," Rev. Sci. Instr. 43, 670-76 (1972).

Hust, J. G., "Electrical Resistance Ratios of Evanohm Heater Wire at Low Temperatures," Rev. Sci. Instr. 43, 1387-88 (1972).

Jackson, H. W., "Quantum Theory of Helium-4 Monolayers," Phys. Rev. 180, 184-92 (1969).

Jura, George and Terrell L. Hill, "Thermodynamic Functions of Adsorbed Molecules from Heats of Immersion," J. Am. Chem. Soc. 74, 1598 (1952).

Kidnay, A. J. and M. J. Hiza, "The Purification of Helium Gas by Physical Adsorption at 76° K," A. I. Ch. E. J. 16, 949-54 (1970).

Kierstead, Henry A., "Pressures on the Critical Isochore of He^4," Phys. Rev. A 3, 329-39 (1971).

Kosterlitz, J. M. and D. J. Thouless, "Long range order and metastability in two dimensional solids and superfluids," J. Phys. C 5, L124-26 (1972).

Lai, Hwa-Wen, Chia-Wei Woo, and F. Y. Wu, "Theory of Helium Submonolayers: Formulation of the Problem and Solution in the Zero Coverage Limit," J. Low Temp. Phys. 3, 463-90 (1970).

Landau, L. D. and E. M. Lifshitz, Statistical Physics, Pergamon London (1958).

Lander, J. J. and J. Morrison, "A LEED Investigation of Physisorption," Surface Sci. 6, 1-32 (1967).

Liang, S. Chu, "Some Measurements of Thermal Transpiration," J. Appl. Phys. 22, 148-53 (1951).

---, "On the Calculation of Thermal Transpiration," Can. J. Chem. 33, 279-85 (1955).

Long, Earl and Lothar Meyer, "The Unsaturated Helium Film," Adv. Phys. (Phil. Mag. supp.) 2, 1-27 (1953).

May, Robert M., "Quantum Statistics of Ideal Gases in Two Dimensions," Phys. Rev. 135, A1515-18 (1964).

McCarty, R. D., "Thermophysical Properties of Helium-4 from 2 to 1500 K with Pressures to 1000 Atmospheres," Nat. Bur. Stand. (U.S.) Tech. Note 631 (1972).

McConville, G. T., "Thermomolecular Pressure Corrections in Helium Vapor Pressure Thermometry: The Effect of the Tube Surface," Cryogenics 9, 122-27 (1969).

McCormick, W. D., D. L. Goodstein, and J. G. Dash, "Adsorption and Specific-Heat Studies of Monolayer and Submonolayer Films of He^3 and He^4," Phys. Rev. 168, 249-60 (1968).

McGlashan, M. L., "The Use and Misuse of the Laws of Thermodynamics," J. Chem. Educ. 43, 226-32 (1966).

--- ed., "Manual of symbols and terminology for physiochemical quantities and units," Pure Appl. Chem. 21, 1-44 (1970).

Mermin, N. D., "Crystalline Order in Two Dimensions," Phys. Rev. 176, 250-54 (1968).

Miller, Michael D., Chai-Wei Woo, and Charles E. Campbell, "Ground State of Two Dimensional Liquid Helium," Phys. Rev. A 6, 1942-46 (1972).

Novaco, Anthony D. and Frederick J. Milford, "Adsorption of Helium on Rare-Gas-Plated Graphite," Phys. Rev. A 5, 783-89 (1972); erratum 6, 526.

---, "Two-Dimensional Evaporation and Substrate Heterogeneity Effects in Submonolayer Helium Films," J. Low Temp. Phys. 9, 457-66 (1972).

---, "Cluster Expansion for Superlattice Physisorption: Helium Adsorbed upon Graphite," Phys. Rev. A 7 to be published (May 1973).

Osborne, Darrell W., Howard E. Flotow, and Felix Schreiner, "Calibration and Use of Germanium Resistance Thermometers for Precise Heat Capacity Measurements from 1 to 25° K. High Purity Copper for Interlaboratory Heat Capacity Comparisons," Rev. Sci. Instr. 38, 159-68 (1967).

Polley, M. H., W. D. Schaeffer, and W. R. Smith, "Development of Stepwise Isotherms on Carbon Black Surfaces," J. Phys. Chem. 57, 469-71 (1953).

Princehouse, D. W., "High-Resolution Heat-Capacity Study of ^{4}He Adsorbed on Bare Copper," J. Low Temp. Phys. 8, 287-303 (1972).

Reynolds, Osborne, "XVIII. On certain Dimensional Properties of Matter in the Gaseous State. Part I. Experimental Researches on Thermal Transpiration of Gases through Porous Plates and on the Laws of Transpiration and Impulsion, including an Experimental Proof that Gas is not a continuous Plenum. Part II. On an Extension of the Dynamical Theory of Gas, which includes the Stresses, Tangential and Normal, caused by a varying Condition of Gas, and affords an Explanation of the Phenomena of Transpiration and Impulsion," Phil. Trans. Roy. Soc. London 170 II, 727-845 (1880).

Rhodin, T. N. Jr., "Low Temperature Oxidation of Copper I. Physical Mechanism," J. Am. Chem. Soc. 72, 5102-06 (1950).

Roberts, Thomas R. and Stephen G. Sydoriak, "Thermomolecular Pressure Ratios for He^3 and He^4," Phys. Rev. 102, 304-08 (1956).

Rollefson, R. J., "Motional Narrowing in Monolayer-He^3-Film NMR," Phys. Rev. Letters 29, 410-12 (1972).

Ross, Marvin and William A. Steele, "Multilayer Adsorption of Helium on Argon," J. Chem. Phys. 35, 871-82 (1961).

Ross, Sydney, "The Homotattic Surface and Adsorption Potentials," 491-501, see (Flood 1967).

Siddon, R. L. and M. Schick, "Second Virial Coefficients of Two-Dimensional Systems of He^3 and He^4," Phys. Rev. Letters, to be published (1973).

Singleton, J. H. and G. D. Halsey, Jr., "The Solution of Argon in Layers of Krypton," J. Phys. Chem. 58, 1011-17 (1954).

Sposito, Garrison, "The Interatomic Potential in Liquid ^{4}He," J. Low Temp. Phys. 3, 491-98 (1970).

Steele, William A., "Adsorbate Equation of State," 307-69, see (Flood 1967).

---, "Thermodynamic Properties of Adsorbed Helium," J. Low Temp. Phys. 3, 257-80 (1970).

Stewart, G. A. and J. G. Dash, "Heat Capacities of Submonolayer He^3 and He^4 Adsorbed on Ar-Plated Copper," Phys. Rev. A 2, 918-32 (1970).

--- and ---, "Heat Capacities of Ar, Ne, ^{4}He-Ar, and ^{4}He-Ne Films Adsorbed on Cu at Low Temperatures," J. Low Temp. Phys. 5, 1-16 (1971).

---, S. Siegel, and D. L. Goodstein, "Elastic Properties of Solid He^4 Monolayers from 4.2° K Vapor Pressure Studies," Proc. 13th Int. Conf. Low Temp. Phys., Boulder Colo. 1972, (1973).

Takaishi, T. and Y. Sensui, "Thermal Transpiration Effect of Hydrogen, Rare Gases, and Methane," Trans. Faraday Soc. 59, 2503-14 (1963).

Thomy, Andre and Xavier Duval, "Adsorption de Molecules Simples sur Graphite I.--Homogeneite de la surface du graphite exfolie. Originalite et complexite des isotherms d'adsorption," J. Chim. Phys. Physiocochim. Biol. 66, 1966-73 (1969); "II.--Variation du potentiel d'adsorption en fonction du nombre de couches adsorbees," 67, 286-90 (1970); "III.--Passage de la premiere couche par trois etats successifs," 67, 1101-10 (1970).

Ubbelhode, A. R. and F. A. Lewis, Graphite and its Crystal Compounds, Oxford Univ. Press (1960).

van Dijk, H., M. Durieux, J. R. Clement, and J. K. Logan, "The '1958 He^4 Scale of Temperatures'," Nat. Bur. Stand. (U.S.) Monograph 10 (1960).

Wallace, John L. and David L. Goodstein, "He^4 on Copper: Some Effects of Preadsorbed Noble-Gas Layers," J. Low Temp. Phys. 3, 283-300 (1970).

Watkins, Reed A., William L. Taylor, and Walter J. Haubach, "Thermomolecular Pressure Difference Measurements for Precision Helium-3 and Helium-4 Vapor Pressure Thermometry," J. Chem. Phys. 46, 1007-18 (1967); erratum 47, 3692.

Weber, Sophus, W. H. Keesom, and G. Schmidt, "Neue experimentelle Untersuchungen bezuglich der thermomolekularen Druckdifferenz, besonders bei tiefen Temperaturen, und Vergleichung mit der Theorie." Commun. Kamerlingh Onnes Lab. Univ. Leiden No. 246a (1937); see also No 223b (1932), Suppl. No. 71b (1933), Nos. 246bcd (1937).

Widom, Allan, "Statistical Mechanics of Ultrathin Films of Quantum Liquids," Phys. Rev. 185, 344-47 (1969).

--- and J. B. Sokoloff, "Remnant Bose Condensation in He^4 Submonolayer Films," Phys. Rev. A 5, 475-76 (1972).